THE UNIVERSITY OF MICHIGAN

INDUSTRY PROGRAM OF THE COLLEGE OF ENGINEERING

EFFECT OF BLOWING CONDITIONS ON DEPHOSPHORIZATION
IN THE BASIC OXYGEN FURNACE

Franklin E. Rote

A dissertation submitted in partial fulfillment
of the requirements for the degree of
Doctor of Philosophy in the
University of Michigan
Department of Chemical and Metallurgical Engineering
1967

September, 1967

IP-789

Preface

Table of Contents

List of Tables

List of Figures

vii

Abstract

The objectives of this investigation were to determine the effect of different operating conditions on dephosphorization and to determine the mechanism of dephosphorization during the steelmaking process in a basic oxygen converter. For this purpose the chemical and thermal gradients in the bath were determined under the different operating conditions which were reported to affect dephosphorization such as lance height above the bath, bath depth and nozzle diameter. To obtain the necessary data, special probes, developed for this investigation, were inserted through the side of the converter.

Substantial chemical gradients were found for P, C, Si and Mn, despite the fact that the bath was only 15 inches in diameter and 6 inches deep. The magnitude of the difference in chemical content was affected most by the degree of penetration of the jet into the bath. For example, with shallow penetration, the P content varied from 0.17% to .0.30% compared to .0.14% to 0.20% P with deep penetration.

Temperature differences also varied with blowing conditions. With the poor mixing accompanying shallow jet penetration a temperature range from 3000°F. to 2500°F. was encountered while with jet penetration to the center of the bath, the temperature range was 3000°F. to 2900°F.

The data indicated marked differences in rate of phosphorus, silicon, carbon and manganese removal depending principally upon the depth of penetration of the jet. If the penetration was relatively shallow (due to increased blowing height, greater bath depth or smaller nozzle diameter) steep compositional gradients were obtained and refining was delayed. The chemical analyses and the thermocouple data all indicated a circulation pattern which was upward at the center and radially outward at the surface.

With supplementary experiments in which metal droplets were collected during the run, the following mechanism of dephosphorization was developed. 1) Silicon is rapidly removed and some iron oxidized in the early stages of the run. This produces, along with the CaO added as flux, a fluid basic slag containing CaO, SiO_2 and FeO. 2) Metal droplets are lifted above the slag by the force of the jet, fall back into the slag and are refined while passing through the slag.

Mathematical models of refinement by bath diffusion, circulation and droplet transfer were presented.

In general, the data reverse the conclusions of many earlier publications recommending avoidance of deep jet penetration in refining.

Introduction

The importance of the basic oxygen steel converter is best illustrated by its growing use in the steel industry. In 1954 the McLouth Steel Corporation installed the first converter in the United States. In January of 1965, 15.4% of the steel made in the United States was produced by the BOF (Basic Oxygen Furnace). The percentage was increased to 21.2% by December of 1965. During 1965 worldwide production by the BOF was 102,000,000 tons of steel. Despite the importance and growing use of this process, important refining reactions such as dephosphorization and decarburization are not well understood. Further, the proper operating conditions to best accomplish refining are established by empirical methods.

The objectives of this research were to determine the effect of different operating conditions on dephosphorization and to determine the mechanism of dephosphorization in a basic oxygen converter. To accomplish these objectives the chemical and thermal gradients in the bath of an operating converter were determined under several different sets of blowing conditions.

New sampling techniques were used to obtain the necessary data on metal composition, metal temperature and slag composition while the converter was in operation. A wide range of operating practices was employed to determine the effect on the conversion process of 1) blowing height (7 inches to 21 inches), 2) bath depth (6 inches to 10 inches), and 3) nozzle diameter (0.162 inches to 0.316 inches). A standard operating practice was established which reflected commercial practice as closely as possible. The 250 lb. to 400 lb. hot model used in this research was distinctive in that it was not externally heated after it was charged with hot metal.

1

Other novel experimental techniques were developed to measure the amount of metal spray above the bath and to determine the effect of this spray on bath dephosphorization.

Review of the Literature

The literature is reviewed in two sections: 1) Commercial Operating Practice and 2) Laboratory Investigations and Hot-Model Studies.   There is some repetition due to the absence of a clear distinction between a small operating converter and a large hot-model.

1)   Commercial Operating Practice

This section is divided into five groups: a) Converter Design, b) Charged Materials, c) Operating Practice, d) Refined Materials, and e) Summary.

a)   Converter Design

The designs of basic oxygen converters reported in the literature vary;   however, the general configuration is the same. In Figure 1 a converter is shown schematically with the generalized dimensions I. D. , height and bath depth.   In Table I these dimensions are tabulated for converters which are described in the literature.
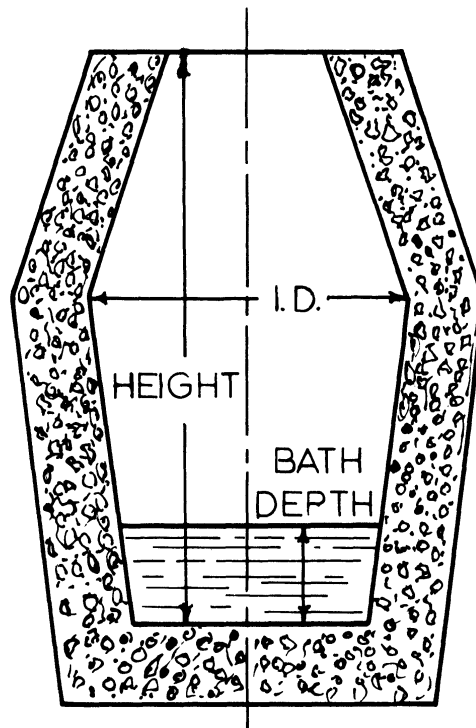
Fig. 1.   Configuration of a Basic Oxygen Converter.

It is evident from the table that the bath depth-diameter ratio is independent of the converter capacity and varies from 0.16 to 0.45 and that only 15% to 20% of the converter volume is occupied by the bath.

Blowing practices reported by several authors are tabulated in Table II in terms of lance height, (height of the oxygen nozzle above the bath), blowing pressure, nozzle diameter, number of nozzles, oxygen jet penetration depth and penetration depth-bath depth ratio.

While blowing practices do vary, the jet penetration depth-bath depth ratio is 0.6 to 0.8 for single nozzle lances.

Table I

Internal Dimensions of Several Basic Oxygen Converters

Capacity (Tons)	I. D. (in.)	Height (in.)	Bath Depth (in.)	Depth to Dia. Ratio	Ht. above Bath (in.)	Reference
55	180	295	31	0.16	264	2
60	123	266	55	0.45	211	3
66	180	328	35	0.19	293	2
77	168	285	39	0.23	246	4
880	153	246	46	0.30	200	5
100	157	318	56	0.35	262	3
120	180	332	56	0.31	276	6
150	204	304	53	0.26	251	7
205	202	334	65	0.33	283	8
230	232	360	65	0.28	295	6
250	234	372	66	0.28	306	6
250	322	324	55	0.17	269	9
300	322	327	62	0.19	265	9
335	280	360	68	0.24	292	10

Table II

Lance Operating Variables,

Jet Penetration and Jet Penetration-Bath Depth Ratio

Lance Height (in.)	Blowing Pressure (psig.)	Nozzle Diameter (in.)	No. of Nozzles	Jet Pen.* (in.)	Ratio	Reference
88	190	2.05	1	32	0.82	4
40	---	1.62	1	32	0.68	11
80	165	2.78	1	35	0.63	6
90	165	2.6	1	33	0.62	7
79	95-105	2.18	3	28	0.41	10

*Jet penetration was calculated according to the empirical relationship developed by Flinn et. al. (11).

b. Charged Materials

The composition of charged hot metal varies depending principally on the source of the iron ore and blast furnace practice. Based on compositions reported by several authors (2,4, 8, 12 - 18), a representative hot metal charge composition is 4.1% C, 0.9% Si, 1.0% Mn, 0.2% P, and 0.04% S. The quantity of steel scrap averaged 22% of the hot metal charge. The range in composition of the charged hot metal is 3.6 to 4.3% C, 0.2 to 1.2% Si, 0.2 to 3.0% Mn, 0.07 to 0.21% P and 0.02 to 0.05% S. The proportion of steel scrap added with the hot metal charge varies between 15% and 30%.

Oxygen consumption has been reported by several authors (3, 4, 12, 13) to be about 2000 cu. ft. per net ton of steel. The oxygen used is at least 99% pure.

Flux compositions were reported by (2, 3, 7, 13, 16, and 18). The average burnt lime addition is 6% of the hot metal charge. The average addition of fluorspar, an agent which speeds lime

solution, is 0.4% of the hot metal charge. The ranges of flux additions are: burnt lime: 4.5 to 6.5% and fluorspar: 0.2 to 0.5% of the hot metal charge.

c. Operating Practice.

Cuscoleca, Rosner and Kuhnelt (16) reported changes in bath composition with blowing time. Their results are summarized in Figure 2. The sequence of oxidation of bath impurities shown in Figure 2, silicon and manganese followed by phosphorus and carbon, is typical of the general oxidation sequence in a converter bath (19).
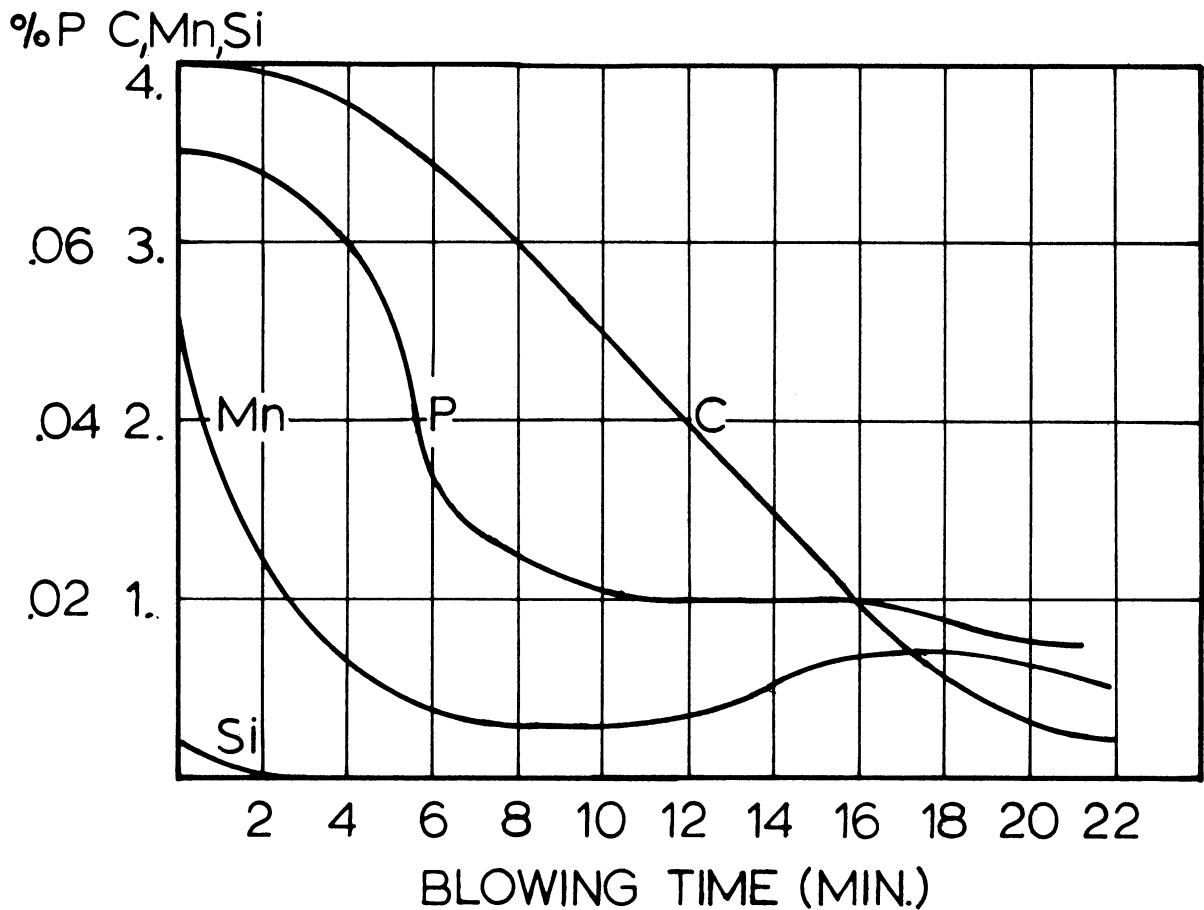
Fig. 2. Sequence of Oxidation of Elements in a Basic Oxygen Converter.

Specific operating practices reported in the literature are summarized below.

Dephosphorization is an essential part of the steelmaking process. Several authors (20-26) were associated with the installation in Austria of the first commercial basic oxygen converters. A summary of their recommendations on an operating practice intended to dephosphorize the metal is to blow pure oxygen gently onto the bath surface, producing large quantities of FeO which in turn fluxes the CaO forming a fluid, basic slag. Behrens and Koenitzer (14) report starting a blow with a 71 inch lance height to enhance the formation of FeO.

Silicon oxidation is not a problem in the converter. It is the first element oxidized (See Figure 2) and the oxidation of silicon can proceed without a basic slag by reaction with dissolved oxygen in any part of the bath.

Decarburization is the main oxidation process. Most authors report conditions which give deep jet penetration (Table II) in conjunction with rapid decarburization and high oxygen efficiencies. Suess (27) specified shallow penetration throughout a run in his American patent on this process. Behrens and Koenitzer (14) report starting a blow with a 71 inch lance height; however, the lance is lowered to 32 inches to hasten decarburization.

Manganese oxidation, like silicon oxidation, is not a problem in the converter.

Bath temperature is controlled by the timing of the addition and amounts of flux and scrap. Petrilli (15) reports adding no flux during the first two minutes of the blow and then adding 80% - 100% of the flux with any remainder being added as a coolant after eighteen minutes of blowing. Cuscoleca et. al. (16) report the addition of flux and scrap after fourteen minutes of blowing to cool the bath.

d. Refined Material

Steel compositions which are produced in the converter range from 0.02% P to 0.05% P, negligible Si, 0.04% C to 0.7% C, 0.1% to 0.4% Mn and 0.02 to 0.03% S (4, 12, 16). Substantial amounts of all the elements except sulfur are oxidized from the bath.

Slag compositions vary with flux and metal contents and with operating procedure. Slag compositions reported by several authors are shown in Table III.

Table III

Composition and Weight of Steelmaking Slags
at the End of the Blow

SiO_2 %	CaO %	MgO %	P_2O_5 %	FeO %	Al_2O_3 %	Fe_2O_3 %	Wt. lb./T.	Ref.
---	---	---	---	---	---	---	250	2
---	---	---	---	20	---	---	---	3
*V=2.7 to 3.2	---	---	---	---	---	---	---	12
V=2.7 to 3.2	---	---	18-23	---	---	---	---	15
12-20	27-40	3-7	0.6-1.5	8-12	---	5.5	350	16
16	48	---	---	15	---	4	---	17
16	43	0.8	4.7	18	2.8	4	300	18
10-20	27-40	3-10	0.6-1.5	10-15	---	---	---	19

*V = % CaO/% SiO_2

e. Summary

Over the wide range of converter capacities which have been reviewed, the following similarities are noted: the bath depth-bath diameter ratio of 0.16 to 0.45, the occupation by the bath of 15% to 20% of converter volume and jet penetration of 60% to 80% of the bath depth. Thus although the Suess patent and some operating instructions specify shallow penetration for dephosphorization, the commercial operations are conducted with penetration to the center of the bath and beyond.

2) Laboratory Investigations and Hot-Model Studies

This section is a review of a) physical phenomona of jet penetration and bath circulation and b) chemical phenomona of mechanisms of bath oxidation, dephosphorization, silicon oxidation, decarburization, and manganese oxidation.

a) Physical Phenomona

Jet Penetration

The question of jet penetration into the bath was mentioned in the previous section. Rellermeyer et. al. (28) and Holden and Hogg (29) maintain that on impact the jet does not penetrate deeply into the bath. Krainer et. al. (30) and Kootz (31) maintain that under certain conditions the jet does penetrate deeply. Philbrook (32) shows deep penetration with a low blowing height and shallow penetration with a high blowing height. Flinn et. al. (11) show that the depth of penetration varies directly with blowing pressure and nozzle diameter and inversely with the square root of the lance height.

Results which lead to the same conclusions as Flinn et. al. (11) were reported by several authors. Krainer et. al. (30) show that the impact momentum is directly proportional to the nozzle area. The reduction of impact pressure by increased blowing height is demonstrated by Kootz, (31), Philbrook (32), and Smith and Dukelow (33). They show that while the momentum of the jet is retained the jet diverges as a cone with increased lance distance/nozzle diameter. This divergence leads to a reduced impact pressure with increased blowing height or decreased nozzle diameter. Philbrook (32) states that changes in the blowing conditions which lead to reduced impact pressure also reduce jet penetration.

Bath Circulation

There is general agreement that the metal bath in an operating converter circulates; however, there is some question as to the direction. Suess (34) states that the circulation produced by the impinging jet is a down in the center up at the sides pattern. Several authors (11, 29, 31, and 35) maintain that the circulation is in the opposite direction rising at the center of the bath (under the jet impingement area) and flowing outward across the surface. Other authors (16, 28, and 36) place emphasis on the spray of metal droplets thrown up by the jet. Krainer et. al. (30) maintain that the circulation pattern is determined by the blowing conditions.

Holden and Hogg (29) state that turbulence in the bath is produced by the mechanical energy of the jet. Others maintain that the turbulence is due to a carbon boil. The carbon boil will be covered later. Flinn et. al. (11) show that circulation patterns are alike when nitrogen or oxygen is blown on the bath. The one difference noted is that the droplets thrown up by the jet burn brightly when oxygen is blown.

b) Chemical Phenomona

Bath Oxidation

Holmes and Thring (36) outline the two theories of the mechanism of bath oxidation. One theory suggests that oxygen reacts at the surface of the jet impingement area forming FeO which is circulated through the bath. The second theory suggests that the iron droplets in the jet spray are oxidized and fall back through the slag into the bath carrying FeO with them. Holden and Hogg (29) point out that the droplet mechanism requires that 40 lb. of 0.12 in. diameter drops be constantly above a 50 ton bath if oxidation rates are to be maintained. This calculation was based on negligible circulation in the drop.

Perbix (37) shows that oxygen efficiency is increased by increasing the oxygen flow rate. Kootz (31) , Smith and Dukelow (33), and Perbix (37) all show decreases in oxygen efficiency with increased blowing height.

Dephosphorization

Equilibrium limits on the extent of bath dephosphorization were established by Winkler and Chipman (38). Their results show that K, the equilibrium constant is given as shown below.

$$
\log K = \log[\ \frac{(4CaO \cdot P_2O_5)}{(CaO')^4 (FeO)^5 [\underline{P}]^2}\ ] = \frac{40067}{T} - 15.06
$$

K is decreased by a factor of 10 by a temperature increase of 100°F. CaO' is the free, unreacted, lime in the slag. SiO_2 and Al_2O_3 react with CaO in 1:2 molar ratios. As shown in the equation above, P_2O_5 reacts with CaO in a 1:4 ratio. Fe_2O_3 reacts with CaO in a 1:1 ratio. All of these oxides detract from the dephosphorizing power of the slag. MnO and MgO are considered to be basic slag constituents equal to CaO in dephosphorizing power. The importance of the FeO content of the slag is shown by its presence to the fifth power in the equilibrium constant.

The mechanism of bath dephosphorization is outlined by Bogandy, Dick and Stranski (39) as $2\underline{P} + 5\underline{O} \rightarrow P_2O_5$ at the slag-metal interface where the reaction $4\ CaO + P_2O_5 \rightarrow 4\ CaO \cdot P_2O_5$ can proceed. Winkler and Chipman (38) show that $\underline{O}$ and (FeO) are both valid sources of oxygen. Kootz and Neuhaus (40) relate bath circulation and the necessity of a slag-metal interface for dephosphorization and conclude that the phosphorus content of the bath varies from one location to another.

Bath turbulence was established as important by Kootz et. al. (41) and they point out that the rate of the dephosphorization reaction in a converter is limited by the metal boundary layer; therefore, it is important to have a large slag-metal interface. Cuscoleca et. al. (16) state that deep penetration causes turbulence in the metal bath and throws up a spray of metal droplets which increases the slag-metal interface. The effect of bath turbulence on dephosphorization was studied by Kato et. al. (42). They found that the rate and extent of dephosphorization are markedly increased by artificially induced bath turbulence.

Bogandy et. al. (39) report that equilibrium is never reached in a basic oxygen converter so that after a blow dephosphorization can continue. They report that a nitrogen purge causes sufficient agitation to reduce the phosphorus content from 0.04% to 0.03% after a converter is turned down. Similar results are achieved with carbon deoxidation and the subsequent CO boil.

Silicon Oxidation

Equilibrium data show that the product $[\%\underline{Si}]\,[\%\underline{O}]^2 =$ 3.6 x 10^{-5} when an iron bath is equilibrated with pure SiO_2 (43). In basic slags of the type found in a converter the mole fraction of SiO_2 is about 0.1 reducing the equilibrium product to 3.6 x 10^{-6} if the slag is an ideal solution. The assumption of ideality is shown to be false by Winkler and Chipman (38). They show that all the SiO_2 is combined with CaO in basic, V > 2, slags.

Decarburization

Equilibrium between carbon and oxygen is determined primarily by the reaction $\underline{C} + \underline{O} \rightarrow CO$ (g) and to a lesser extent by $\underline{C} + 2\,\underline{O} \rightarrow CO_2$ (g). At one atmosphere pressure of pure CO, 0.1% $\underline{C}$ is in equilibrium with 0.02% $\underline{O}$ in an iron bath at $1600^\circ C$.

At higher carbon contents the solubility product is increased due to changes in the activities of the carbon and oxygen (43). Pearson et. al. (44) report that in a converter bath at 2980°F containing 0.1% $\underline{C}$ the oxygen content is 0.04% to 0.1% $\underline{O}$.

The mechanism of decarburization is $\underline{C} + \underline{O}$ or $\underline{C} + 1/2\ O_2$ going to CO gas. No slag-metal interface is required as a reaction site. Several authors (16, 19, 24, and 32) maintain that the decarburization reaction proceeds through a carbon boil. Philbrook (32) discusses the carbon boil in detail concluding:

1.　　CO volumes of 2 to 2.5 times the bath volume are evolved every second with usual blowing practice, the bath is virtually a bubble-metal slurry,

2.　　no upper limit of oxygen absorption by the bath is found,

3.　　concentration gradients are minimized by the carbon boil,

4.　　greater mixing of slag and metal including ejection of slag streamers and metal droplets into the oxidizing gas phase is induced by the carbon boil.

Krainer et. al. (30) report data showing that decarburization is accomplished principally in an area immediately adjacent to the jet impingement area. Coupling this finding with the fact that the bath volume is not sufficiently increased to accomodate the required boil during the rapid decarburization period, they conclude that no more than one third of the CO is evolved from the bath. They contend further that the majority of the CO is evolved from the surface of the impact area, and report temperatures of 4500°F in this region.

Flinn et. al. (11) mention the brightly burning droplets of iron thrown up by the oxygen jet. Baker et. al. (45) report data on decarburization of iron drops showing that a 1/4 inch diameter drop could be decarburized from 3.5% C to 0.1% by pure oxygen in two or three seconds under the conditions found in a converter. They show further that if CO_2 is substituted for oxygen the decarburization time is increased 4 fold.

Smith and Dukelow (33) and Perbix (37) found that the decarburization rate of a bath is linearly increased by increasing the delivery rate of oxygen.

Manganese Oxidation

Equilibrium data for Fe, Mn, O, MnO, FeO show that the equilibrium manganese content of the metal bath is approximated by % Mn = 0.4 x (MnO)/(FeO) (43).

The mechanism of manganese oxidation is the same as silicon oxidation in that it can proceed without a slag and that it begins immediately upon the initiation of blowing.

Planning the Experiments

Three areas of substantial disagreement exist in the literature concerning the proper operation of a basic oxygen converter: 1) Dephosphorization - Some authors state that large amounts of FeO produced by shallow jet penetration are necessary to achieve good dephosphorization while other authors contend that bath turbulence produced by deep jet penetration is necessary.
2) Decarburization - Some authors contend that a substantial carbon boil is responsible for decarburization while others state that direct jet-bath interaction either at the jet impingement area or in the metal droplets is responsible for decarburization. 3) Bath Circulation - Some authors state that the converter bath is generally turbulent, others contend that a discernible down in the center circulation pattern exists while the majority assert that the circulation is up in the center.

If a soft blow is necessary to achieve appreciable dephosphorization the rate and extent of dephosphorization should be greater in soft blown heats. On the other hand, if agitation is most important to good dephosphorization, heats blown hardest should be the most completely dephosphorized.

If a carbon boil is responsible for decarburization then the metal bath should expand well beyond its normal limits. If the boil is minimal or non-existent, the bath would retain its normal limits.

If bath circulation is down in the center, the center of the bath should be the hotter and lower in alloy content; but if bath circulation is up in the center, the surface of the bath should be hotter and lower in alloy content than the rest of the bath. If the bath is generally turbulent then the temperature and composition should be uniform.

15

To resolve these points, it was decided to determine the chemical and thermal gradients in a converter under different operating conditions. To determine the mechanisms of element removal it is far more important to know the distribution of elements in a converter bath than to know only the average bath composition.

The plan of the experiments is shown schematically in Figure 3. At the center are the "standard" conditions. Ranging around them are the variations in practice made to test the effects on the conversion process of blowing height, bath depth, blowing pressure and nozzle diameter.

```
┌─────────────────────────────┐      ┌─────────────────────────────┐
│ BATH  DEPTH      : 6 in.     │      │ BATH  DEPTH      : 6 in.     │
│ BLOWING  HEIGHT  : 21 in.    │      │ BLOWING  HEIGHT  : 7 in.     │
│ BLOWING  PRESSURE: 20psig.   │      │ BLOWING  PRESSURE: 25psig.   │
│ NOZZLE  DIAMETER : .316 in.  │      │ NOZZLE  DIAMER   : .162 in.  │
└─────────────────────────────┘      └─────────────────────────────┘
        BLOWING  HEIGHT                      NOZZLE  DIAMETER

            ┌─────────────────────────────┐
            │ BATH  DEPTH        : 6 in.   │
            │ BLOWING  HEIGHT    : 7 in.   │
            │ BLOWING  PRESSURE  : 20psig. │
            │ NOZZLE  DIAMETER   : .316 in.│
            └─────────────────────────────┘

        BATH  DEPTH                          BLOWING  PRESSURE

┌─────────────────────────────┐      ┌─────────────────────────────┐
│ BATH  DEPTH      : 10 in.    │      │ BATH  DEPTH      : 10 in.    │
│ BLOWING  HEIGHT  : 7 in.     │      │ BLOWING  HEIGHT  : 7 in.     │
│ BLOWING  PRESSURE: 20psig.   │      │ BLOWING  PRESSURE: 35psig.   │
│ NOZZLE  DIAMETER : .316 in.  │      │ NOZZLE  DIAMETER : .316 in.  │
└─────────────────────────────┘      └─────────────────────────────┘
```

Fig. 3.   Physical Design of the Experiments.

Experimental Procedure

This description of experimental procedure is divided into two sections 1) Development of Techniques, and 2) Conduct of the Experiments.

1) Development of Techniques

Before making any heats three techniques were developed: A) Sampler Preparation, B) Converter Preparation and C) Charge Preparation.

A) Sampler Preparation

A brief description of the development of the sampler may help others to avoid some of the problems experienced in this work. Once the concept of determining chemical gradients was established the problem of gathering the data had to be solved.

a) Top Sampling

The first thoughts on the matter suggested sampling by extending probes down into the bath from above. This technique was abandoned after preliminary tests because it was unsuitable on three points. First, any sampling device which is lowered into the bath passes through the slag taking some down into the metal. This unnatural mixing of slag and metal could cause local dephosphorization thus making the metal sample nonrepresentative. Second, probing from the top involved a distance of more than 38 inches making accurate sampler location very difficult. Third, the area directly over the converter mouth was exposed to the molten slag and metal which were ejected from the converter during a heat.

b) Metal Sampler Probes

When it was clear that the converter would have to be sampled through the side wall the initial sampling probe was developed. Three areas of development were studied simultaneously: a sampling device, a refractory coating to protect the sampling device and a support for the system.

The sampling device (sampling tubes) were required to take and retain a metal sample from a specified location in the converter bath. The sample had to be taken after the probe was in place but before it was destroyed. The first technique considered was vycor tubing shielded with a metal foil window. When the foil melted the sample was taken as metal flowed into the open tube. This design was found to be poor due primarily to fabrication problems. The second technique considered was to insert evacuated vycor tubes into the bath. This too was abandoned because the vycor tube slowly collapsed during immersion.

The successful design utilized evacuated pyrex tubes which were insulated from the bath by refractory except at a tip which protruded through the insulation. The location of the pyrex tube in the bath was determined with guides on the support and in the converter wall.

The opening time of the exposed tip of the sampling tube depended upon bath temperature, exposed area and the thickness of the tip.

The dependence of opening time on bath temperature is shown in Figure 4. In the temperature range of experimental interest the opening time was 5 seconds at $2500^{\circ}F$ to 1 second at $3300^{\circ}F$. Analysis of movies taken of the sampling procedure indicated that a sampling probe was located in the bath in 1/8 to 1/4 second and tests on the system showed that the probe was not damaged after a 15 second exposure to steel at $3200^{\circ}F$.

TUBE OPENING TIME (SEC.)
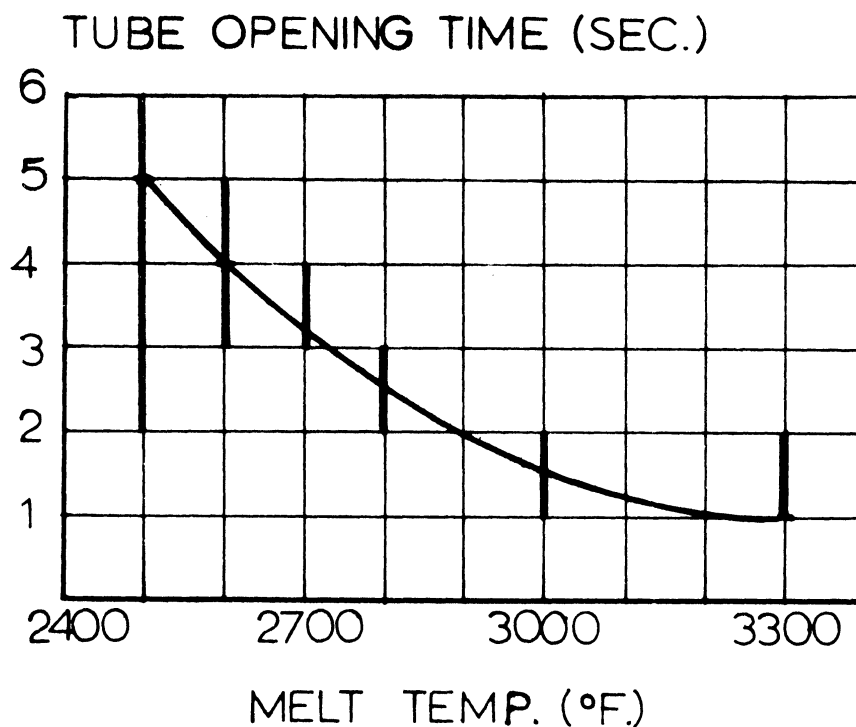
MELT TEMP. (°F.)

Fig. 4. Tube Opening Time Versus Melt
Temperature.

The opening time depended only slightly on the exposed

area of the tip; however, care was taken to insure that the exposed

area was a circle roughly 9 mm. in diameter.

The opening time varied almost directly with tip thickness

in the range 0.01 inches to 0.03 inches. The data in Figure 4 were

for a tip thickness of 0.015 inches $\pm$ 0.002 inches. This was the

specification for tip thickness throughout the investigation. The

tip thickness was checked periodically to insure production within

the range specified.

The refractory insulation was required to pack around the

tubes easily but densely, to resist spalling when inserted at room

temperature into a metal bath at $3200^{\circ}F$ and to liberate no gas when

inserted into the bath. The refractory could be preheated to

$1000^{\circ}F$ (a limit set by the creep properties of pyrex) but had to be

cooled to near room temperature immediately before use.

A wide range of refractories was tested and most of them failed either because of spalling or gas liberation. It was found that most refractories could successfully be packed around the tubes as a thick slurry. The optimum refractory insulation was found to be a slurry of fines taken from commercial MgO refractory. After the slurry was applied and air dried the probe was slowly heated to 1000°F, held 48 hours and furnace cooled before use. After this treatment the refractory neither spalled nor liberated gas for at least 15 seconds after immersion into steel at 3200°F.

The support of the sampler probe was required to be chemically inert in a steel bath before the sample was taken, to be strong enough to pierce a patch in the converter wall and not to disturb the bath.

Earlier experience with vycor showed that this material was inert in a bath for long periods so the first supports were fabricated from 25 mm. vycor tubing. While chemically inert, the vycor tubes cracked when the assembly was preheated to 1000°F. This cracking was due to the greater thermal expansion of MgO than vycor. This problem was solved by lining the vycor tube with asbestos which served as a cushion for the thermal expansion of the MgO.

Vycor supports were not strong enough to pierce the thin refractory patches in the converter. Whenever an attempt was made to pierce a patch with a vycor support it cracked and then shattered. This difficulty was never overcome and vycor supports were abandoned.

The strength of steel allowed steel supports to pierce a wall patch easily; however, bath contamination by the probe had to be checked.

Comparative samples were taken for chemical analysis with a steel probe and with a vycor tube and suction bulb from baths at 2850°F. The result of this comparison was that the respective phosphorus contents were 0.45% and 0.48% in one test and 0.18% and 0.17% in a second test. In the second test a chill cast slug was also poured which contained 0.18% P. In both tests the silicon contents were found to be 0.72% $\pm$ 0.02% for all samples. The range of carbon contents was 4.2% versus 4.3% and 4.3% versus 4.3% in the two tests. Manganese contents were the same for all samples. On the basis of these results it was decided that steel probes could be used without fear of sample contamination.

The design of the probe was a 1 inch diameter cylinder with a pointed end. The amount of bath disturbance when a sampler probe was inserted was determined with water-model experiments. Streamline flow of water was established in a steel trough at a velocity of 5 inches/second. Dye was fed into the stream to mark the flow direction. A sampler probe was inserted into the stream with the result that within roughly 1/4 inch of the probe the flow lines were deformed to accommodate the probe. Beyond this distance no disturbance of the flow lines was noted.

Initially it was hoped that the samplers could be inserted into the converter and then be removed. Considerable time was spend attempting to transform this concept into a working procedure; however, this was not possible because of one or the other of two recurring problems. The sampler was usually frozen into the converter wall by bath metal which filled the 1/16 inch gap between the sampler and the wall of the sampling hole. On those rare occassions when the sampler was retrieved the resulting hole in the converter wall was so large that substantial metal was lost from the bath before the hole was botted.

The final sampler probe design is shown in Figure 5.

These probes remained in the converter wall throughout the heat.

The preparation procedure and the specific dimensions of the probe

are given below.
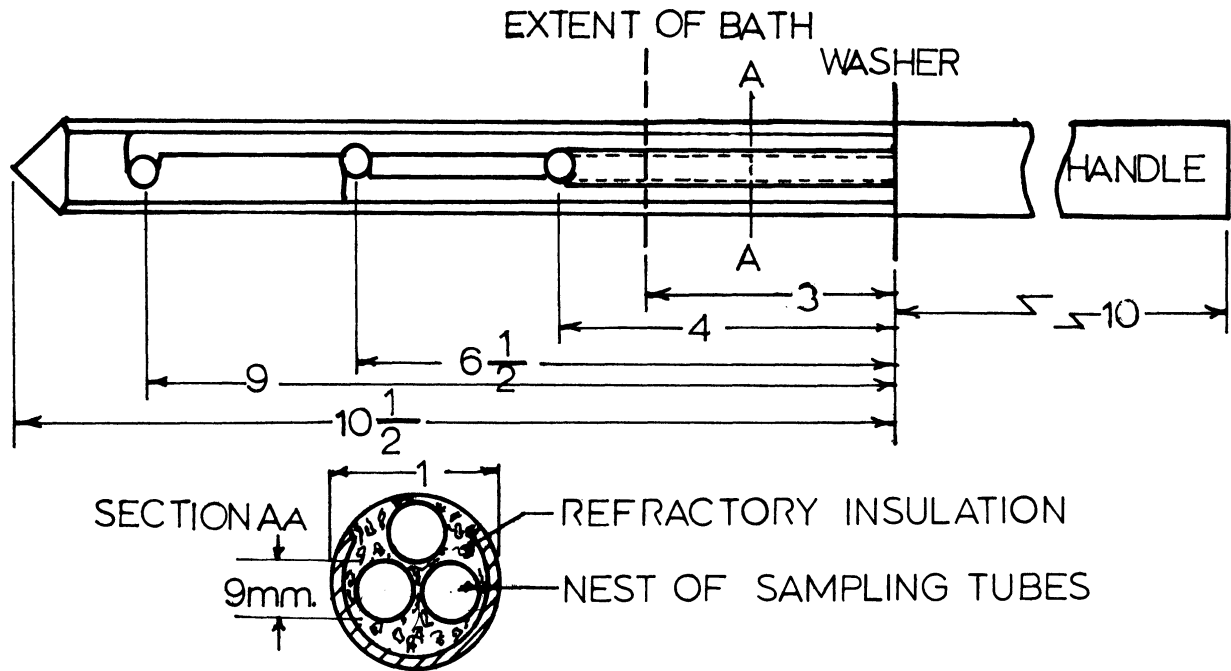
Fig. 5.   Metal Sampler Probe.

9 m. m. O. D. , tipped sampling tubes were evacuated to

less than 1 μ Hg after a weighed amount of 24 gauge aluminum wire

was inserted.   Sufficient wire was used to add 0. 4% Al to the sample.

The sampling tubes were nested into the support in a strictly

maintained arrangement to insure proper identification of the

samples after a run.

When the tubes were in place the support was filled with a

thick slurry of MgO fines.   The handle was filled with a fire-clay

slurry. The fire-clay was used to guard against a broken tube causing a leak and to supply a heat sink to solidify the samples rapidly. After fabrication the samplers were slowly heated to 1000°F., held 48 hrs. and furnace cooled.

The steel support cylinder was a slotted 3/4" low C steel pipe. The slot was 5/8 inch to 7/8 inch wide. A solid steel point was welded into one end of the cylinder and a handle was welded to the other. The handle was fabricated from 3/4" low C steel pipe and a 2" O. D. washer.

Immediately prior to a run a fireclay collar was applied in front of the washer and a cone of fire-clay was applied behind the washer.

Reproducibility of sample location was checked first by inserting sampler probes through unpatched holes into an empty, cold converter. By measuring the distance from the converter wall to the tips of sampling tubes the error in radial location was determined. The error in vertical location was determined by measuring the angular deviation of the sampler probes from a horizontal axis after an experiment. Errors in radial sample location were found to be $\pm$ 1/4". Inclination of the sampler probe averaged 1° as most were horizontal. The range of inclination was $\pm$ 5°. At $\pm$ 5°, the worst condition, the location error of the 6 inch tip was $\pm$ 1/2 inch, the 3-1/2 inch tip, $\pm$ 3/8 inch and the 1 inch tip, $\pm$ 1/8 inch.

The location of the volume of metal taken as a sample was determined in water-model experiments. J probes were bent from a length of 9 m. m. pyrex tubing, fitted with suction bulbs and immersed into a water-turpentine bath. The turpentine being immiscible in water floated on the bath surface. The open end of the J probe was first positioned 6 inches from the water-turpentine

interface and moved upward to within 1/2 inch of the water-turpentine interface before it was disturbed when the suction bulb was released and a 15 c. c. sample taken. The experiment was repeated with light machine oil and with alumina particles held afloat by surface tension. In these cases the results were the same. Horizontal tests were made by holding the open leg of the J probe just below the surface of the water-alumina model and taking a sample. In this case the crosssection of the sample volume was roughly a semicircle 1/2 inch in radius.

Reproducibility of sample analyses was checked by taking samples from two similar runs at the same location and blowing time. The results of this check are shown in Table IV along with the results of comparative analyses of the same sample. The error in comparative analyses is of the same magnitude as the variation between samples.

Table IV

Reproducibility of Sample Compositions
for Standard Blowing Conditions

Element	P	Mn	C	Si
Similar Samples from Different Heats				
Average Comp.	0.17	0.15	3.5	0.07
Average Variation	0.03	0.02	0.25	0.03
$\pm$ % Variation	$\pm$ 8%	$\pm$ 7%	$\pm$ 4%	$\pm$ 23%
No. of Samples	14	20	16	12
Comparative Analyses of the Same Sample				
Average Comp.	0.16	0.14	2.0	0.06
Average Variation	0.027	0.02	0.25	0.02
$\pm$ % Variation	$\pm$ 8%	$\pm$ 7%	$\pm$ 6%	$\pm$ 16%
No. of Samples	9	11	9	8

c)   Slag Sampling Probe

The slag sampling probes were fabricated from 3/4 inch low C steel pipe in much the same way as metal samplers. The slotted portion was 7 inches long separated from the handle by a 2-1/2 inch length of spacer pipe. The handle was filled with fire-clay and the spacer pipe was rammed solid with MgO refractory. The slotted portion was left open. Before a run the slotted portion was washed with a zirconia slurry to ease separation of the sample.

d)   Thermocouple Probe

The preparation of the thermocouple tube deserves special attention because of the harsh environment of a converter bath. Figure 6 shows schematically a probe after installation. The
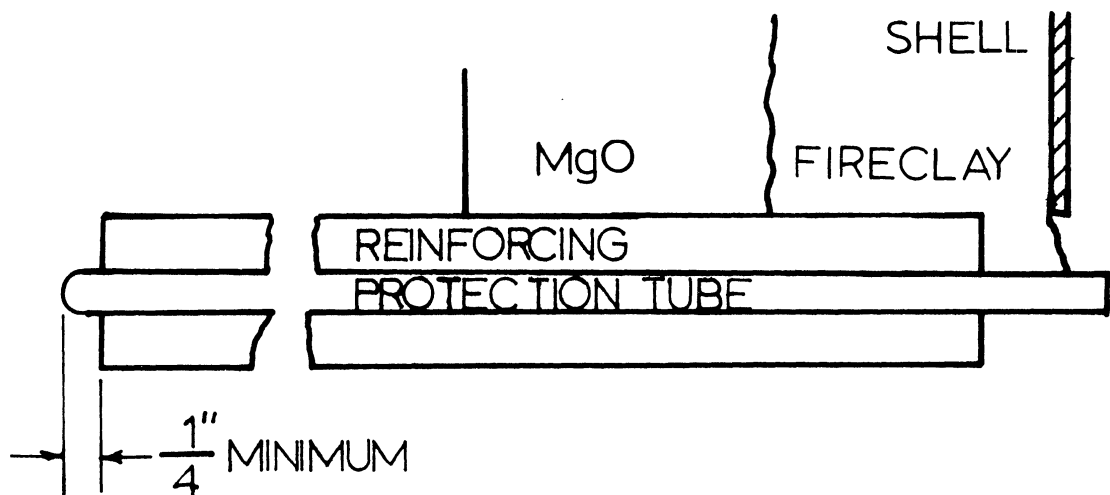
Fig. 6.   Temperature Probe after Installation.

protection tube was high purity alumina (99. 7% Al_2O_3) and was covered with a layer of castable alumina (99. 3% Al_2O_3) which mechanically strengthened the structure. The reinforcing layer was applied as a slurry of fines. The tip of the protection tube extended about 1/4 inch beyond the reinforcing layer, for sensitivity of response.

After fabrication the assembly was allowed to air set for three hours and then was slowly heated to 800°F. and furnace cooled. The tubes were located by ramming refractory around them while they were held in place. The ramming sequence is shown in Figure 6. After ramming was complete the wall was washed with MgO fines to fill any small rifts.

The thermocouples were fabricated from 26 gauge Pt-Pt + 10% Rh wires which were fused in a carbon arc without flux. Response to temperature was tested in a bunsen burner flame which also cleaned any trace of grease from the thermocouple lead.

The thermocouple wires were insulated with high purity alumina two hole insulators. The assembly was put into the previously installed tubes and sealed in place with refractory cement.

Contact to a recorder was made with compensating leads through a switching arrangement which allowed up to twelve thermocouples to be read sequentially at one second intervals.

The schematic wiring diagram is shown in Figure 7. Included in the drawing are two constant potentials: the "marker" and the "buck". Both constant potentials were supplied by potentiometers. The marker was wired into the output circuit to mark a point in the reading sequence so that the output of each of the thermocouples could be identified. The buck was wired into the input circuit in opposition to the thermocouples lowering their voltage 3.3 m.v.. This effectively increased the range of the recorder 500° F to 2500° F to 3500°F. The error in temperature readings was estimated to be ± 30°F.
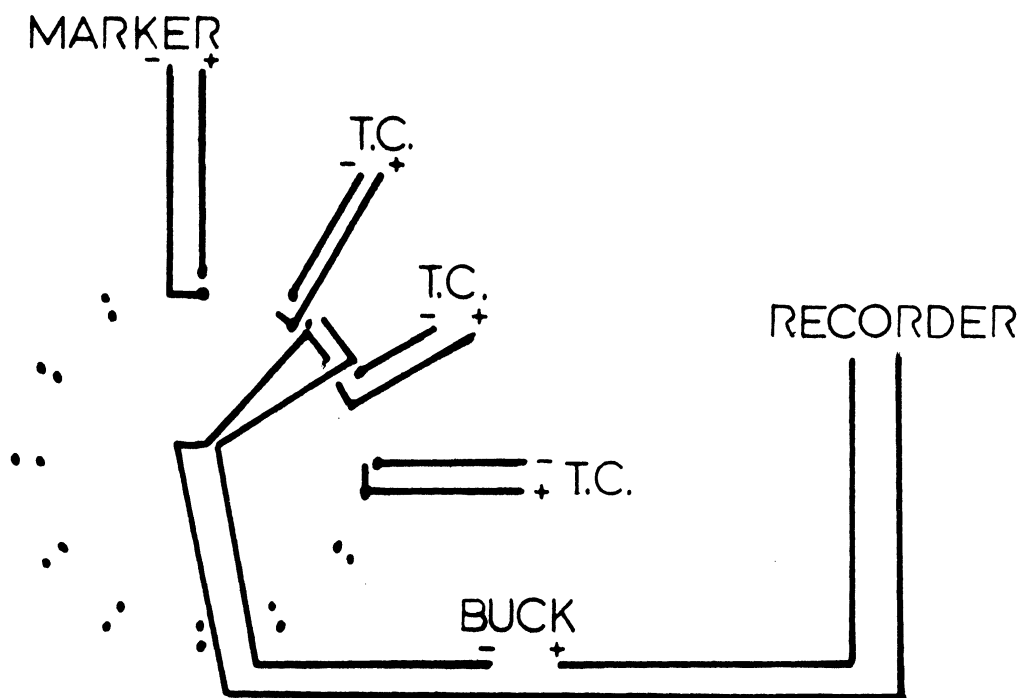
Fig. 7. Schematic Thermocouple - Switch Wiring Diagram.

Errors in thermocouple probe location were $\pm$ 1/4 inch. The response time of the thermocouple assembly was 1 second, $2000^{\circ}F$. to $3000^{\circ}F.$, and limited by the recorder.

B) Converter Preparation

The 15 inch converter used in the experiments is shown in Figure 8.

The lining away from the sampling area was cleaned and patched before each run and the bottom was checked for damage. The lining in the sampler hole area was completely removed so that cast sampler hole forms could be set in place and accurately located.

The location of the cylindrical portion of the form was determined as shown in Figure 9. The level assures that the cylinder axis is horizontal. The rule was centered by suspending it directly
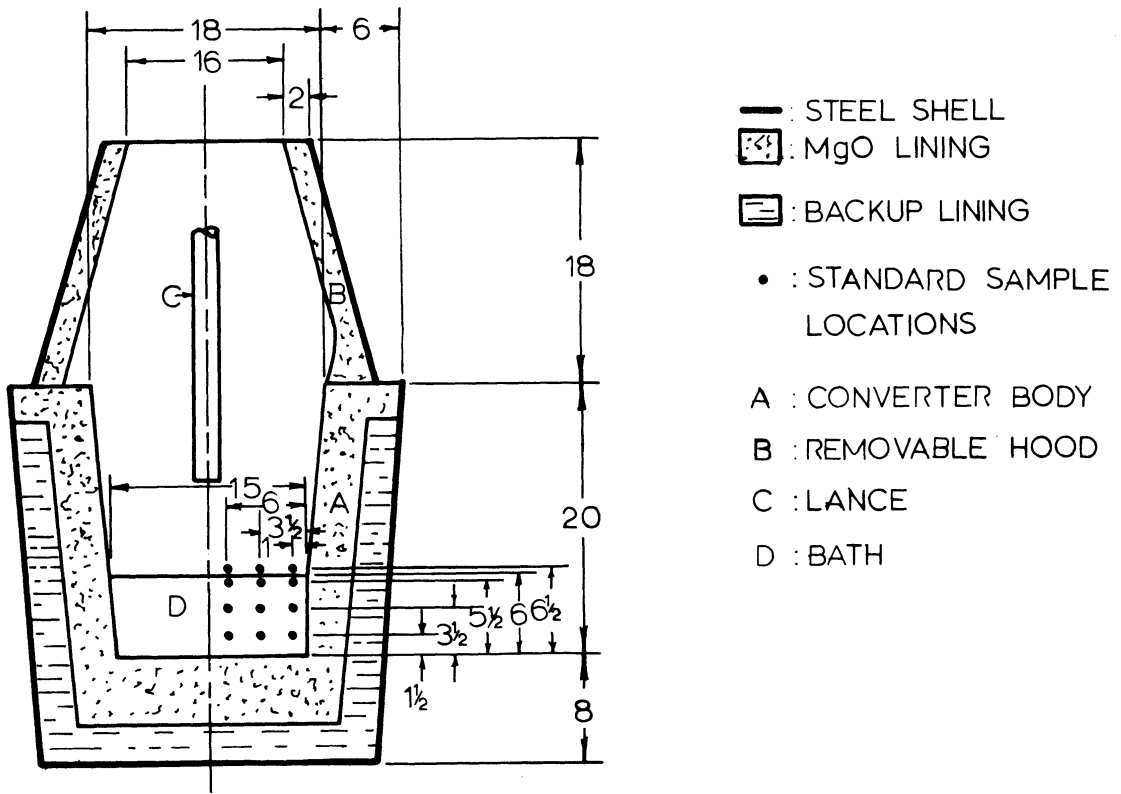
Fig. 8.   Hot-Model Basic Oxygen Converter Used in These Experiments.

Fig. 9.   Locating a Sampling Hole.

under the nozzle of the lance. With the angle iron it was possible
to determine both the cylinder height and the axis orientation relative
to the center of the converter.

The ramming sequence for the sampler hole area is shown
in Figure 10. The shape of the hole is significant. The 1-1/6 inch
diameter cylinder was a slip fit with a sampler, allowing it to
slide through; the 2 inch length allows only axial motion. The patch
was rammed after the rest of the lining was in place. Once the wall
was patched it was washed with MgO fines to fill any pores or rifts.
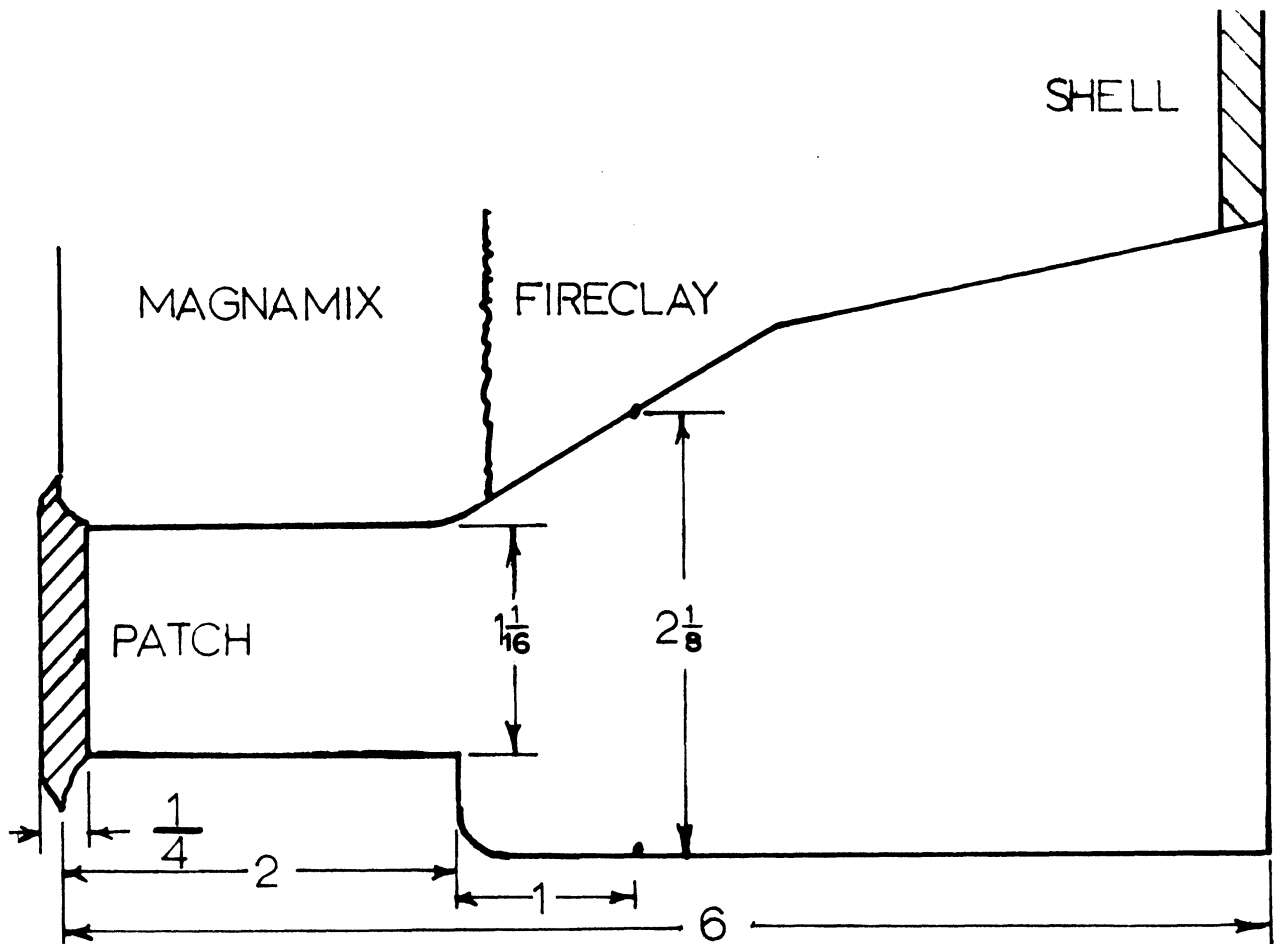
Fig. 10. Shape of a Sampling Hole.

The thickness and material used for wall patches were
determined by careful experimentation. Hollow refractory cones
were prepared and patched with several refractories in thickness
from 1/8 inch to 1 inch. These cones were immersed in cast iron
or steel baths and held for 10 minutes at temperatures up to $3500^{\circ}F$..
If the patch had not leaked and was still easily pierced it was acceptable.
A 1/4 inch patch rammed with MgO cement met both criteria and
was used.

C) Charge Preparation

The charge for a run consisted of hot metal and flux. Both
components were weighed to accuracies of $\pm$ 1%. Representative
weights of all components of the charge are shown in Table V along
with the source and reported composition.

Table V

Representative Weights, Source, and Composition of Charge Components

Hot Metal

Component	Weight (lbs)	Source	Reported Comp. Major Elements
pig iron	246	Great Lakes Foundry Supply Co.	C - 4.3% Si - 0.62% Mn - 0.54% P - 0.08%
50% Fe-Si	.25	Union Carbide Corp.	Si - 50%
75% Fe-Mn	.20	Union Carbide Corp.	Mn - 75%
Fe-P	2.0	Great Lakes Foundry Supply Co.	P - 24%

Flux

Lime	18.0	Wyandotte Chemical Co.	CaO - 91% MgO - 3.5% SiO_2 - 1.3%
Fluorspar	.90	Great Lakes Foundry	CaF_2 - 88%

The pig iron was received as 35 lb. pigs which were broken into thirds and the pieces were stored in separate containers. The 246 lb. charge was taken from one container. This practice and the anticipated mixing of the pigs prior to delivery produced a uniform charge. The alloy additions were taken from shipping containers; the lime was obtained directly from a carloading facility and the fluorspar from two pound bricks.

The flux was weighed out into 6 paper bags each containing 3 lbs.. Two distinctly marked bags each contained 0.45 lbs. of fluorspar. The weights were increased to 4.8 lbs. and 0.72 lbs. respectively when 400 lb. heats were run.

2) Conduct of the Experiments

a) Melting the Charge

The metallic charge was melted in two 3000 c. p. s.,
50 KVA induction furnaces with 200 lb. and 110 lb. individual
capacities. Both units were MgO lined.

The alloy additions were placed in the bottom of the furnace
and it was filled with pigs. Neither furnace would hold its full
cold charge so additions were made as melting progressed. During
the melt down period the molten metal temperature did not exceed
2700°F. Prior to tapping the melts were superheated to 2850°F.

When 400 lb. heats were run the additional 160 lbs. were
melted as two charges in the 110 lb. induction furnace. The metal
was transferred to a clay-graphite crucible in a gas-fired holding
furnace. The heating capacity of this unit was such that tap
temperatures of 2650°F. to 2680°F. were attained.

Charging the Converter

Prior to a run the converter was preheated to a 2000°F.
surface temperature. This was accomplished in about 18 hrs. with
a natural gas-air torch.

When all the metallic charge was molten and superheated
it was tapped into a 100 lb. ladle and transferred to the preheated
converter.

b) Pre-Run Checks

When the converter was fully charged it was raised to an
upright position and the bath depth was measured. A 1 inch by
1/4 inch steel bar was lowered along the lance to the bottom of
the converter. The bar was held in position for 6 seconds, lifted
out and placed on the lab floor where the bath depth was measured.

The extent of the bath is clearly evident on the bar as shown in Figure 11. The bath was adjusted to $\pm$ 0.1 in. of the desired depth.
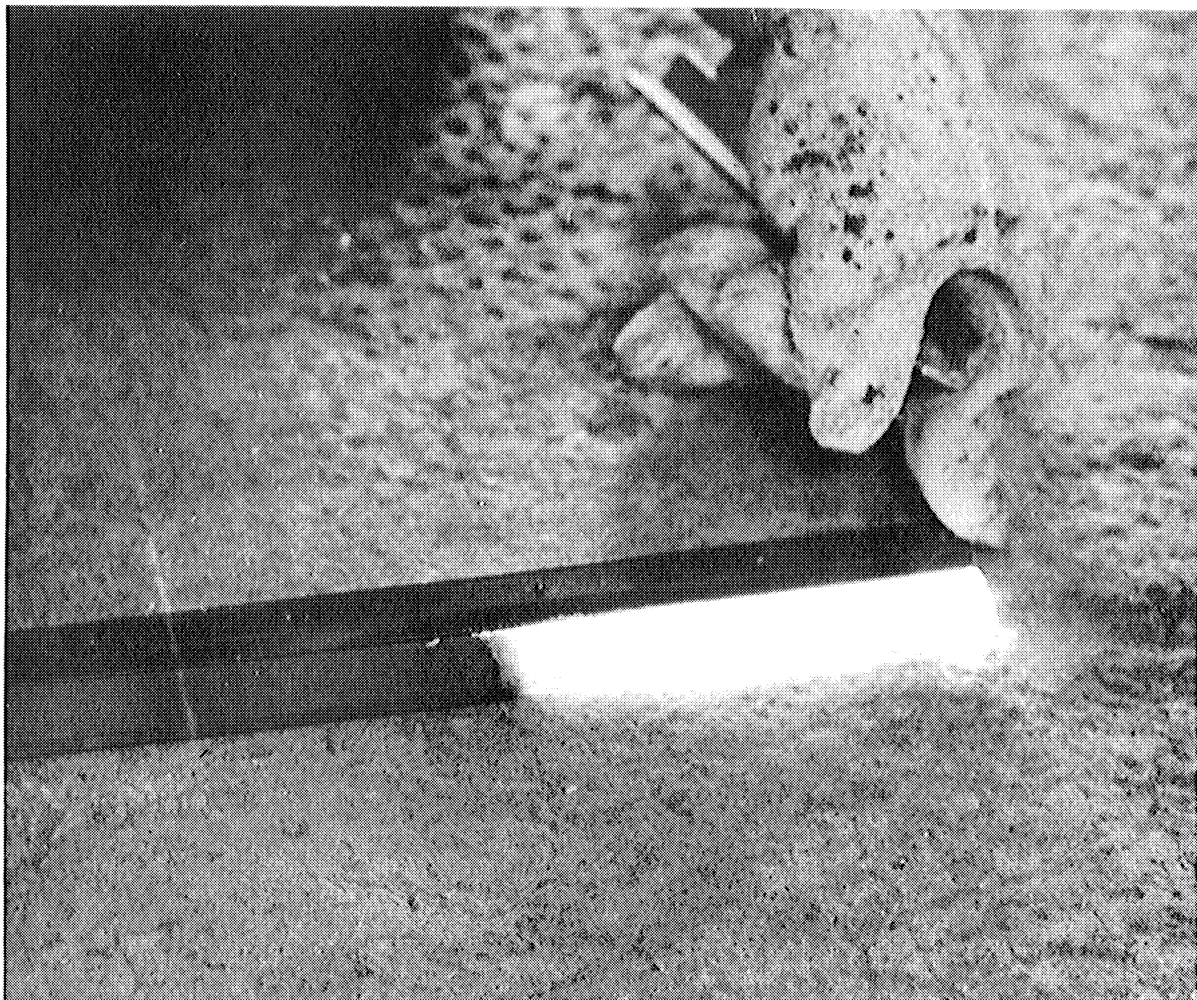
Fig. 11. Depth of the Bath Indicated on a Steel Bar.

The bath temperature was followed to $2550^{\circ}F$. with an optical pyrometer. During this time any loose slag was removed from the bath surface. When the converter bath reached 2550° F., sample M-1 was taken. The sample was poured from the converter into a 5 lb. ladle and then chill cast in a core sand mold.

This procedure produced an average starting analysis of 0.24% P, 0.6% Si, 4.1% C, and 0.55% Mn. The range of analyses was 0.2% to 0.4% P, 0.4% to 0.7% Si, 3.9% to 4.3% C, and 0.4% to

0. 7% Mn.   The starting analysis of the individual heats is given in
Appendix I, Data.

The converter was now turned upright, and a safety
catch basin which fitted the contour of the converter and an overhead
protective shield were put in place.   While these changes were being
made the lance was lowered to the proper blowing height.

Figure 12 is a detailed drawing of the oxygen lance with the
0. 316 inch diameter nozzle.   The other lance used in this investiga-
tion was the same except the nozzle diameter was 0. 162 inches.
Both lances were fabricated   of   copper and all joints were brazed.
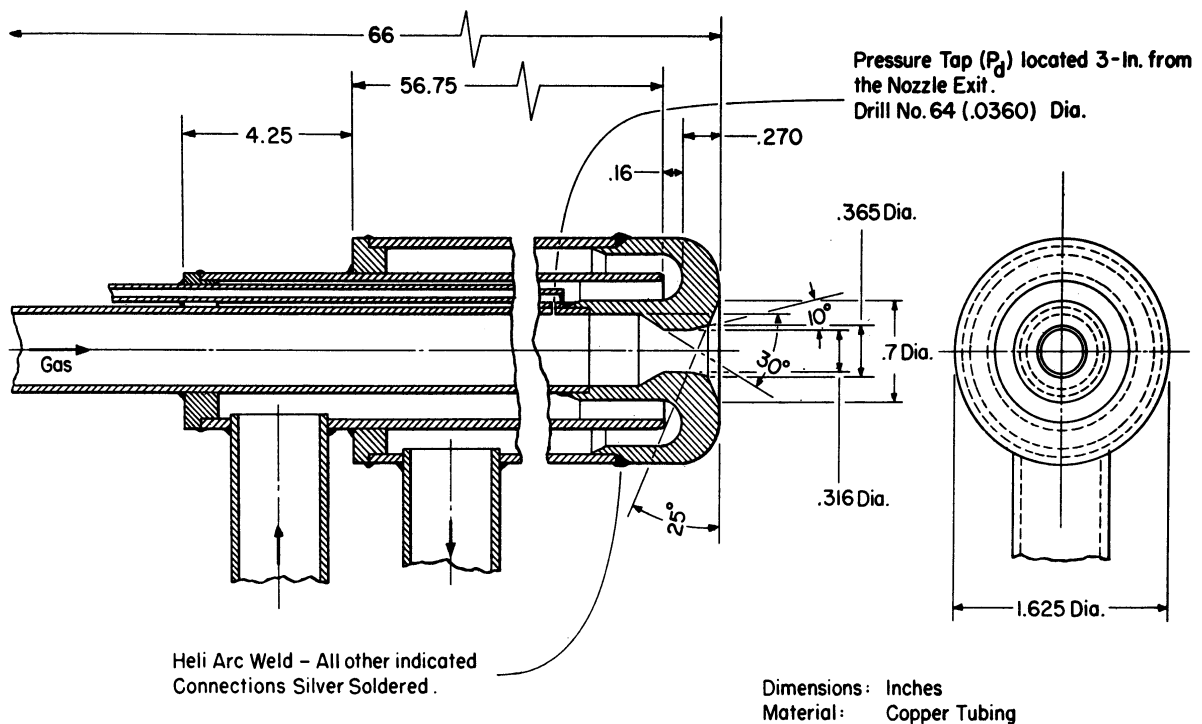
Fig. 12.   Detail Drawing of the Lance with the
0. 316 inch Diameter Nozzle.

The effects on converter phenomona of the individual variables which make up a set of blowing conditions were determined by varying each of them individually. In Table VI the blowing practices used in this investigation are tabulated along with sampling locations and the particular variables being studied.

Table VI

Compilation of Blowing Conditions

(1) Blowing Height (in.)	(2) Bath Depth (in.)	(3) Blowing Pressure (psig.)	(4) Nozzle Diameter (in.)	Sample Heights Above Bottom * (in.)	Variable Studied
7	6	20	0.316	6, 5, 3, 1	Standard
21	6	20	0.316	7, 5, 3, 1	(1)
7	10	20	0.316	10, 8, 5, 2	(2)
7	10	35	0.316	10, 8, 5, 2	(3)
7	6	25	0.162	6, 5, 3, 1	(4)

* Heights are measured to sampler centerline. Sample location is 1/2 inch above the centerline. In all cases samples were taken on a radius 1, 3-1/2, and 6 inches from the wall of the converter. The bath radius was 7-1/2 inches.

The significant point of Table VI is that metal samples were usually successfully taken only 1/2 inch above the level of a quiet bath; however, when a 21 inch blowing height was used metal samples were taken 1-1/2 inches above the level of a quiet bath. Slag samples were taken 2 inches and 5 inches above the level of a quiet bath.

c) Making the Run

The run time was begun when the oxygen was turned on. The six bags of flux were added at 0, 5, 10, 15, 20, and 25 seconds. The two bags containing fluorspar were added at 0 and 5 seconds. Flux was added with a long-handled trough as shown in Figure 13. Also evident in Figure 13 are the safety catch basin and the shield.
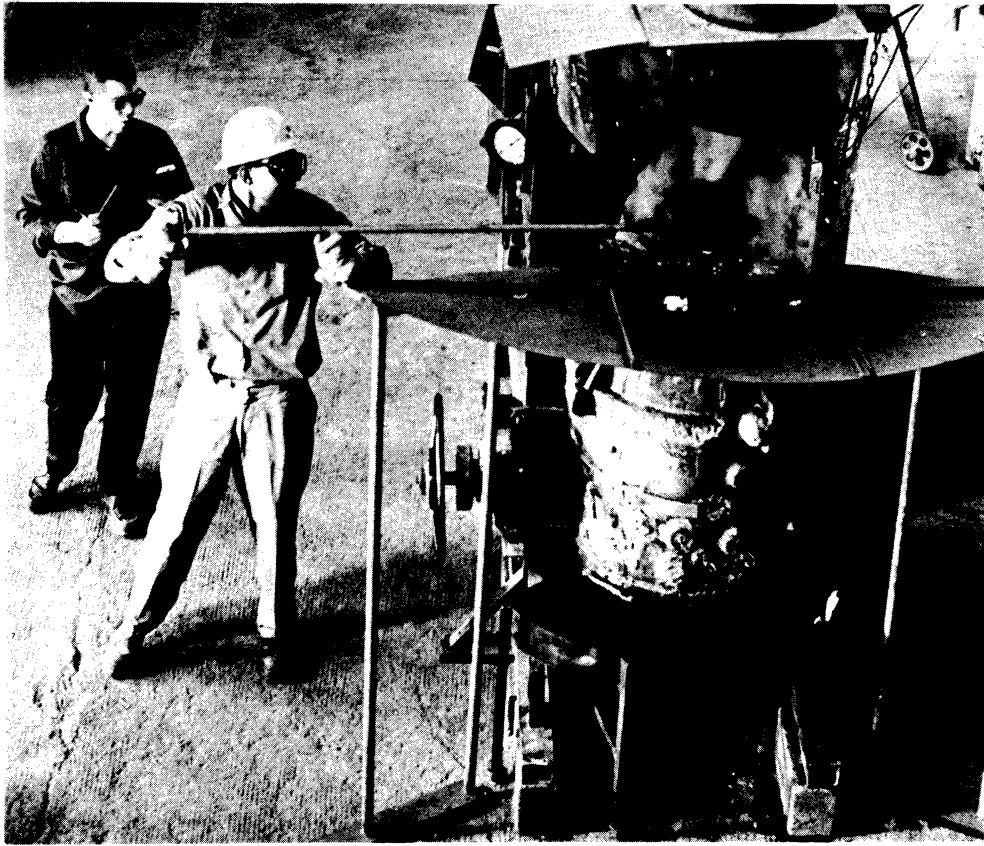
Fig. 13.   Addition of Flux During a Run.

Metal samples were taken by piercing the specially prepared sampling locations with the pointed end of the sampler and continuing to push the sampler into the bath until the locating collar stopped motion.   After the sampler was in place the fire-clay cone was rammed around the sampler.   This procedure is shown in Figure 14.   Slag samples were taken through holes higher in the vessel.   In this case the sampler was retrieved at once and the hole packed with clay. Sampling times were recorded to $\pm$ 1 second.   When all the samples were taken and temperature data collected the O_2 was turned off and the total blowing time recorded.

After the blow the safety catch basin and shield were removed and a pig mold positioned.   Before tapping the converter a spoon sample of slag, sample S-2, was taken and another chill cast metal sample, sample M-2, poured.
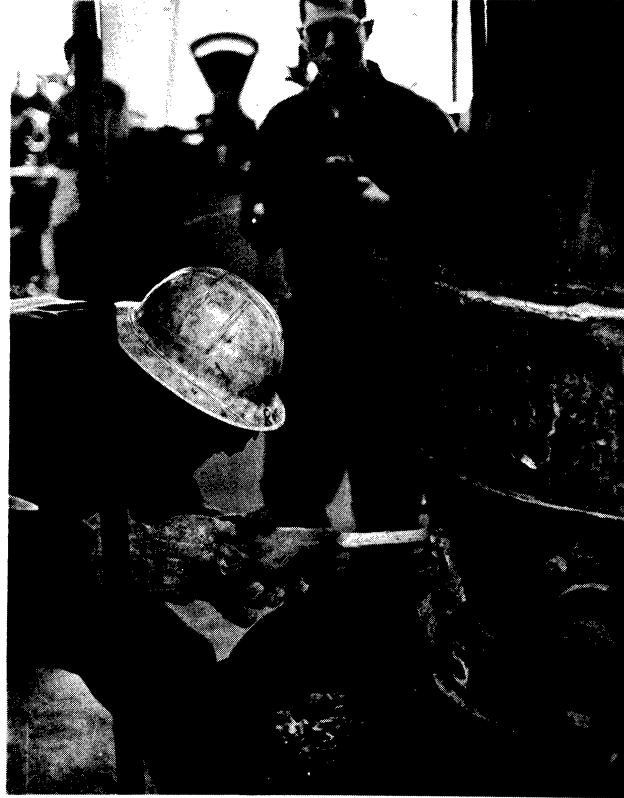
Fig. 14. Insertion of a Metal Sampler Probe.

After a run the individual samples were collected and identified. The metal samples were analyzed for P, Si, C, and Mn and the slags for P_2O_5, CaO, SiO_2, MgO, MnO, Al_2O_3, and in most cases FeO and Fe_2O_3 and spot checked for ZrO_2.

d) Special Run

A special run was made to determine the amount and size distribution of the droplets thrown up by the oxygen lance under various blowing conditions. Figure 15 shows the collecting device. Prior to use, it was filled with a fire-clay slurry and covered. It was inserted through a 2 inch by 7 inch hole in the converter wall which was 2 inches above the surface of a quiet metal bath. The lance was set at a predetermined height and the O_2 jet turned up to a predetermined blowing pressure. The collector was uncovered for 5 seconds, recovered and removed and the jet turned off.
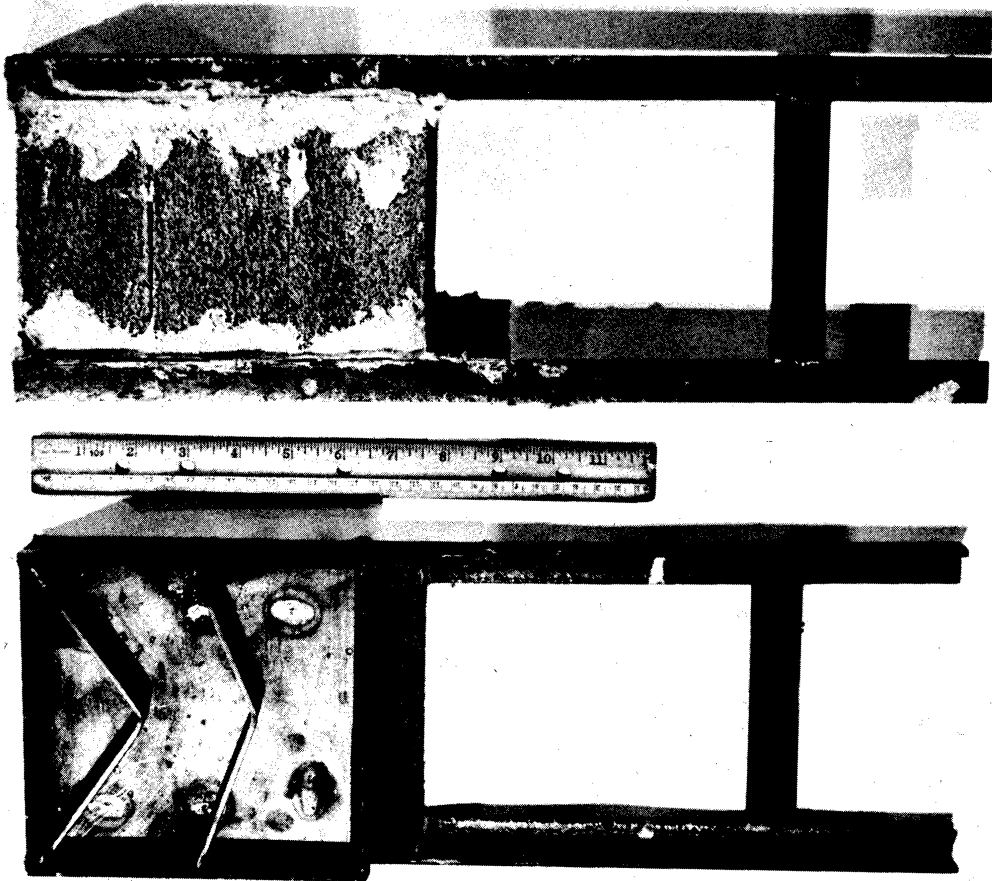
Fig. 15.   Droplet Collecting Trays.

The collected droplets were weighed, sized and in one case examined metallographically to allow an estimate of the carbon content.

Results and Discussion

The results are reported under the following headings:
1) General Features, 2) Phosphorus, 3) Silicon, 4) Carbon,
5) Manganese, 6) Temperature, 7) Slag, 8) Special Heats,
9) Summary of Results, and 10) Mathematical Analyses.

1) General Features

Before describing the specific effects of the various blowing
conditions on the composition and temperature, the general effects
of the different blowing conditions upon the melts should be reviewed
as background.

a)   Standard Conditions

The standard experimental conditions (6 inch bath depth,
7 inch blowing height, 20 psig. blowing pressure and 0.316 inch lance)
were scaled from commercial practice. The 0.4 bath depth to bath
diameter ratio and the deep jet penetration were taken directly from
commercial practice. The oxygen rate was 380 scfm. per ton which
is higher than that used commercially; however, total oxygen
consumption of 1900 cubic feet per ton is the same as commercial
practice.

These standard conditions resulted in slight throw out of slag
and metal droplets throughout the heat. Metal samples could be
taken no higher than 1/2 inch above the level of the quiet bath. At
greater heights only slag was obtained (with a few metal droplets).
Experimental runs were complete after 5-1/2 minutes of blowing
(5: 30) at which time the final slag sample had the viscosity of thick
oil.

39

b) Effect of Blowing Height

The experimental conditions designed to determine the effect of blowing height (6 inch bath depth, 21 inch blowing height, 20 psig. blowing pressure and 0.316 inch diameter lance) produced a substantially different appearance. The early portion of the heat was marked by little ejection of slag or metal droplets; however, after approximately 5 minutes and 20 seconds blowing time (5:20) a foamy slag overflowed from the mouth of the converter. Metal samples were successfully taken 1-1/2 inches above the level of the quiet bath. Runs were halted when the slag overflowed and delays of up to 3 minutes were required before the converter could be safely approached. The final slag sample was gas-filled and very thick.

c) Effect of Bath Depth

When the bath depth was increased to 10 inches, the runs appeared similar to those conducted under standard conditions. Metal samples were taken 1/2 inch above the level of a quiet bath. The runs required 8:30 and the final slag sample was thick and dry.

The effect of blowing pressure was determined by modifying the condition above with a 35 psig. blowing pressure (10 inch bath depth, 7 inch blowing height, 35 psig. blowing pressure and 0.316 inch diameter lance). This change increased metal and slag ejection to the extent that the converter operation was quite violent. Because of this a limited number of samples were taken. Metal samples were successfully taken 1/2 inch above the level of a quiet bath. The run was completed in 5:30. The final slag sample is fluid and very flat.

d) Effect of Nozzle Diameter

The heats with a smaller nozzle diameter (0.162 inches) produced some difficulty in maintaining adequate temperature. The ejection of metal and slag droplets was slight. The flux formed a solid crust on the bath surface completely shielding it from the oxygen jet. This crust had to be manually broken up to continue the heat. Metal samples were taken 1/2 inch above the level of a quiet bath. Heats were run for as long as 13:38 at which time the slag was very thick.

To summarize these observations, the amount of metal ejected from the converter was generally proportional to the depth of jet penetration except in the case of an increased blowing height when slag overflowed the converter.

The uppermost metal samples were usually taken 1/2 inch above the level of a quiet bath. The one exception was the 21 inch blowing height condition where the samples were taken 1-1/2 inches above the level of a quiet bath. While there were some differences in bath expansion for different blowing conditions it is significant to note that the bath expansion was usually 1/2 inch, 10%, and in the exceptional case reached a maximum of 25%.

In all cases, the final slag samples had a medium to heavy consistency.

The slag sampling holes were placed 1-1/2 inches above the uppermost metal sampling holes when the converter was rammed. During a run little metal flowed out of these slag sampling holes when they were opened; therefore, at points only 1-1/2 inches from the metal bath the emulsion of slag and substantial amounts of metal (spoken of by most investigators) is not present in the converter.

With these general features produced by the various blowing conditions in mind, the chemical and thermal gradients of a converter bath and the composition of converter slags can now be described.

2) Phosphorus

a) Standard Conditions

The phosphorus content of the bath under standard experimental conditions is shown in Figure 16 as a function of time and bath location. The points on the individual plots are data points.* The origin of each individual plot is located at a sampling location. For example, the origin of the uppermost, left-hand plot in Figure 16 is located 6-1/2 inches above the bottom and 1 inch from the wall. This is sampling location 61. In designation "61" the "6" indicates approximate height and "1" the approximate distance from the wall. Similarly, the origins of the other two plots 6-1/2 inches above the bottom are 3-1/2 inches and 6 inches from the wall, sampling locations 63 and 66 respectively. The other rows of plots are 5-1/2 inches, 3-1/2 inches, and 1-1/2 inches above the bottom.

With standard experimental conditions the greatest dephosphorization is found at the top of the bath, 0.02% P at 4:15, and the least at the bottom of the bath 0.10% P at 4:30.

The maximum dephosphorization rate is 0.12% P/min. at the top of the bath near the wall at 1:00 while 0.06% P/min. is found at the bottom of the bath at 2:30.

The variations in dephosphorization lead to substantial gradients as shown in Figure 17. The range of phosphorus is 0.14% to 0.20% from the top to the bottom of the bath at 1:00. The constant composition curves are all nearly horizontal. The gradient in phosphorus content is steepest at the top of the bath (0.03% P/inch) and very slight in the lower half of the bath.

*The data are tabulated in Appendix I, Data.

IN. ABOVE BOTTOM

Fig. 16. % Phosphorus Versus Blowing Time for all Sampling Locations (6 in. bath, 7 in. bl. ht., 20 psig., 0.316 in. nozzle).
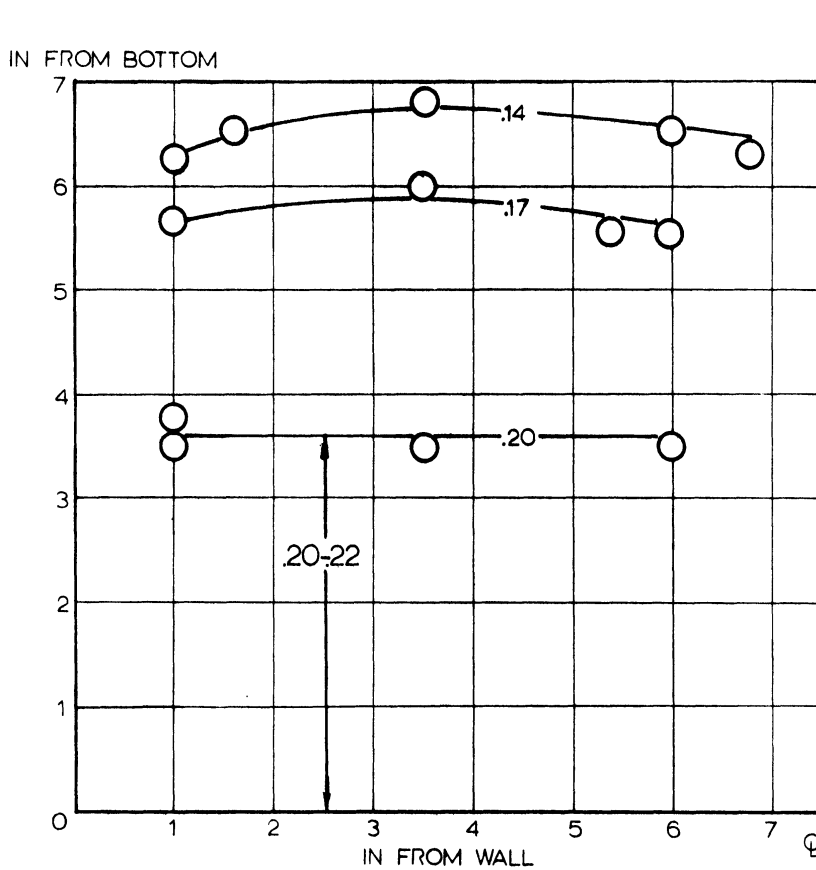
Fig. 17. Constant % Phosphorus Versus Bath Location at 1 Minute Blowing Time
(6 in. bath, 7 in. bl. ht., 20 psig., 0.316 in. nozzle).

b) Effect of Blowing Height

Increasing the blowing height from 7 inches to 21 inches produces the phosphorus pattern shown in Figure 18. The top of the bath dephosphorized earlier and to a greater extent than the bottom, 0. 05% P versus 0. 12% P at 3: 00. Maximum dephosphorization rates of 0. 15% P/min. are found throughout the bath. The difference in phosphorus content is due to the later initiation of rapid dephosphorization lower in the bath.

The phosphorus gradients at 1: 00 are shown in Figure 19. The range of phosphorus content in the bath is 0. 17% to 0. 30% P, top to bottom. The constant composition lines curve upward near the wall of the converter. The top of the bath is 50% dephosphorized while the bottom of the bath is virtually unrefined.

IN ABOVE BOTTOM

IN. FROM WALL

Fig. 18. % Phosphorus Versus Blowing Time for all Sampling
Locations (6 in. bath, 21 in. bl. ht., 20 psig., 0.316 in. nozzle).
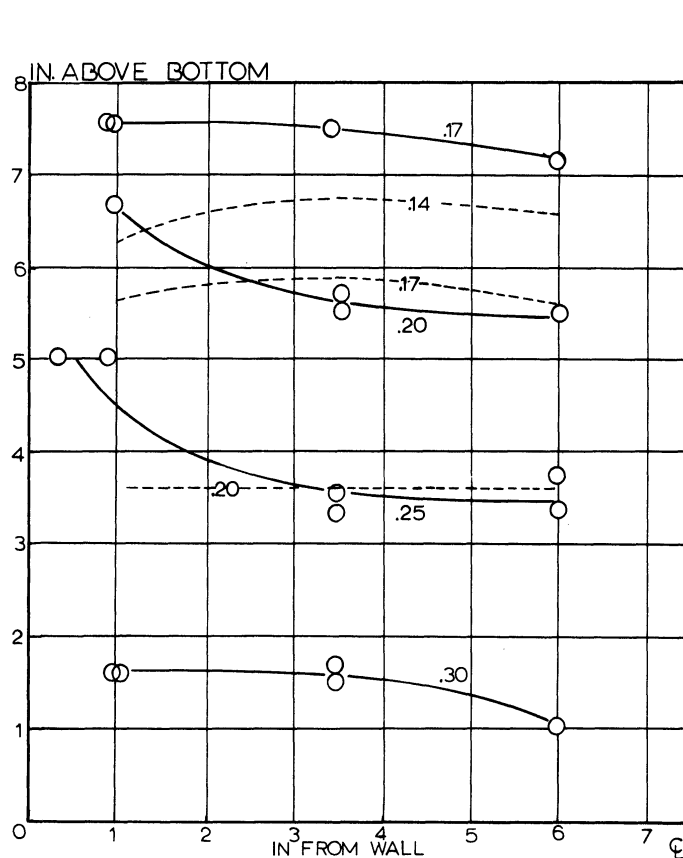
Fig. 19. Constant % Phosphorus Versus Bath Location at 1 Minute Blowing Time (6 in. bath, 21 in. bl. ht., 20 psig., 0.316 in. nozzle).

The vertical phosphorus gradient is generally smallest near the top of the bath and nearly constant below the 6 inch depth at 0.025% P/inch. At the top of the bath near the wall the gradient is increased to 0.03% P/inch.

The effect of blowing height on the dephosphorization is clearly shown when Figures 16 and 18 are compared. At all sampling locations throughout the heat the phosphorus content of the bath blown under standard conditions is lower than that of the bath blown with a 21 inch blowing height. The dotted lines on Figure 19 are standard condition data emphasizing the difference in the two blowing practices. The effect of the deep penetration is especially apparent near the bottom. The upward trend of the constant composition lines with the 21 inch blowing height is in direct contrast to the nearly horizontal lines resulting from the 7 inch blowing height. The differences in phosphorus gradients for these two conditions are

caused solely by increased blowing height as all other conditions are constant.

c) Effect of Bath Depth

In Figure 20 the solid points and curve show the effect of increasing the bath depth to 10 inches (400 lb. of hot metal). Initially rapid dephosphorization is found at the bath surface followed by slow dephosphorization. The major portion of the bath was slowly dephosphorized. This system does not produce a substantial gradient because so little phosphorus is removed.

The data points drawn as open circles in Figure 20 show the effect of increasing blowing pressure to 35 psig. with a 10 inch bath depth. The bath is dephosphorized rapidly and extensively, e. g. , 0. 03% P at 5: 22 at sample location 51.

The rate of oxygen input with 20 psig. and a 10 inch bath depth is 0. 12 scfm/lb. while at 35 psig. the rate is 0. 17 scfm. /lb. or a 40% increase. Increased pressure increases the jet penetration from 4-1/2 to 7-1/2 inches. As was noted earlier the slag on the 10 inch bath blown at 20 psig. was dry and very thick at 8: 30 which accounts for the poor dephosphorization with these conditions. Increasing the blowing pressure to 35 psig. produces a fluid slag at 5: 30. The dotted lines in Figure 20 in the 10-1/2 inch row and the 5-1/2 inch row are data from the standard conditions at the 6-1/2 inch and 5-1/2 inch sampling heights respectively. In the former case the sampling heights are the same distance below the slag-metal interface while in the latter case the sampling heights are the same distance above the bottom.

Regardless of whether the reaction location (slag-metal interface) or the bottom of the bath is used as a level the data show that at corresponding locations the rate and extent of dephosphorization

%P

ALL DATA IN THE TOP ROW IS EQUIDISTANT FROM THE SLAG

.3
.2
.1

11

2 4 6 8

IN. ABOVE BOTTOM

10

8

6

4

2

2 4 6

IN. FROM WALL

Fig. 20. % Phosphorus Versus Blowing Time for all Sampling
Locations (10 in. bath, 7 in. bl. ht., 20 psig., 0.316 in. nozzle -
solid lines) and (10 in. bath, 7 in. bl. ht., 35 psig., 0.316 in.
nozzle - open points).

is greater with the standard 6 inch bath than with a 10 inch bath and 20 psig. blowing pressure. Further, the standard data correspond very closely with the data from the heats blown at 35 psig. In other words, as bath depth is increased, penetration and oxygen delivery rate should be correspondingly increased.

d) Effect of Nozzle Dimater

The effect of decreasing nozzle diameter to 0.162 inches and using 25 psig. blowing pressure is shown in Figure 21. The time scale has been changed on the plots to accommodate the longer blowing time. The bath is dephosphorized at all sampling locations with the usual pattern of most rapid and extensive dephosphorization taking place at the bath surface. Dephosphorization rate is 0.03% P/minute at the surface and as low as 0.01% P/minute at the bottom of the bath at the initiation of blowing.

The dotted lines in Figure 21 represent comparative data from the standard conditions. The oxygen input rate with the 0.162 inch diameter nozzle is 30% of the rate under standard conditions. As would be expected, decreasing the oxygen input rate has decreased the rate of dephosphorization. As will be seen later this heat was not fully decarburized in 13:38 so the maximum dephos-phorization is not known.

Summary - Dephosphorization

Under all conditions a phosphorus gradient is established with the lowest phosphorus in the upper layers of the bath. The difference in phosphorus content from the top to the bottom of the bath is least in the cases with deep penetration, e.g., standard conditions and the 10 inch bath with 35 psig.. The high lance, deep bath and small nozzle conditions produce good surface dephosphor-ization but are less effective in the lower portions of the bath.
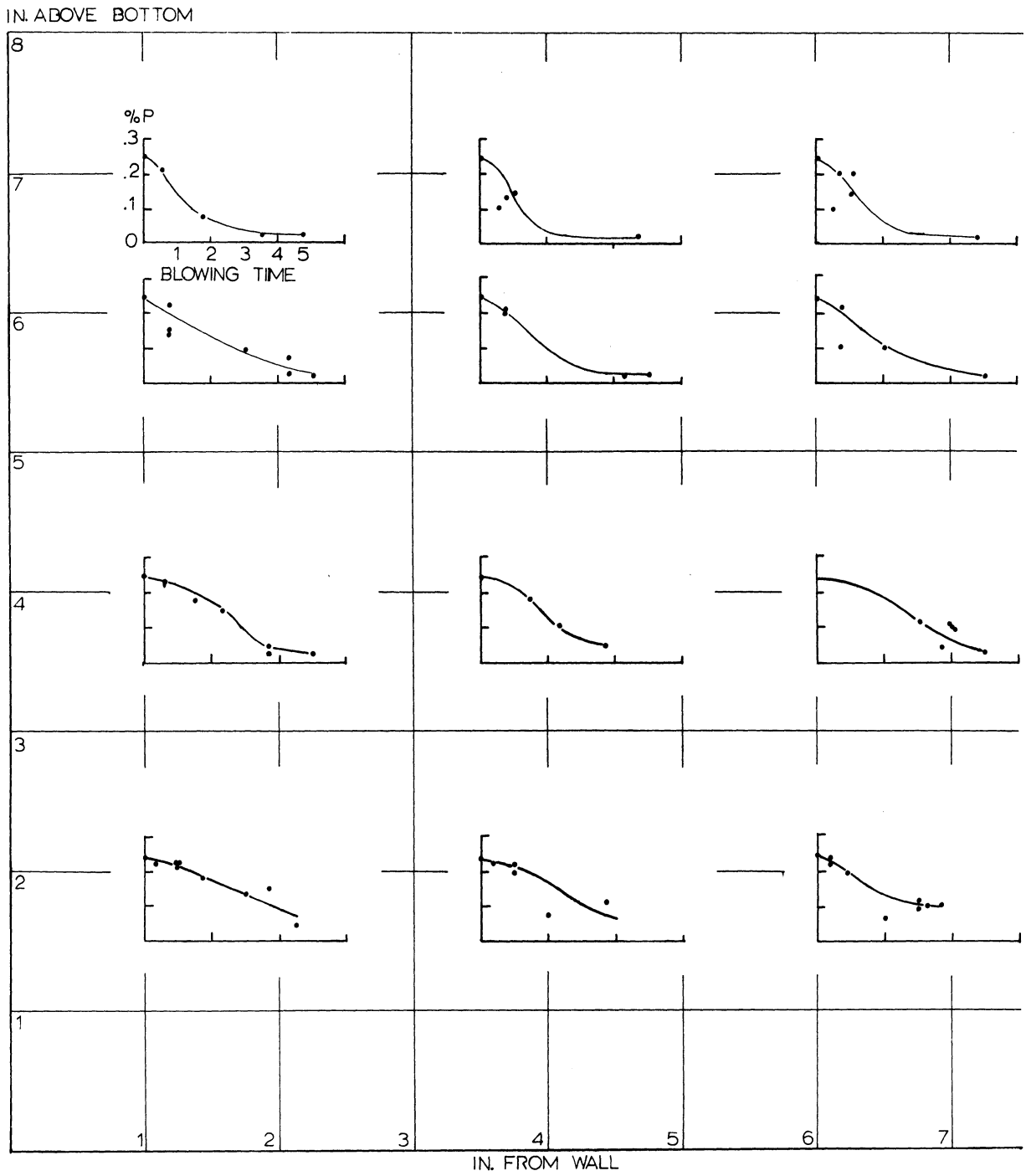
Fig. 21. % Phosphorus Versus Blowing Time for all Sampling Locations (6 in. bath, 7 in. bl. ht. 25 psig., 0.162 in. nozzle).

3) <u>Silicon</u>

a) Standard Conditions

The silicon content of the bath blown with standard conditions is plotted in Figure 22 as a function of blowing time and location in the bath using the same locations as for phosphorus. The silicon is oxidized most rapidly at the initiation of blowing and finally decreases to less than 0.05% at all sampling locations. At the iniation of blowing the rate of silicon removal at the top and bottom of the bath are respectively (1.5%/min.) and (0.5%/min.).

Gradients of silicon are established in the bath by these differences in the rate of silicon oxidation as shown in Figure 23. The composition lines are lowest in the bath near the center and then move upward and become horizontal as the lines approach the wall. After 0:30 the silicon content has been reduced by 2/3 at the bottom of the bath and at the top of the bath the metal is virtually silicon free (<0.05% Si). The gradient of silicon content is steepest at the top of the converter being 0.10% Si/inch and is reduced to 0.02% Si/inch between the 5-1/2 and 1-1/2 inch bath depths.

b) Effect of Blowing Height

A substantial reduction in the rate of silicon oxidation is caused by increasing the blowing height to 21 inches as shown in Figure 24. The silicon content at the bath surface is reduced at a rate of 0.5% Si/min or 1/3 the rate found when the blowing height is 7 inches. At the bottom of the bath the rate is 0.15% Si/min. compared with 0.5%/min for the 7 inch lance height. Maximum silicon oxidation rates are found at the initiation of blowing. The silicon content is reduced to less than 0.05% Si at the top of the bath and to 0.06% Si 3-1/2 inches above the bottom of the bath at 5:30.

IN. ABOVE BOTTOM
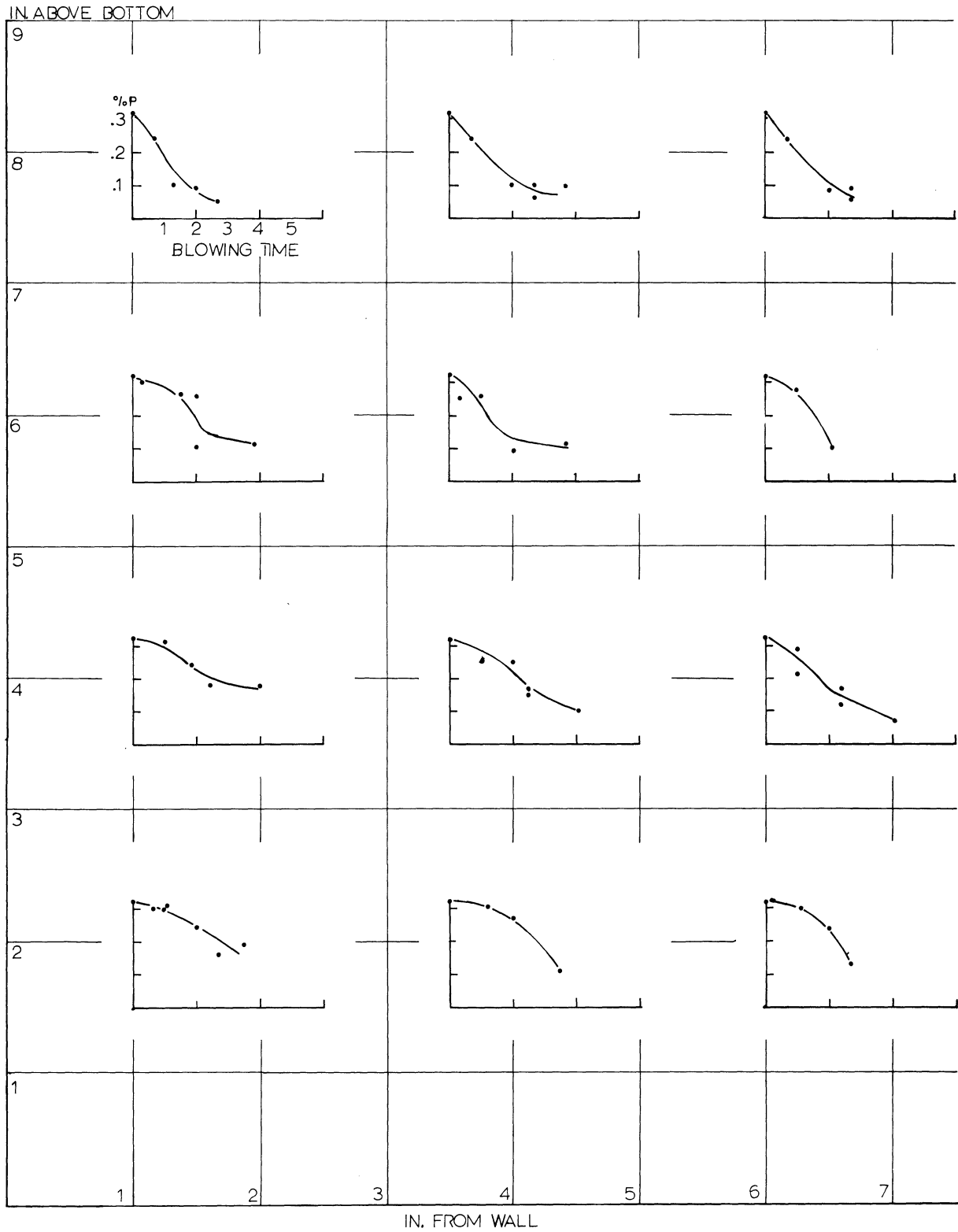
Fig. 22.   % Silicon Versus Blowing Time for all Sampling Locations
(6 in. bath, 7 in. bl. ht., 20 psig., 0.316 in. nozzle).

Fig. 23. Constant % Silicon Versus Bath Location at 1/2 Minute Blowing Time (6 in. bath, 7 in. bl. ht. , 20 psig. , 0.316 in. nozzle).

Fig. 24. % Silicon Versus Blowing Time for all Sampling Locations (6 in. bath, 21 in. bl. ht., 20 psig., 0.316 in. nozzle).

Constant composition lines at 0:30 are shown in Figure 25.
The lines higher in the bath have a definite upward curve from the
center to the edge of the bath. Lower in the bath the 0.5% Si line
is horizontal. The bottom 3 inches of the bath are at nearly constant
composition averaging 0.54% Si or 90% of starting silicon. At the
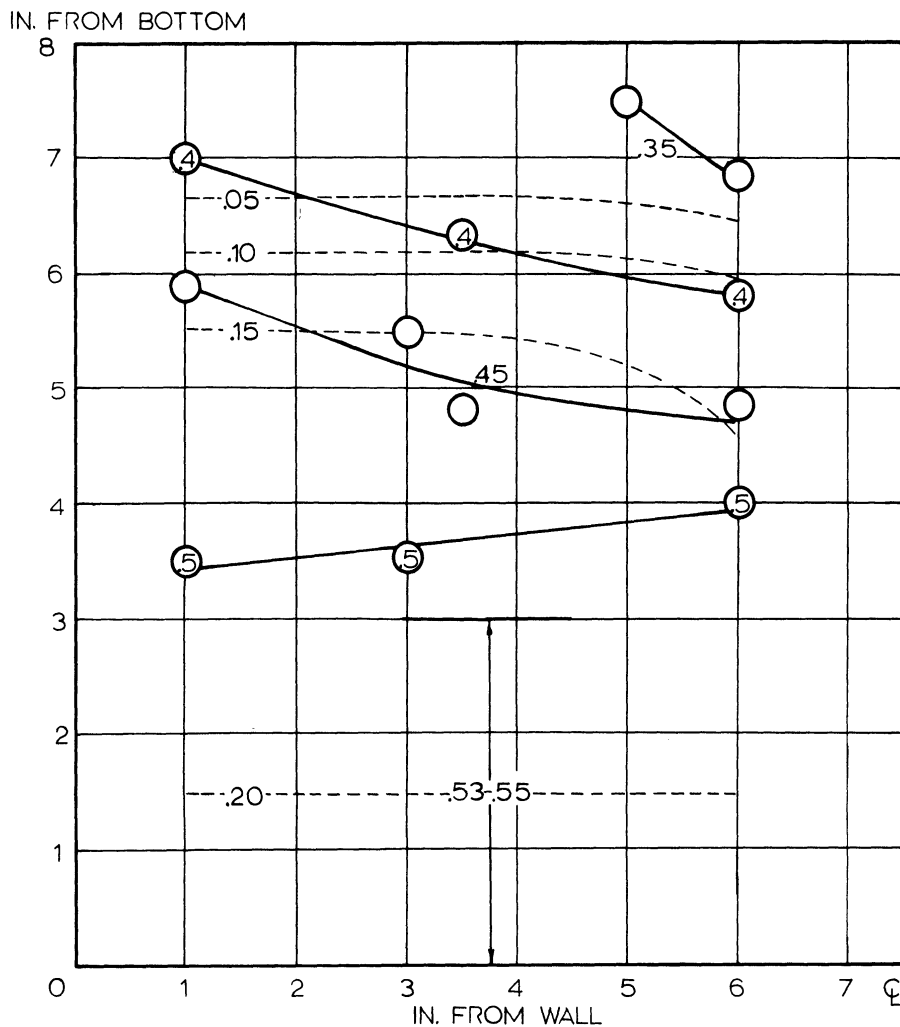
Fig. 25. Constant % Silicon Versus Bath Location at 1/2 Minute Blowing Time
(6 in. bath, 21 in. bl. ht., 20 psig., 0.316 in. nozzle).

centerline, high in the bath the silicon content is reduced to 0.30%
or 50% of starting silicon. The silicon gradient is 0.05% Si/inch
in the uppermost 4 inches of the bath. Below this there is no
appreciable silicon gradient. The dotted lines in Figure 25 are

standard condition data. The difference in rates of silicon oxidation is shown clearly by comparison. Silicon has been removed three times as rapidly when the bath was blown from 7 inches.

c) Effect of Bath Depth

In Figure 26 the solid curves and points are the % Si-time relationships for the sampling locations in a 10 inch bath blown at 20 psig. The silicon at the bath surface is oxidized very rapidly to 0.03% Si after 0:15 blowing time yielding a silicon oxidation rate of 2.3% Si/min. at the start of the blow. The silicon content at the bottom of the bath is reduced to 0.03% after 4:00. The initial rate of silicon oxidation is 0.15% Si/min. at the bottom.

The open circles in Figure 26 are % Si versus time data from heats run with a 10 inch bath blown at 35 psig. Silicon content is reduced to 0.01% at the top of the bath at 5:15, and to less than 0.05% Si at location 51 at 5:22.

Early in the run silicon at the bath surface is more rapidly oxidized when 20 psig. blowing pressure is used than when 35 psig. blowing pressure is used. Near the bottom of the bath (location 21) the opposite is true.

The dotted lines in Figure 26 at the bath surface are data from the standard runs. Silicon at the bath surface of the 10 inch bath blown at 20 psig. is oxidized more rapidly than at the surface of baths blown under standard conditions. Surface oxidation in 10 inch baths blown at 35 psig. is somewhat slower than under standard conditions.

The dotted lines in the 5-1/2 inch row of Figure 26 show, as expected, that at the same distance from the bottom of the converter silicon in the 6 inch bath is oxidized more rapidly than silicon in a 10 inch bath when both are blown at 20 psig.
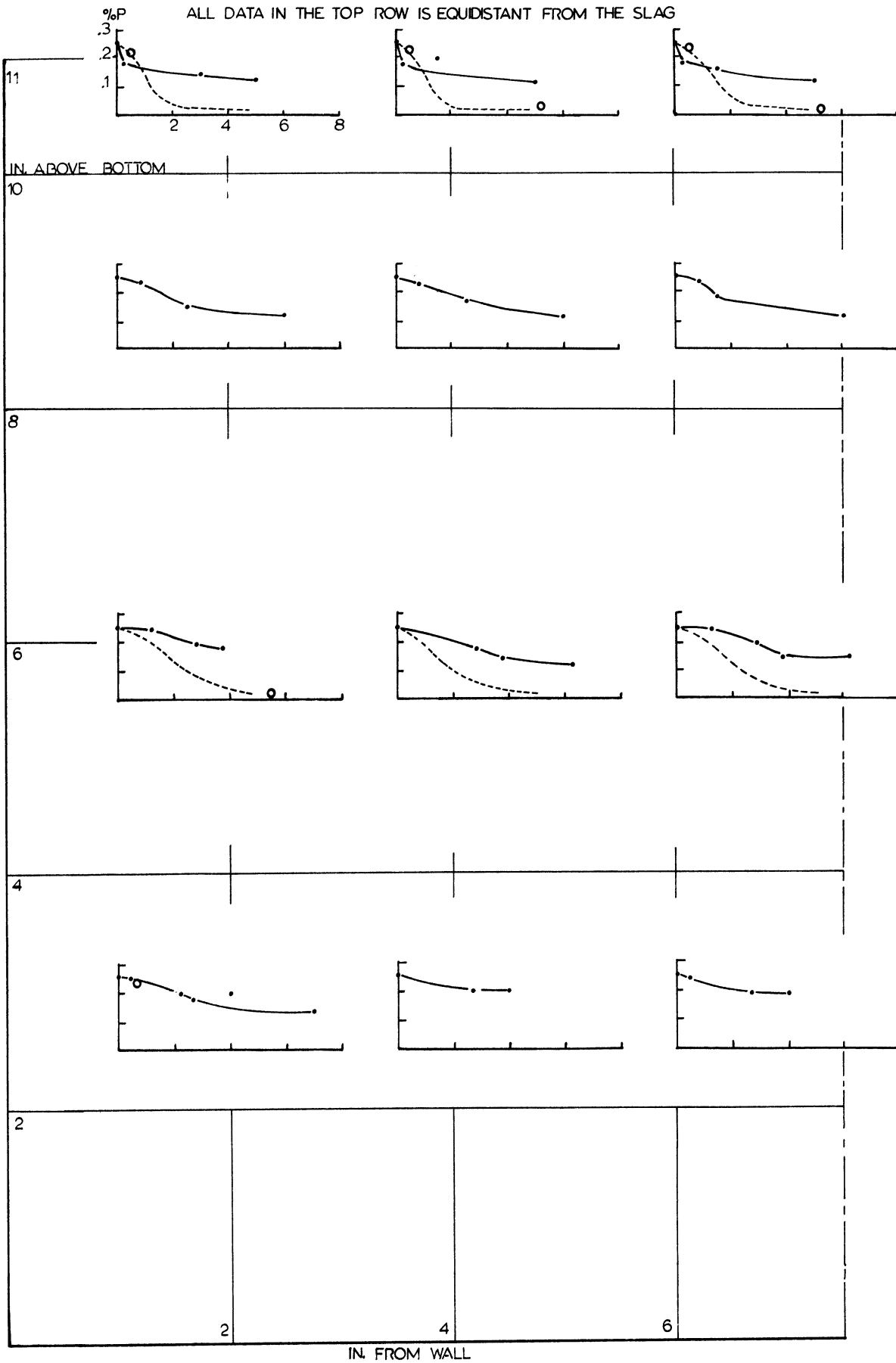
Fig. 26.   % Silicon Versus Blowing Time for all Sampling Locations
(10 in. bath, 7 in. bl. ht., 20 psig., 0.316 in. nozzle - solid line)
and (10 in. bath, 7 in. bl. ht., 35 psig., 0.316 in. nozzle - open
points).

d)   Effect of Nozzle Diameter

The % Si-time relationships for the heats blown at 25 psig. with a 0.162 inch nozzle are shown in Figure 27. The usual pattern of most rapid silicon oxidation at the bath surface is apparent. The surface silicon content is reduced to 0.01% at 11:30 with an initial rate of 0.4% Si/min.. The silicon content at the bottom of the bath is reduced to 0.04% Si at 10:00 with an initial rate of 0.1% Si/min..

The dotted lines on the plots are data from standard runs. The slower rate of silicon oxidation with the smaller lance is clearly apparent. For example, the blowing time required to reach 0.05% Si at sample location 53 is 2:00 for standard conditions as opposed to 6:00 when the small nozzle is used.

Summary - Silicon Oxidation

In contrast to phosphorus removal, silicon removal depends only on contact with oxygen, either as gaseous or dissolved oxygen or as iron oxide. Accordingly, silicon oxidation is completed under all blowing conditions to below 0.05% Si in the bath. As expected, the rate is roughly proportional to the oxygen input; however, with shallow jet penetration the rate is slower at the bottom of the vessel. Apparently when the silicon is oxidized at the surface in this case, the oxygen reacts with other elements in this region. By contrast, with deep penetration and stirring by the jet as in standard conditions, the silicon is oxidized throughout the bath giving a smaller gradient.

In all cases the most rapid rate of silicon removal is at the start of blowing because the silicon is the most reactive element in the bath. As the silicon content decreases its activity falls and phosphorus and carbon can react with more of the oxygen.
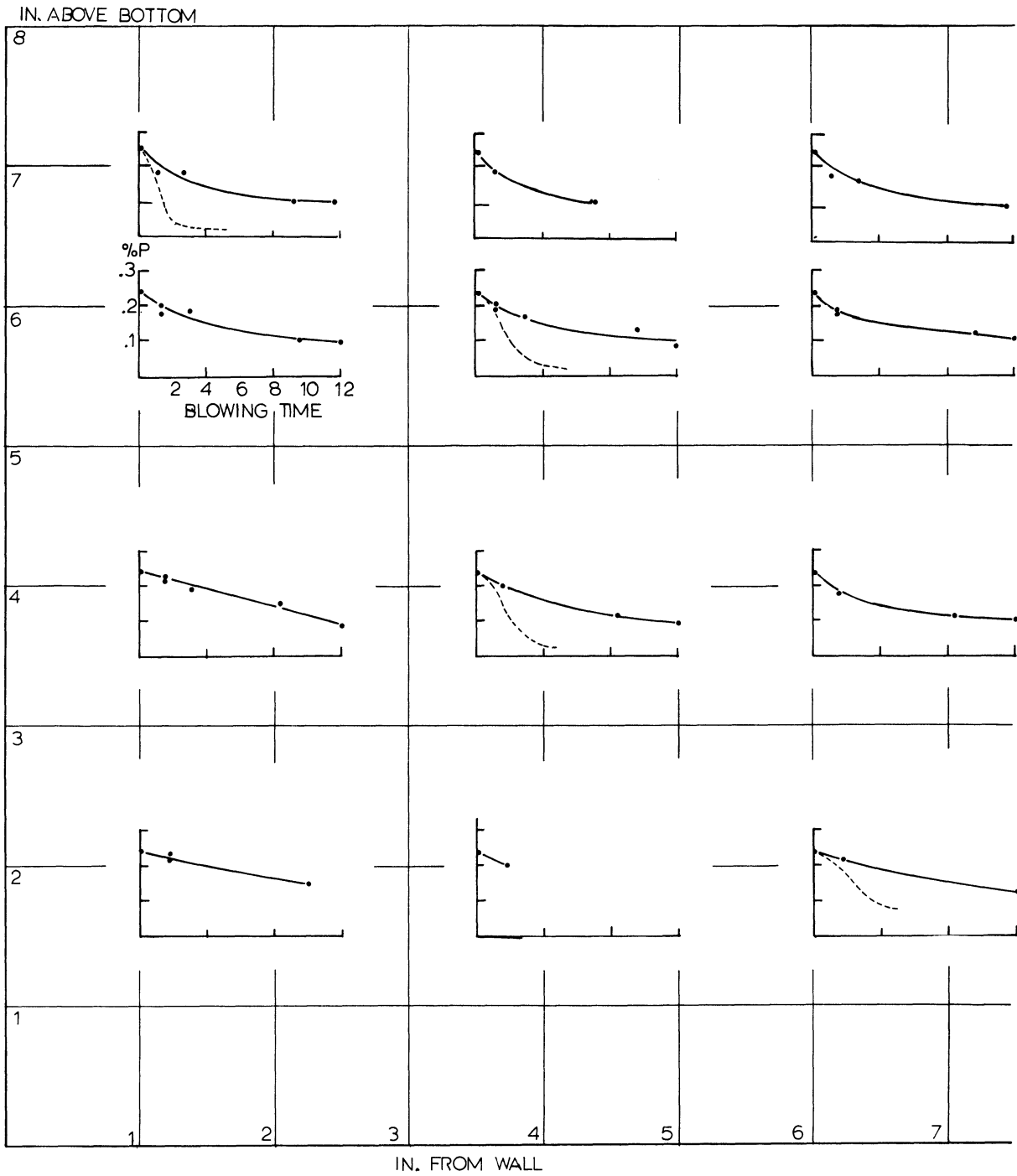
Fig. 27. % Silicon Versus Blowing Time for all Sampling Locations (6 in. bath, 7 in. bl. ht. , 25 psig. , 0.162 in. nozzle).

4) Carbon

a) Standard Conditions

The carbon content-time plots for standard experimental conditions are shown in Figure 28. Decarburization is most rapid at the bath surface. Carbon content is reduced to 0.04% C at 4:45. The rate of surface decarubrization is 1.1% C/min. after 0:30. Decarburization is slowest at the bottom of the bath. A minimum carbon content of 0.1% C was found at the bottom corner at 4:30. The maximum decarburization rate at the bottom of the bath is 0.8% C/min. at 3:00.

The differences in the time of initiation and the rate of maximum decarburization produce substantial gradients of carbon in the bath. Constant % C lines are shown for standard blowing conditions in Figure 29. The range of carbon content is 1.0 to 2.6% C at 2:30. This gradient is particularly interesting because at 2:30 the entire bath is undergoing rapid decarburization which is alleged by some authors to minimize chemical gradients by the boiling action. In the upper portion of the bath the constant composition lines are horizontal while lower in the bath the lines curve downward from the edge of the bath to the center. The line representing 2.6% C is nearly vertical. The maximum carbon gradient is 1% C/inch at the surface of the bath.

b) Effect of Blowing Height

The % C-time relationship for a bath blown from 21 inches is shown in Figure 30. Of greatest significance is the reduced decarburization. The minimum carbon content of the bath is 1.98% C at the centerline at the top of the bath after 5:25 compared to 0.04% C at the same location and time for standard conditions. The maximum rate of decarburization at the top of the bath is 0.3% C/min. at
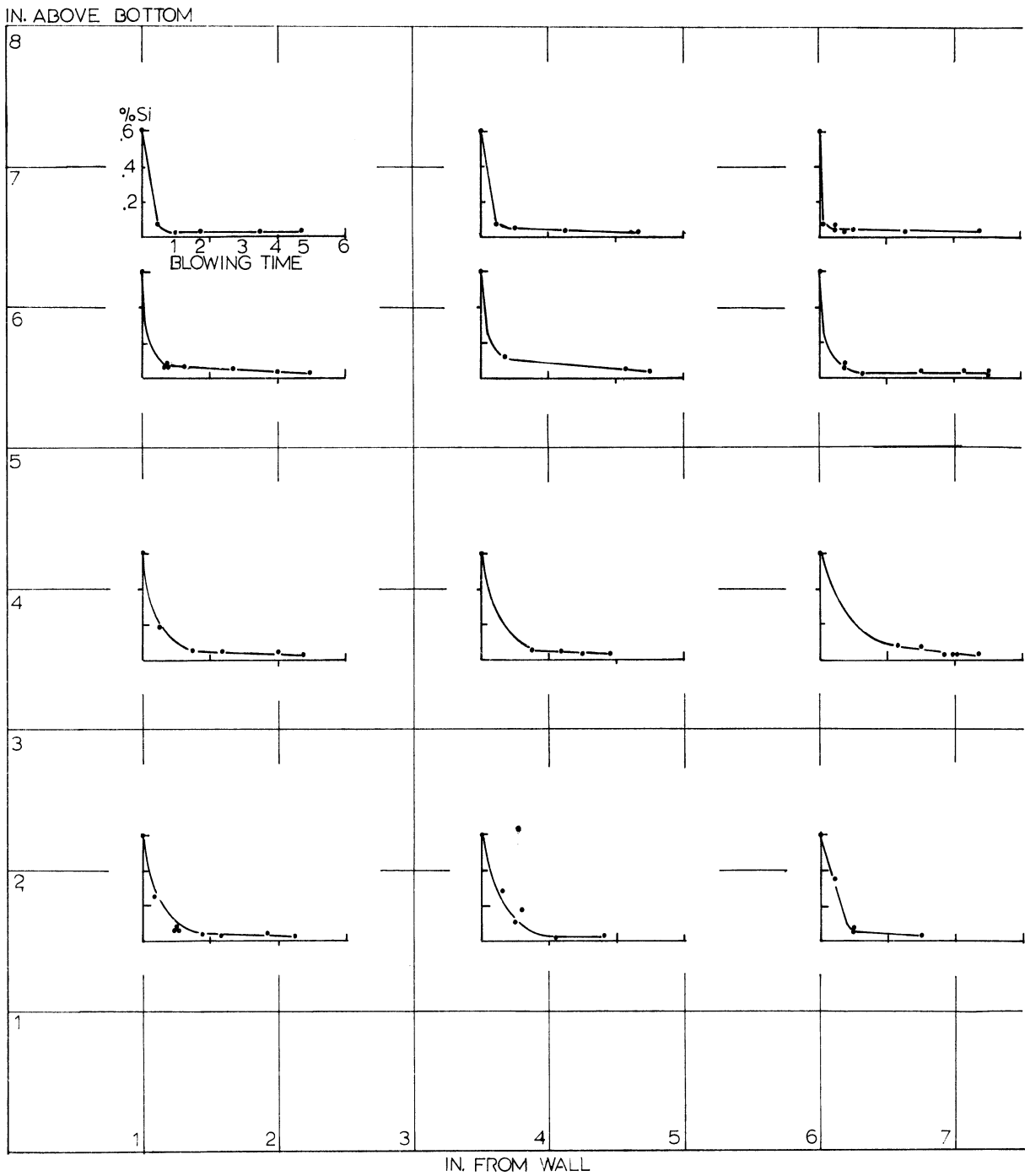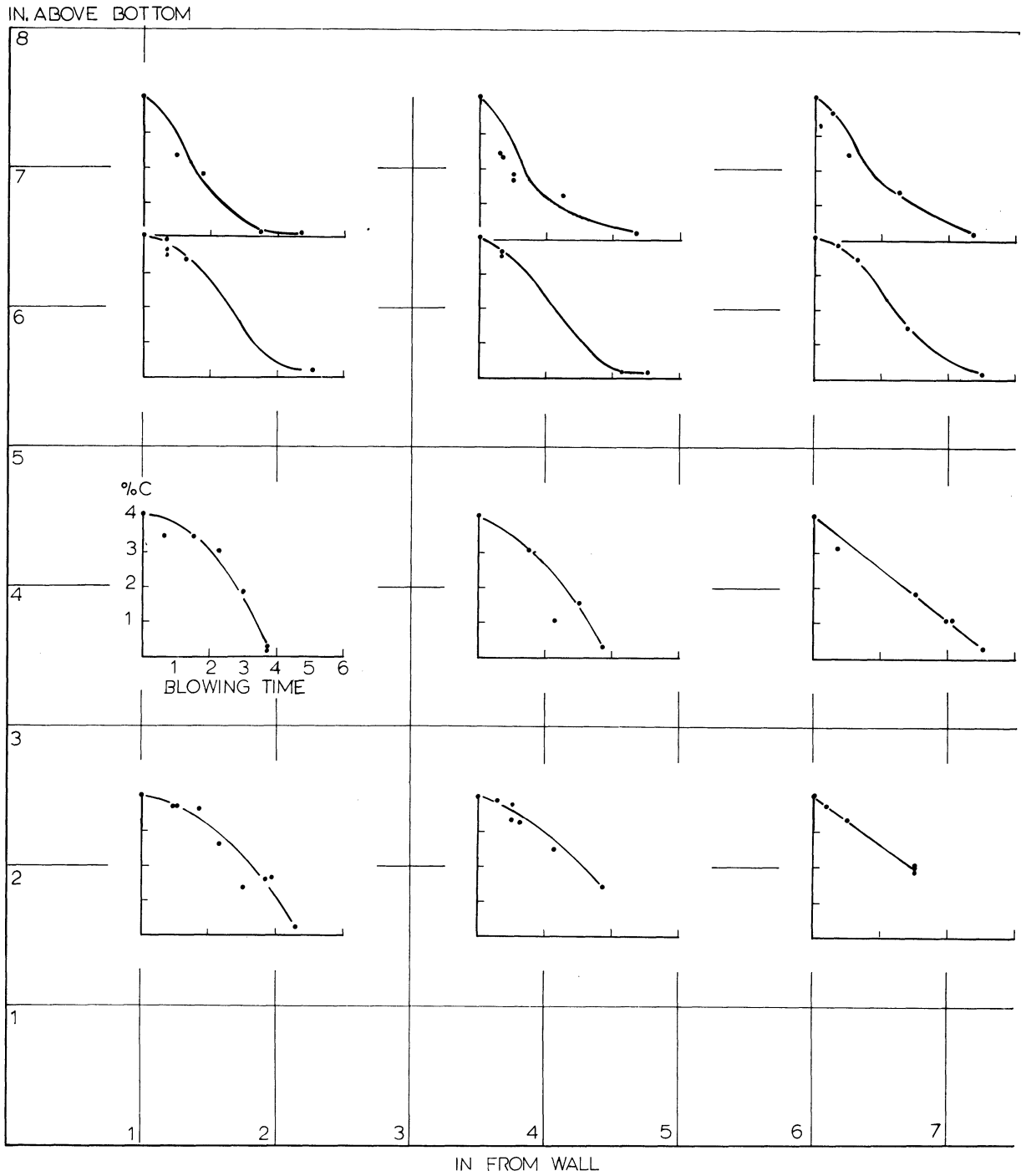
Fig. 28. % Carbon Versus Blowing Time for all Sampling Locations (6 in. bath, 7 in. bl. ht., 20 psig., 0.316 in. nozzle).
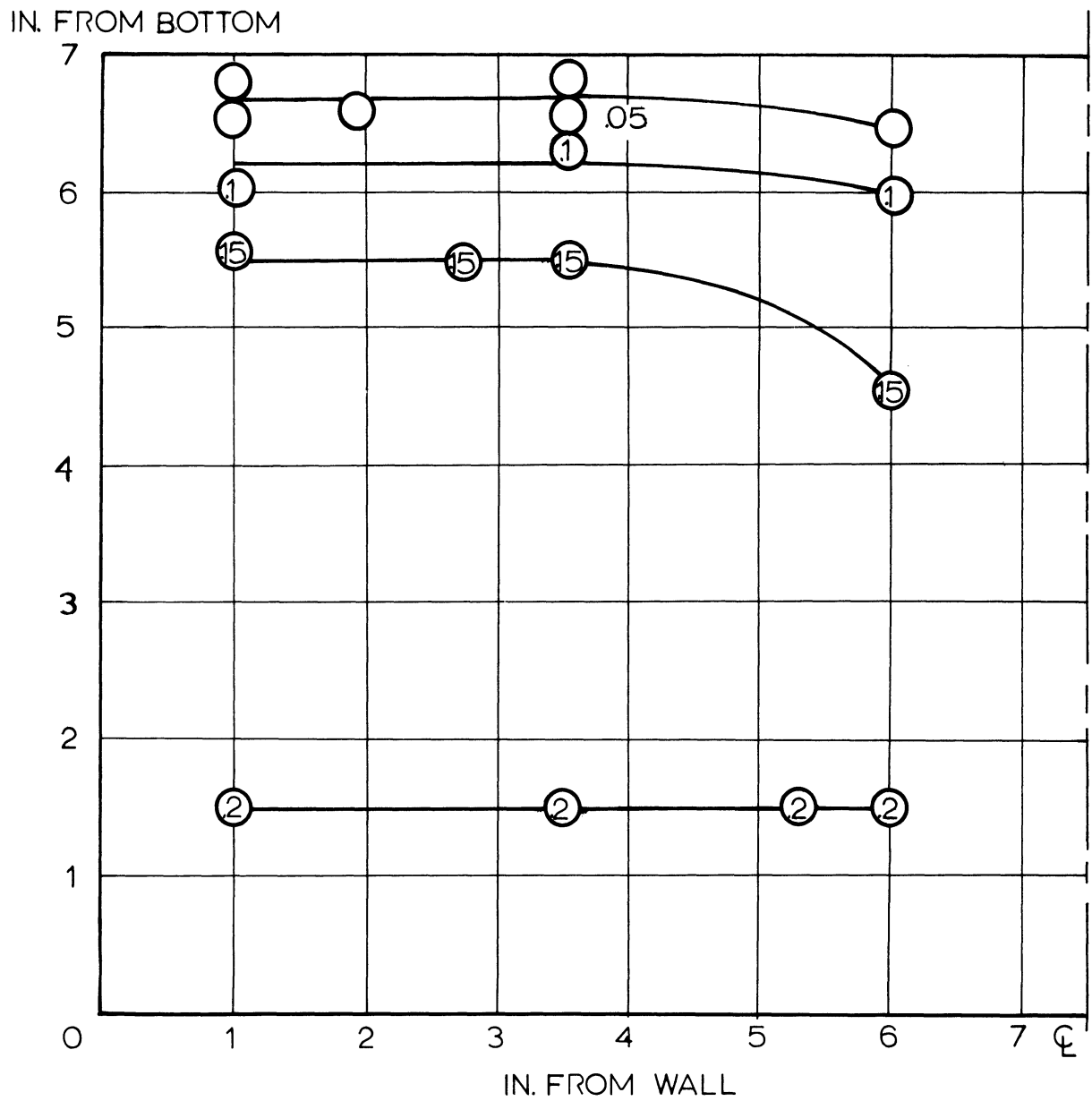
Fig. 29. Constant % Carbon Versus Bath Location at 2-1/2 Minutes Blowing Time (6 in. bath, 7 in. bl. ht., 20 psig., 0.316 in. nozzle).
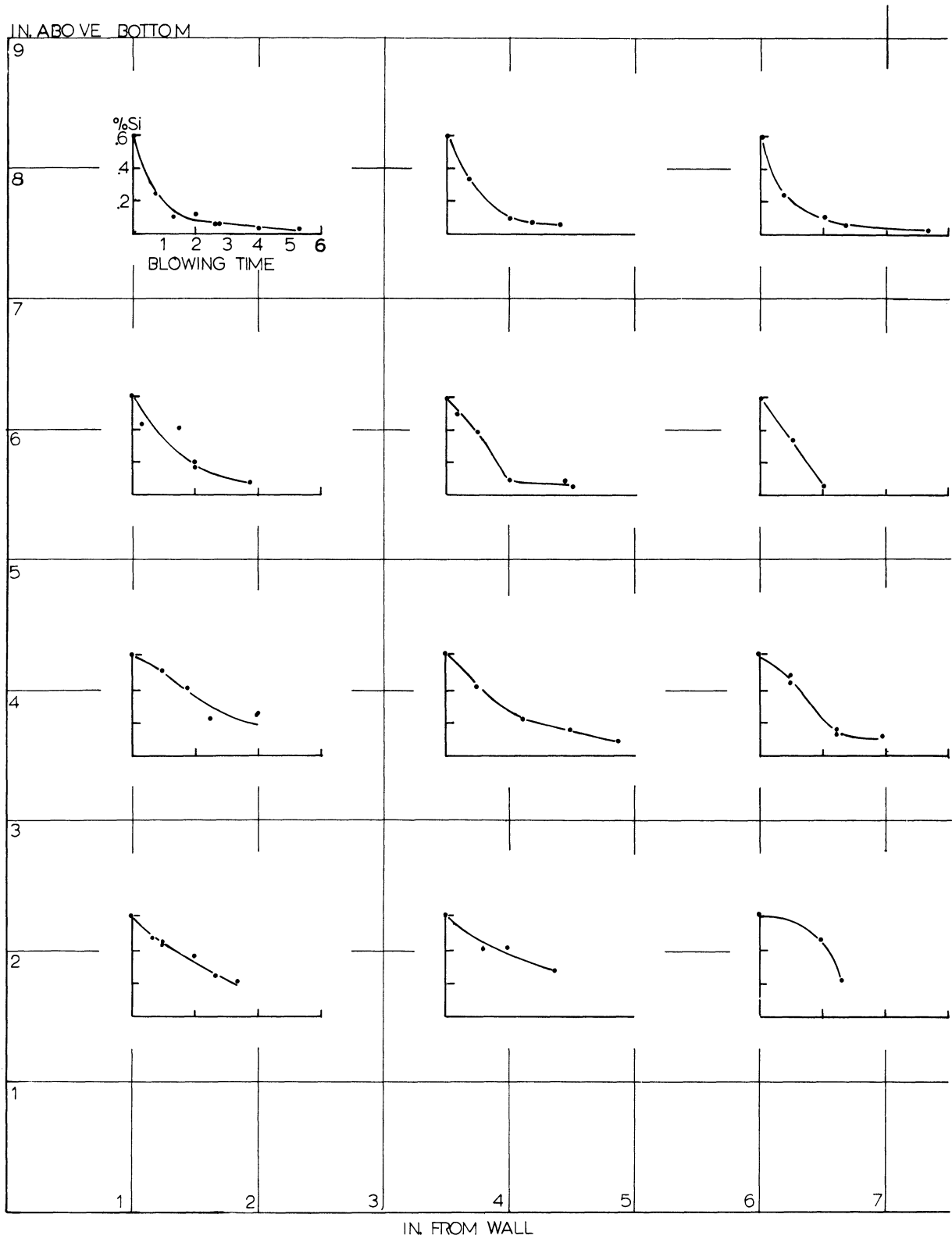
63
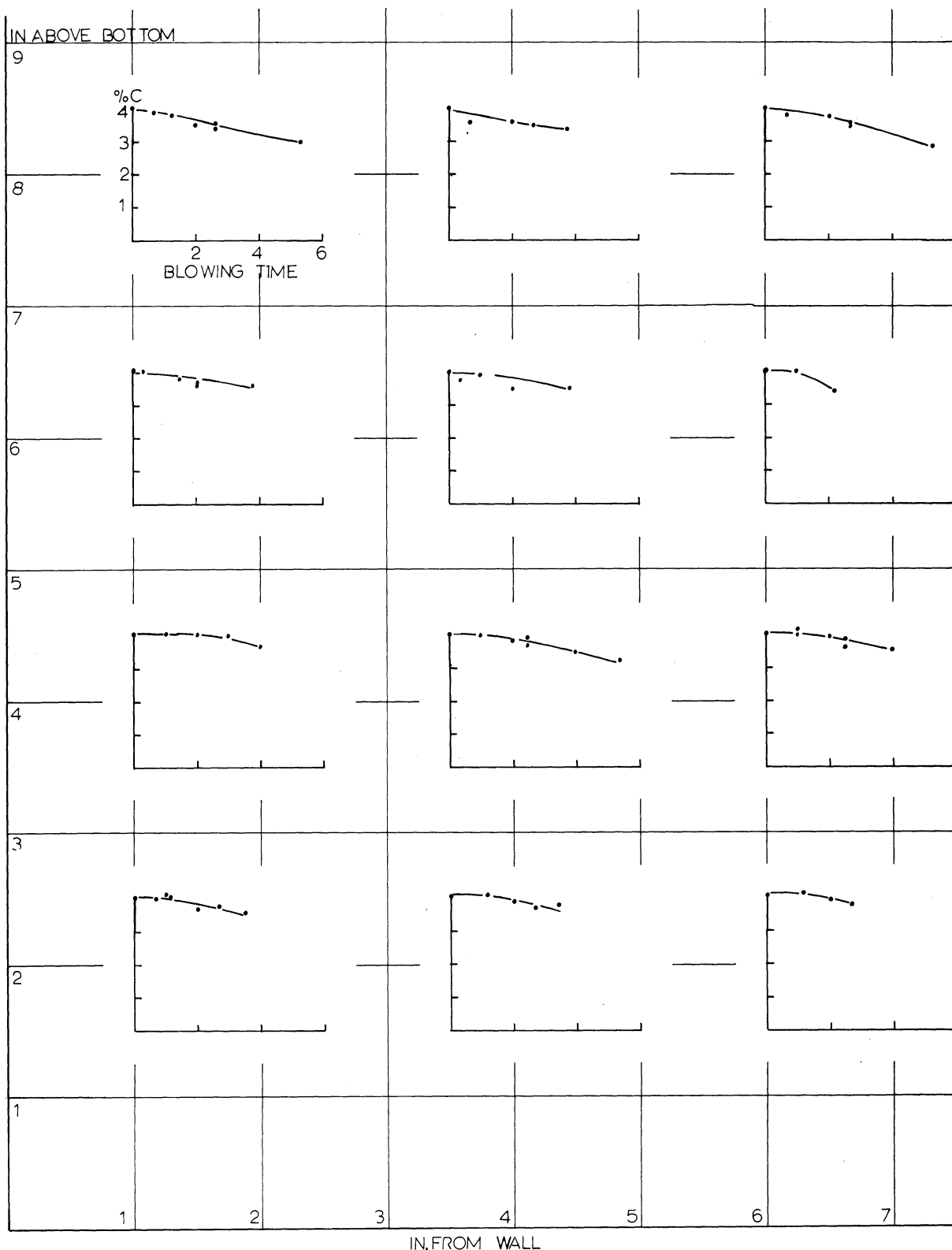
Fig. 30. % Carbon Versus Blowing Time for all Sampling Locations
(6 in. bath, 21 in. bl. ht., 20 psig., 0.316 in. nozzle).

5: 00 as compared to 1.1% C/min. at 0: 30 for standard conditions.
Great differences also exist at the bottom of the bath. The extent
and rate of decarburization are extremely slow under the 21 inch
blowing height condition.

c)   Effect of Bath Depth

Decarburization patterns for heats run with a 10 inch
bath depth and 20 psig. are shown by the solid points and curves
in Figure 31. As is usual, decarburization is most extensive and
rapid at the surface of the bath (0. 2% C at 5: 00 with a maximum
rate of 0. 7% C/min. at 3: 30). The bottom of the bath is the least
effectively decarburized (0. 3% C at 7: 00 with a maximum rate
of 0. 6% C/min. at 4: 30).

The open circles on the plots are data from 10 inch
baths blown at 35 psig. Decarburization at the bath surface is the
same as when the bath was blown at 20 psig. Lower in the bath
decarburization proceeds faster when the 35 psig. blowing pressure
is used.

The dotted lines in the 10-1/2 row of plots and the 5-1/2
inch row of plots are data taken from standard runs. Decarburization
is faster with the standard experimental conditions at all bath
locations than it is when the bath depth is increased to 10 inches (20 psig.).
The carbon content of the runs made with a 10 inch bath blown at
35 psig. correspond closely to those blown under standard conditions.
The specific rate (scfm./lb. of metal) of oxygen delivery is the
highest for the standard conditions (0. 19 scfm. /lb.), lower for
35 psig. - 10 inch bath conditions (0. 17 scfm. /lb.), and lowest for
the 20 psig. - 10 bath conditions (0. 12 scfm. /lb.). The rate of
decarburization varies directly with the rate of oxygen delivery.
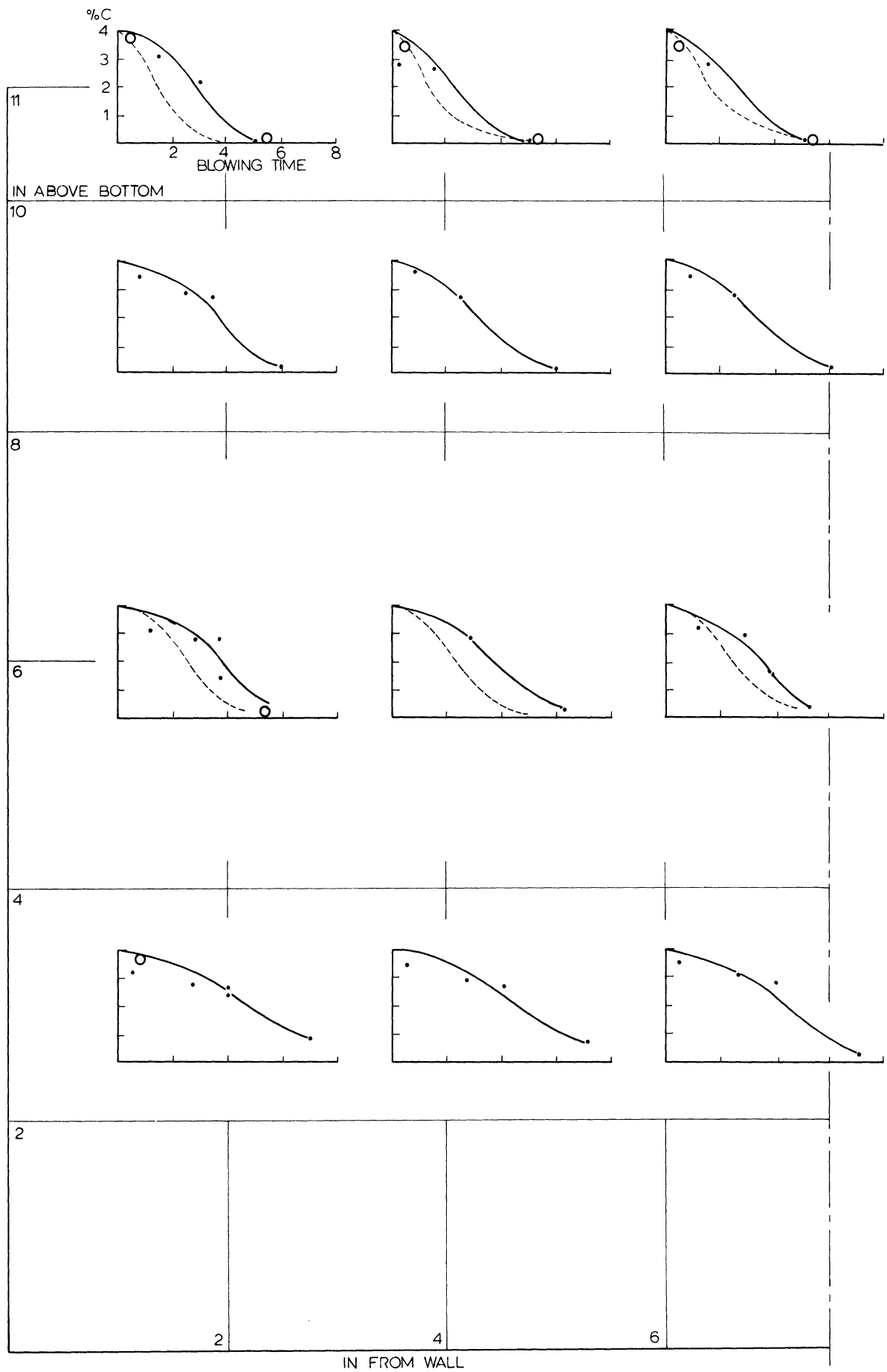
Fig. 31. % Carbon Versus Blowing Time for all Sampling Locations (10 in. bath, 7 in. bl. ht. , 20 psig. , 0.316 in. nozzle - solid lines) and (10 in. bath, 7 in. bl. ht. , 35 psig. , 0.316 in. nozzle - open points).

d) Effect of Nozzle Diameter

The effects of blowing a 6 inch bath with a 0. 162 inch diameter lance are shown in Figure 32. Decarburization is slow throughout the bath; however, the pattern of slowest decarburization at the bottom of the bath is maintained. At the bath surface the carbon content is reduced to 2. 3% C after 11: 30. The rate of decarburization is 0. 5% C/min. at 2: 00. The carbon content at the bottom of the bath is reduced to 3% C at 10: 00. The maximum decarburization rate is 0. 2% C/min. at 4: 00.

The dotted lines in Figure 32 show the decarburization in a standard run. Oxygen is supplied 3. 4 times as fast under standard conditions as it is when the bath is blown with a 0. 162 inch diameter lance. This is roughly the ratio of the decarburization rates of the two conditions.

Summary - Decarburization

In contrast to Si elimination, C oxidation proceeds more slowly and in some cases the heat is stopped before low levels are reached. In the case of the 21 inch blowing height for example, a violent foaming condition is encountered by the time the carbon reaches 1. 98% and the heat was discontinued. Similarly, with the small lance the heat was stopped after the silicon was oxidized but before the carbon was eliminated. In this case the highest carbon was found all across the bottom layers of the vessel even directly beneath the nozzle.
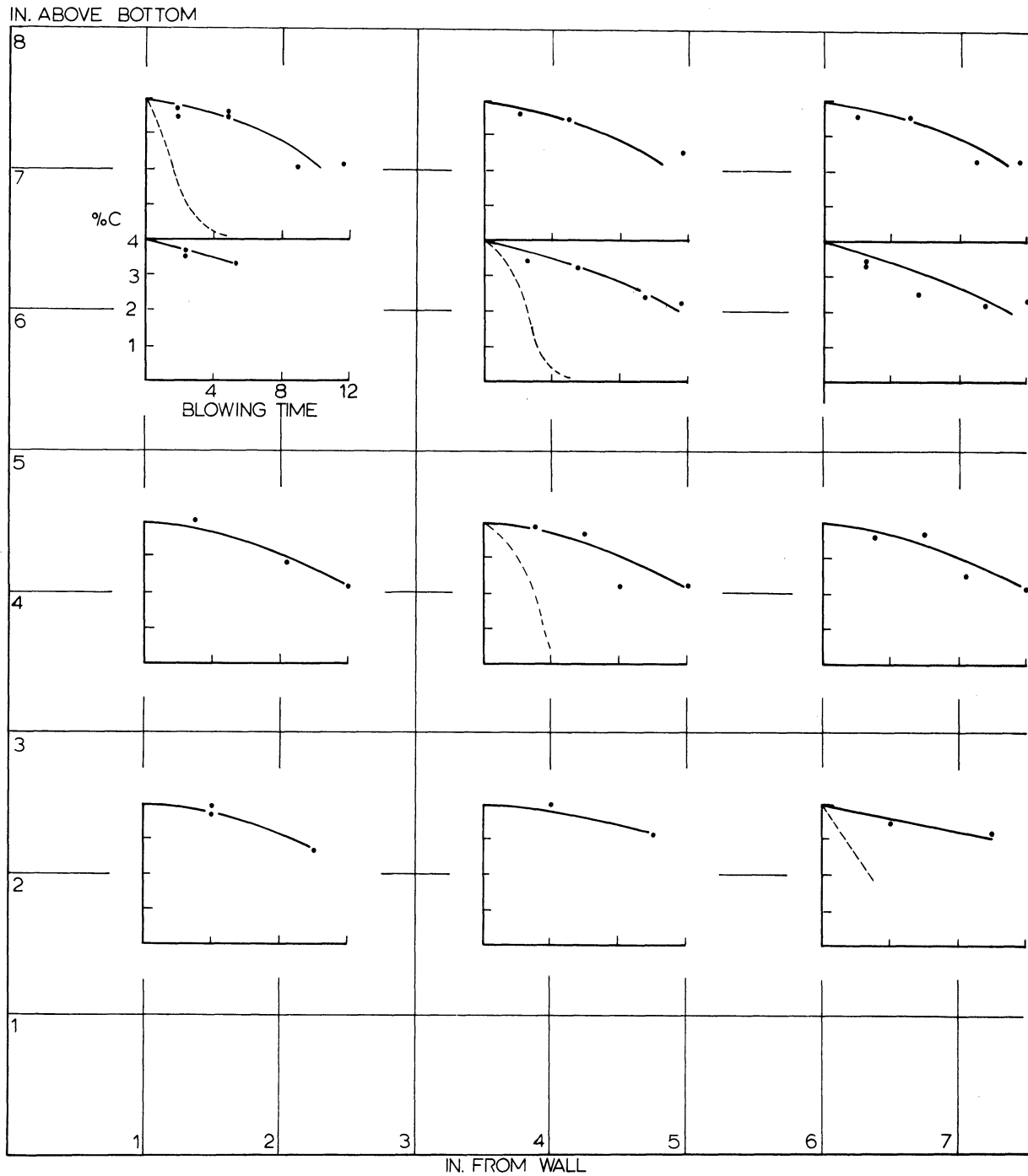
Fig. 32. % Carbon Versus Blowing Time for all Sampling Locations
(6 in. bath, 7 in. bl. ht., 25 psig., 0.162 in. nozzle).

5) Manganese

    a) Standard Conditions

The manganese distribution in a 6 inch bath blown with
standard conditions is shown in Figure 33. As expected, the curves
resemble those for silicon. Manganese content is reduced throughout
the bath to 0.08% Mn by the end of the blow. The rate of manganese
oxidation at the start of a run is 0.7% Mn/min. at the surface of the
bath and 0.3% Mn/min. at the bottom of the bath. Manganese oxidation
is always most rapid at the initiation of blowing.

    b) Effect of Blowing Height

In Figure 34 the manganese pattern in a 6 inch bath blown
from 21 inches is shown. Similar to silicon, the pattern of most
rapid oxidation at the top of the bath is found (3% Mn/min. versus
0.07% Mn/min. at the bottom of the bath.). Of greater significance
is the extensive reduction in manganese content at the top-center of
the bath while the rest of the bath is maintained at much higher
manganese levels. As an example, after 3:00 the manganese content
is 0.07% at the top-center and 0.38% at the bottom corner. The
difference in concentrations reflects the poor circulation from the
jet impingement area to the bottom of the converter with shallow
jet penetration. The initial rate of manganese oxidation is 0.6% Mn/min.
at the top-center of the bath.

    c) Effect of Bath Depth

The % Mn-time relationships for a 10 inch bath blown at
20 psig. are shown by the solid lines and points in Figure 35. The
bath manganese content is reduced to 0.14% at all locations. The
maximum rate of manganese oxidation at the bath surface is 0.5%
Mn/min. while the rate is 0.3% Mn/min. at the bottom. In both cases
the maximum rate is found at the start of the run.
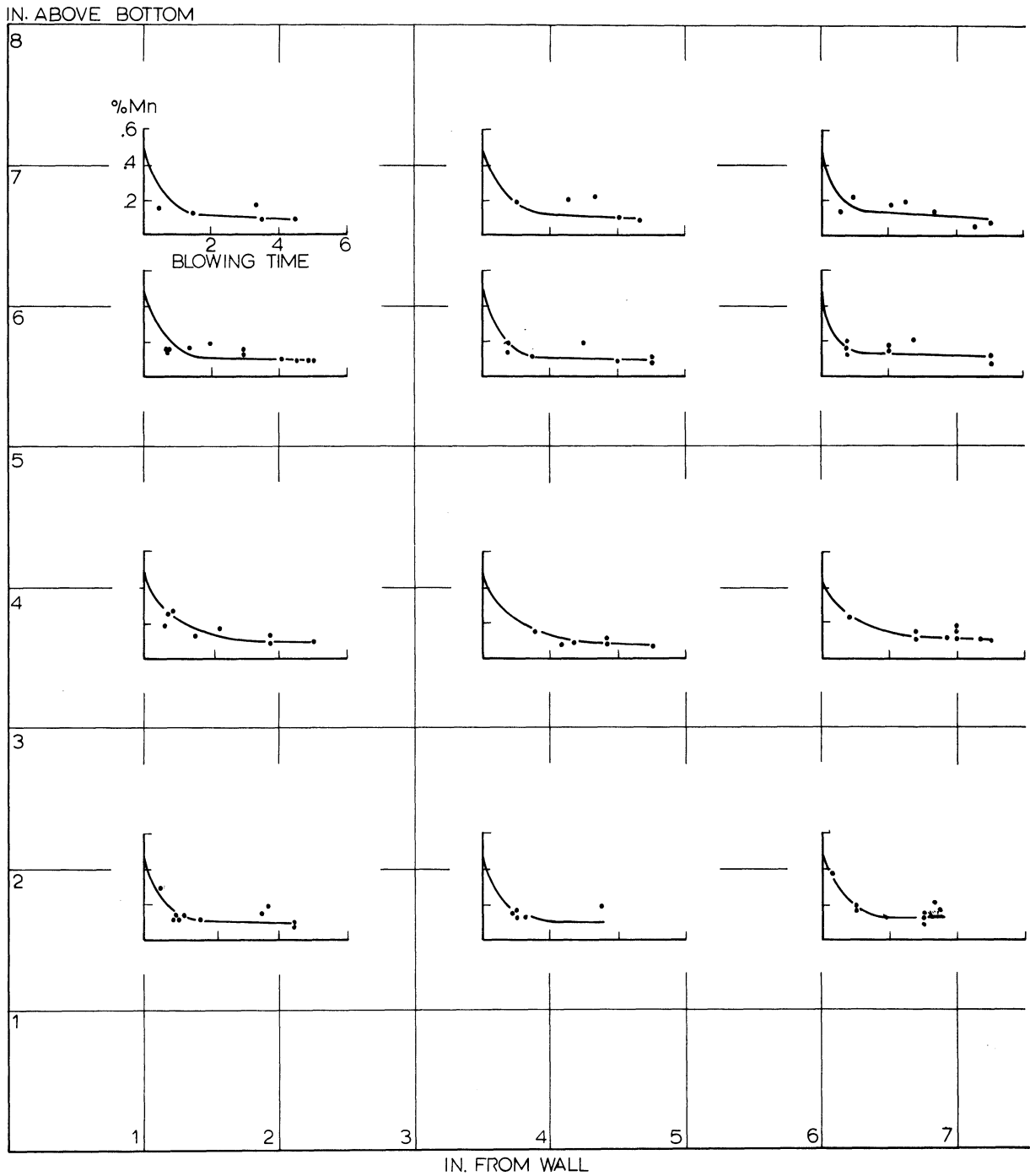
Fig. 33. % Manganese Versus Blowing Time for all Sampling Locations (6 in. bath, 7 in. bl. ht., 20 psig., 0.316 in. nozzle).

IN. ABOVE BOTTOM

IN. FROM WALL
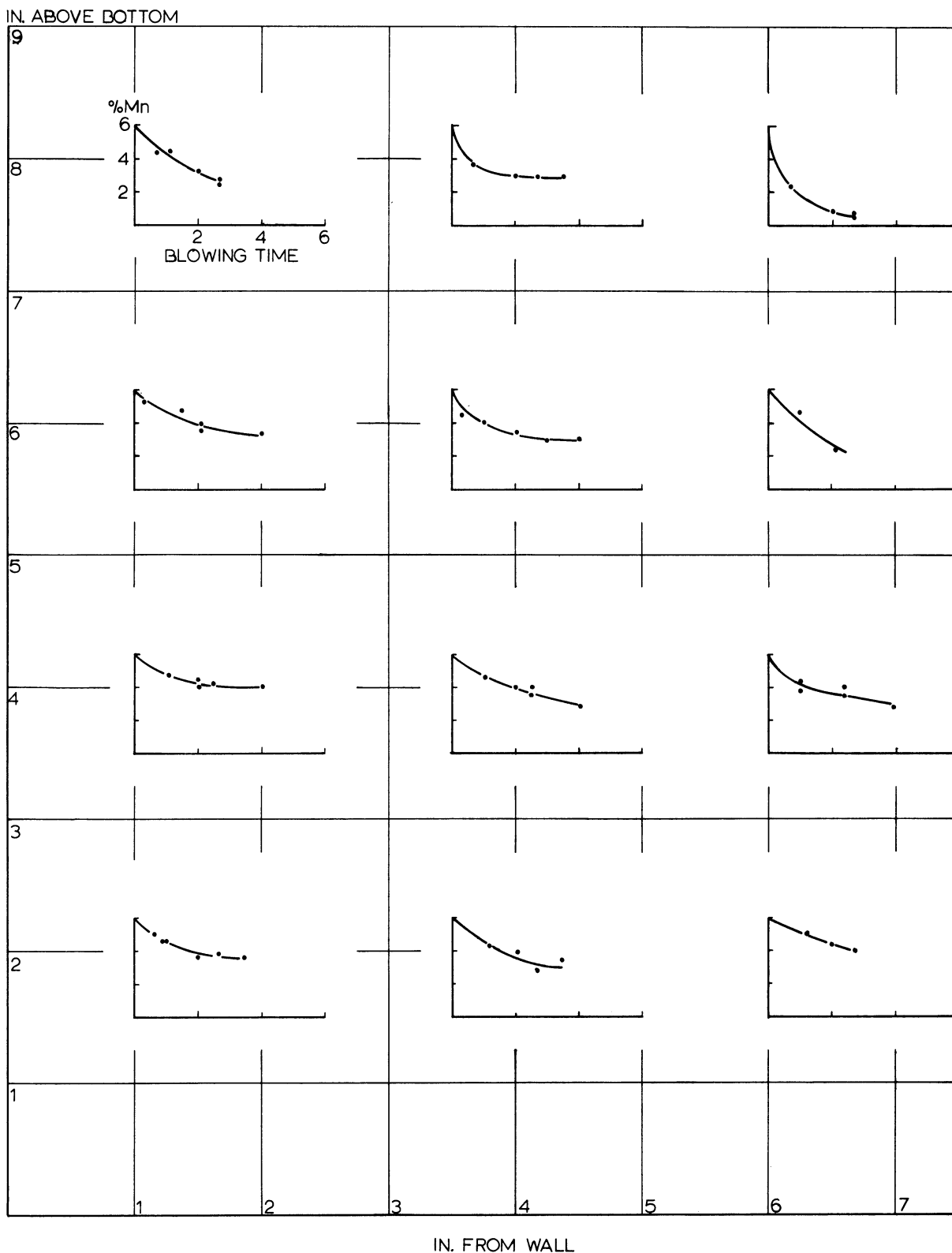
Fig. 34. % Manganese Versus Blowing Time for all Sampling
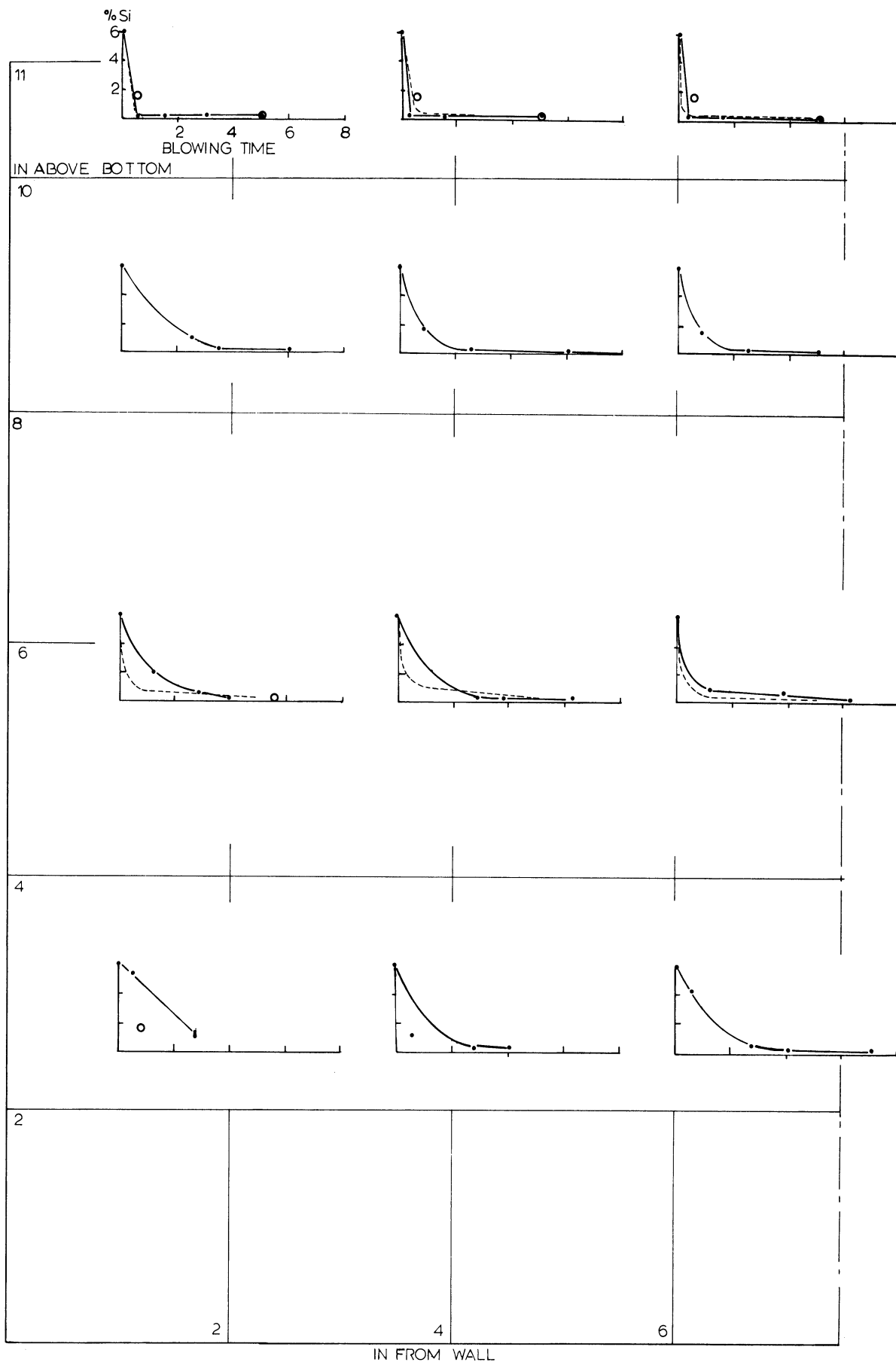Locations (6 in. bath, 21 in. bl. ht., 20 psig., 0.316 in. nozzle).
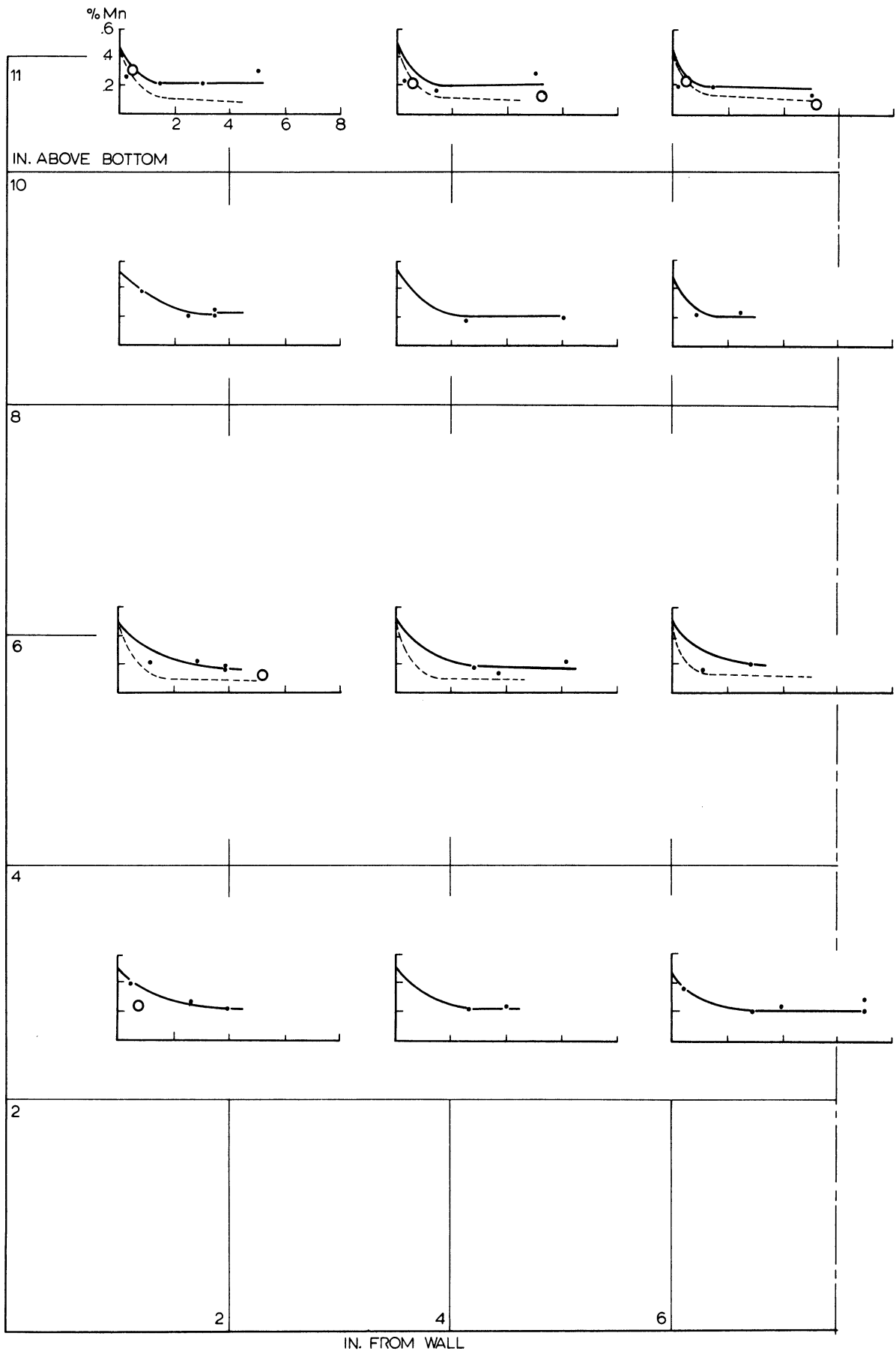
Fig. 35. % Manganese Versus Blowing Time for all Sampling
Locations (10 in. bath, 7 in. bl. ht., 20 psig., 0.316 in. nozzle -
solid lines) and (10 in. bath, 7 in. bl. ht., 35 psig., 0.316 in.
nozzle - open points).

The open circles in Figure 35 are data from runs with a
10 inch bath blown at 35 psig. In this case manganese oxidation is
more extensive and the rate is slightly faster than in a 10 inch bath
blown at 20 psig.

d) Effect of Nozzle Diameter

In Figure 36 the manganese pattern in a 6 inch bath blown
with a 0.162 inch diameter lance is shown. The bath manganese
content is reduced to 0.14% at 13:38. The maximum rate of manganese
oxidation is 0.3% Mn/min, at the top of the bath and 0.05% Mn/min.
at the bottom of the bath. In both cases the rate of oxidation is
greatest at the initiation of blowing.

Summary - Manganese Oxidation

Manganese is not quite as active as silicon and the gradients
found are intermediate between silicon and carbon. Under conditions
of deep penetration, e.g., standard conditions, the elimination of
Mn is rapid throughout the bath, reaches a maximum rate early and
falls to 0.08% by the end of the blow. By contrast, where circulation
is poor, as with the high lance position, there is still appreciable
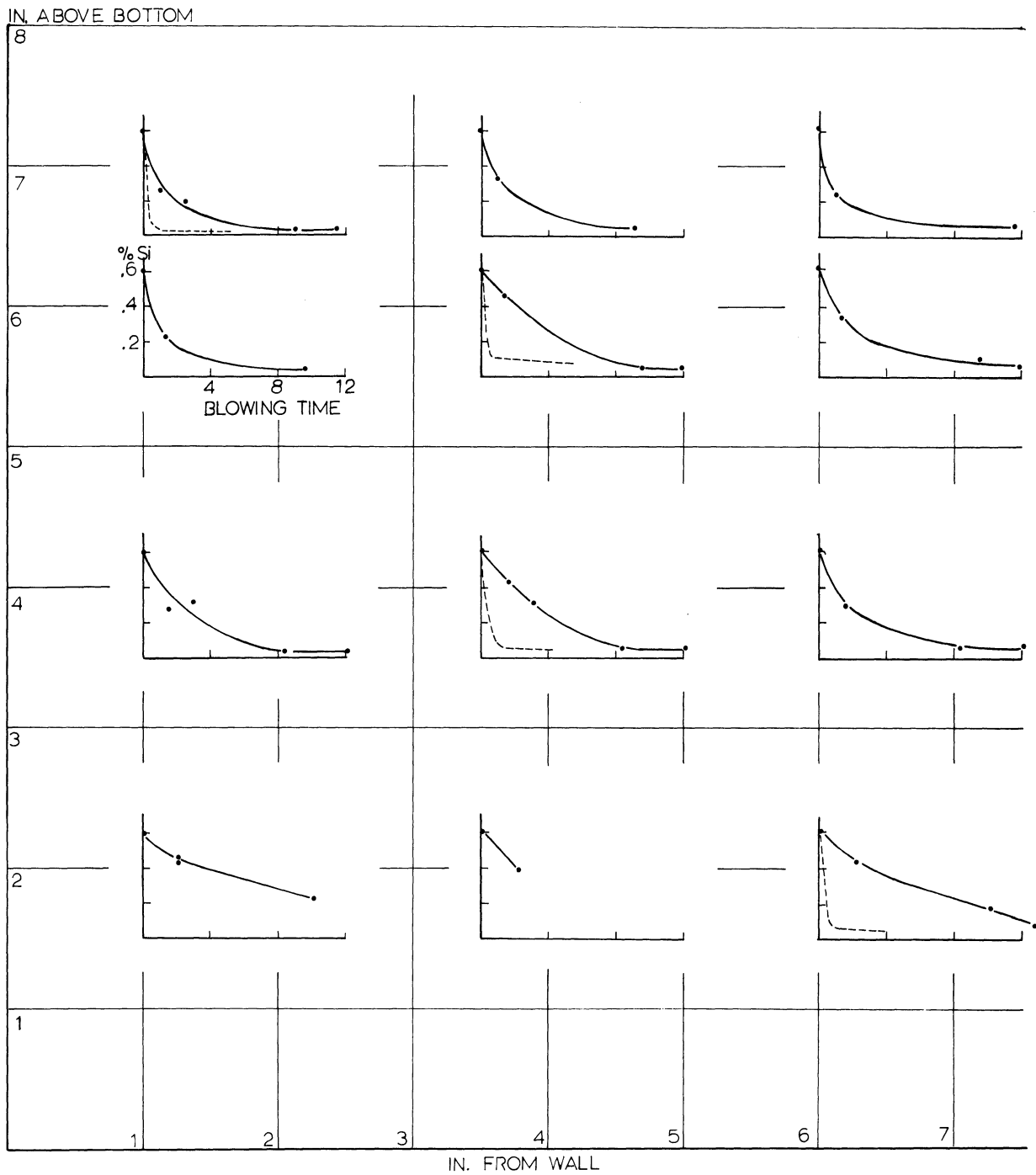Mn (0.14%) at the end of the heat.
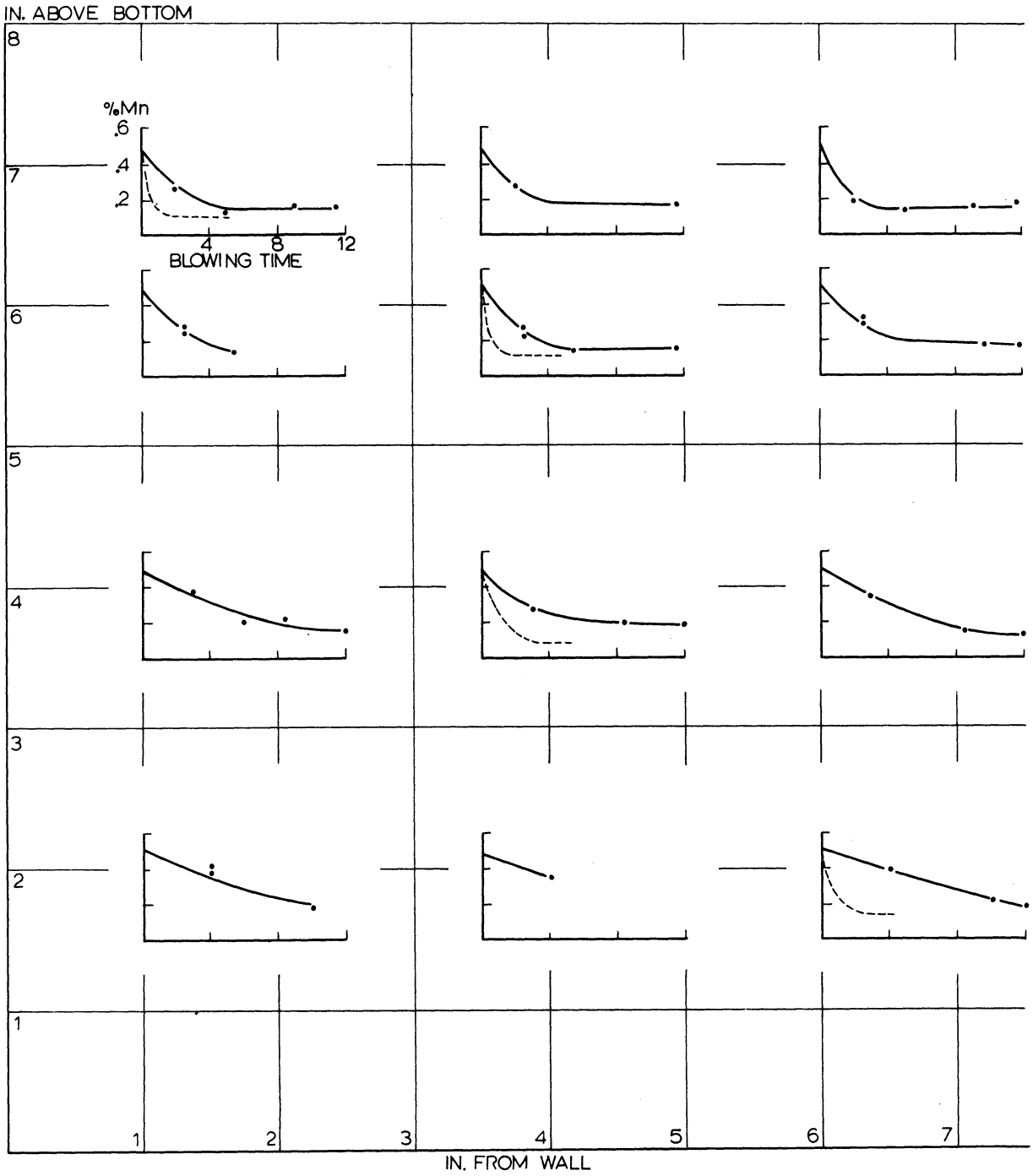
Fig. 36. % Manganese Versus Blowing Time for all Sampling
Locations (6 in. bath, 7 in. bl. ht., 25 psig., 0.162 in. nozzle).

6) <u>Temperature</u>

a) Standard Conditions

The temperature distribution in a bath under standard conditions is shown in Figure 37. Surface and bottom-center temperatures increase smoothly at $200^\circ F/min$. to $3000^\circ F$. at 2:30. The bottom-corner temperature is linearly increased to $3000^\circ F$ at 3:30 giving a rate of $150^\circ F./min$.

b) Effect of Blowing Height

The temperature pattern is markedly changed by increasing the blowing height to 21 inches as shown in Figure 38. The bottom temperatures increase only to $2600^\circ F$. in 5 minutes. At the top of the bath the temperature rises slowly at first then rapidly at $150^\circ F/min$. to $2950^\circ F$. at 3:00 and then slowly to $3000^\circ F$. at 5:30.

c) Effect of Bath Depth

When the bath depth is increased to 10 inches the temperature patterns shown in Figure 39 are produced. The top-center temperature increases at $300^\circ F./min$. to $2800^\circ F$. at 1:00 and then much more slowly to $2950^\circ F$. at 3:30. The top edge temperature is increased smoothly to $3100^\circ F$. at 7:00 at a rate of $100^\circ F./min$.. The bottom temperatures show a two minute delay before rising.

Temperatures at all locations are increased when the 10 inch bath is blown at 35 psig. as shown in Figure 40. The surface rises initially at $250^\circ F./min$. and then more slowly to $3100^\circ F$. at 3:00. The bottom of the bath is heated slowly for the first minute and then the temperature is increased at $200^\circ F./min$. to $2900^\circ F$. at 3:00.

IN. ABOVE BOTTOM

IN FROM WALL
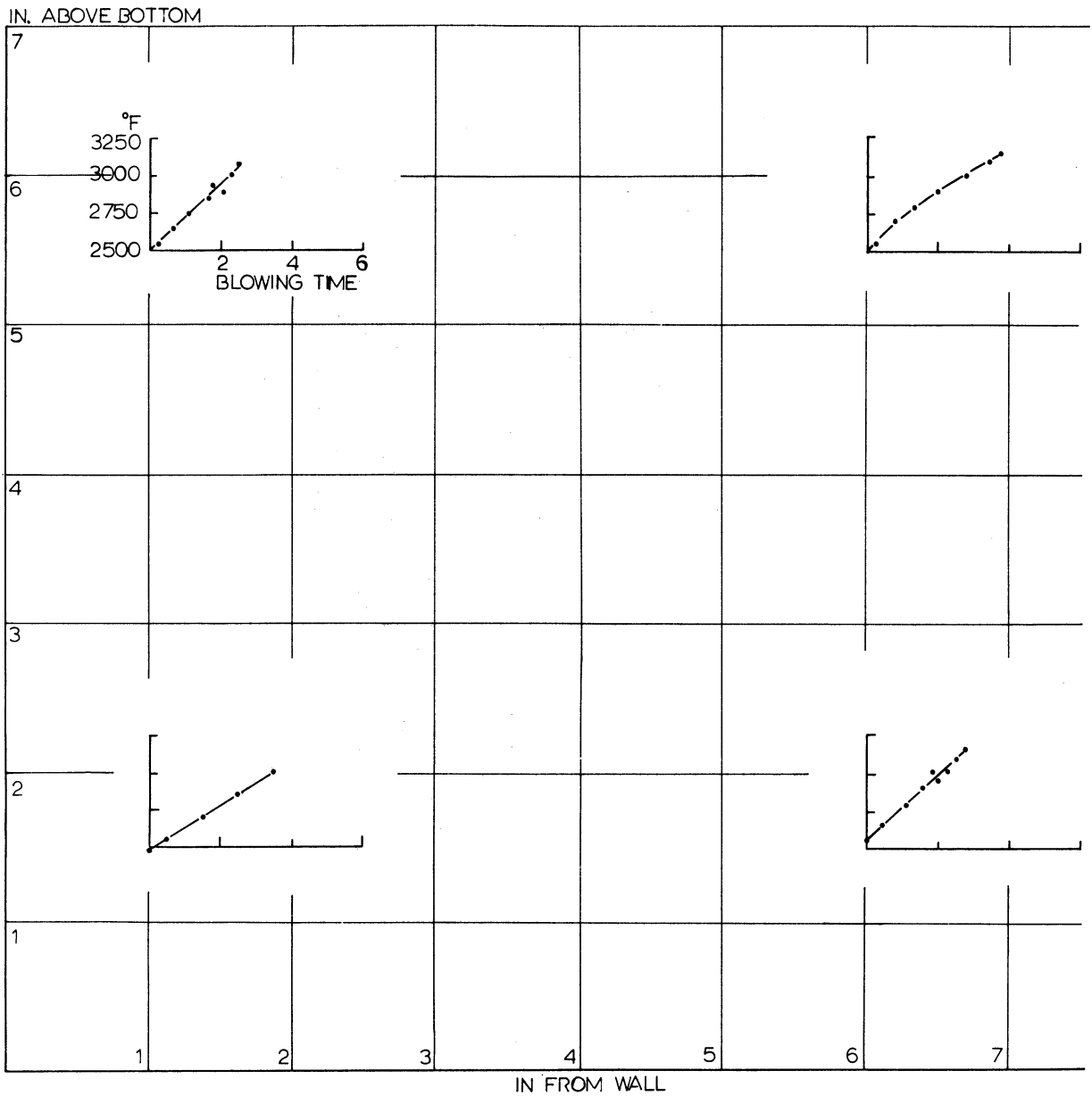
Fig. 37.   Temperature Versus Blowing Time at 4 Locations
(6 in. bath, 7 in. bl. ht., 20 psig., 0.316 in. nozzle).

76
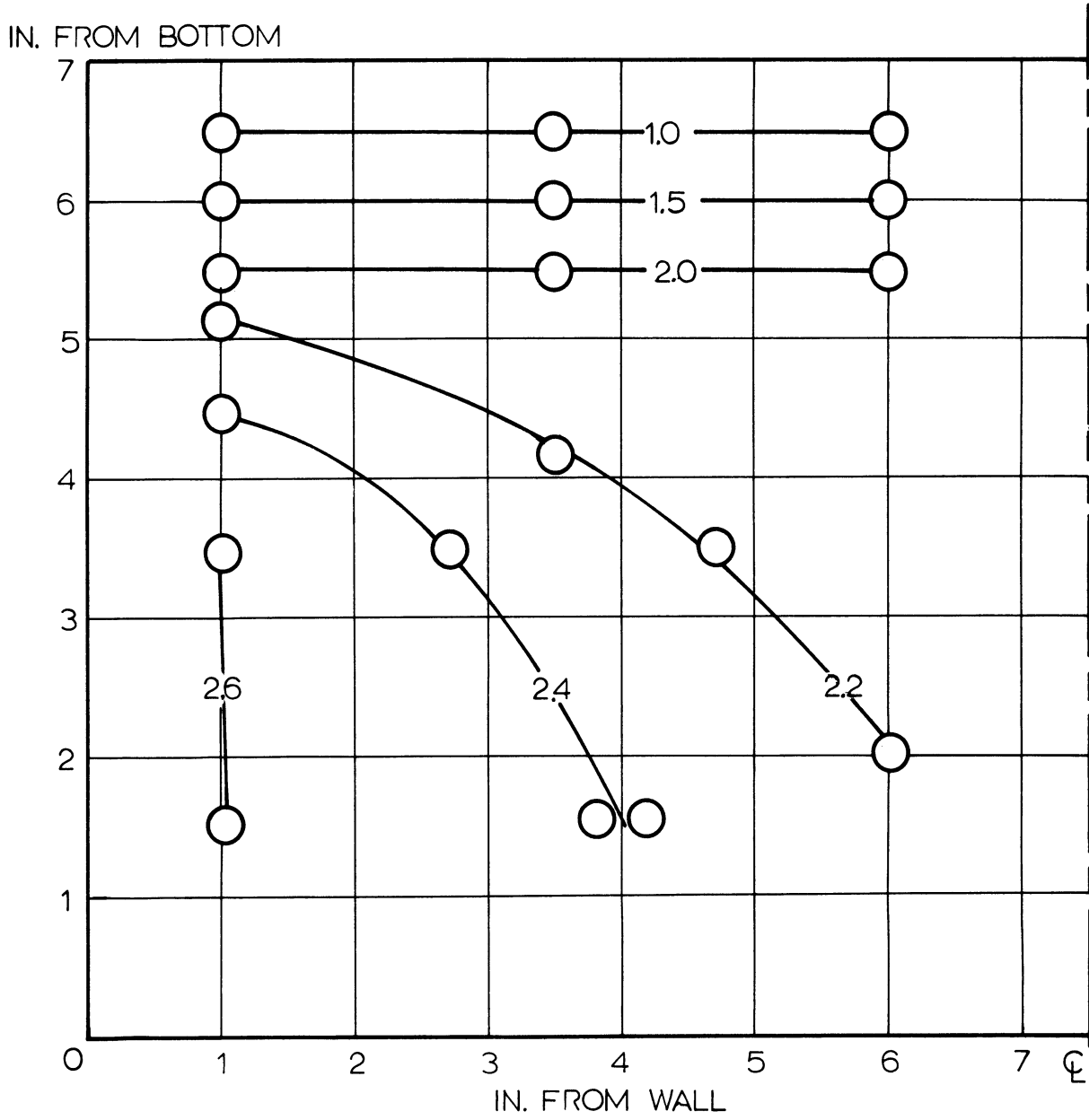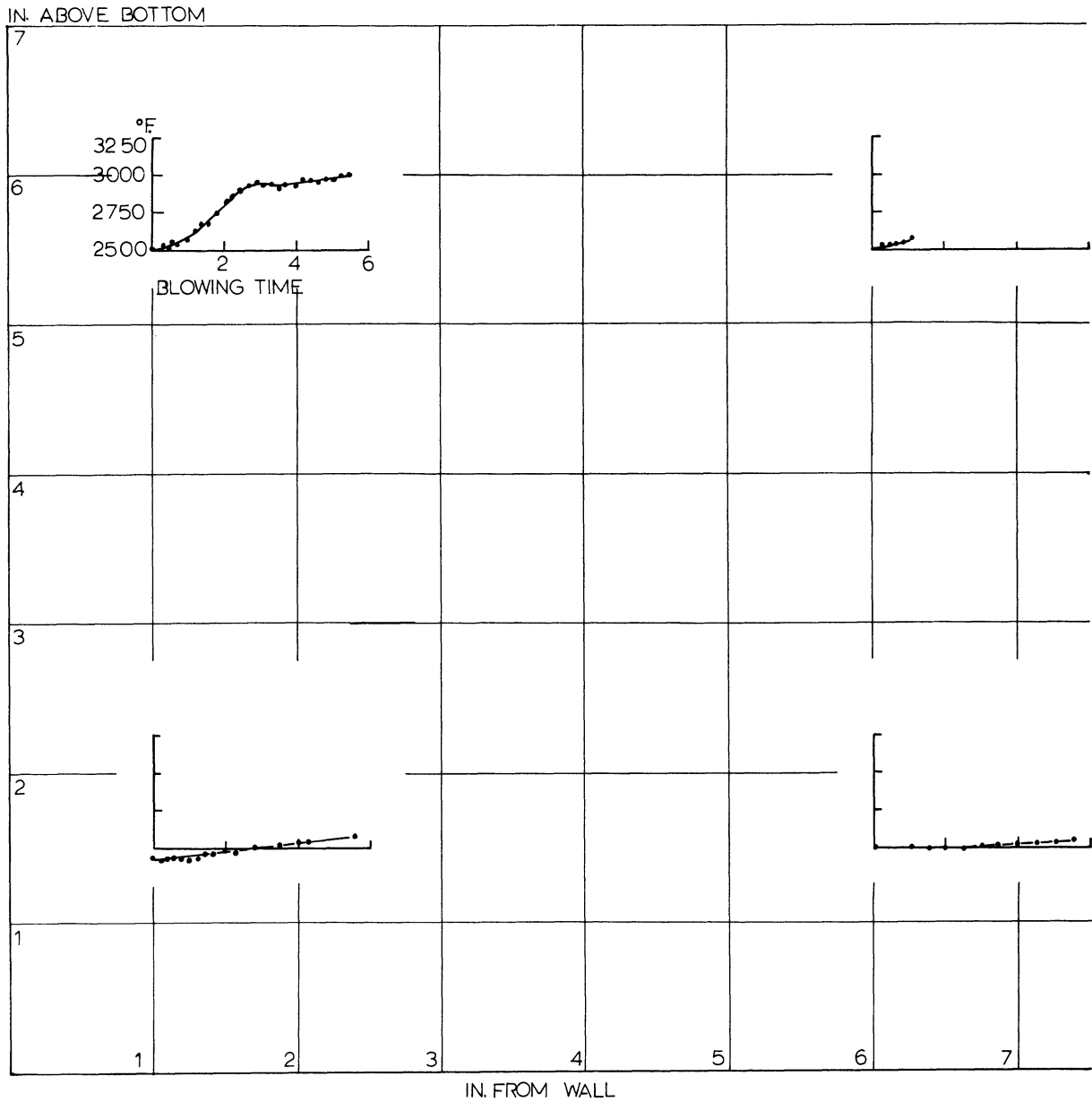

Fig. 38. Temperature Versus Blowing Time at 4 Locations
(6 in. bath, 21 in. bl. ht., 20 psig., 0.316 in. nozzle).
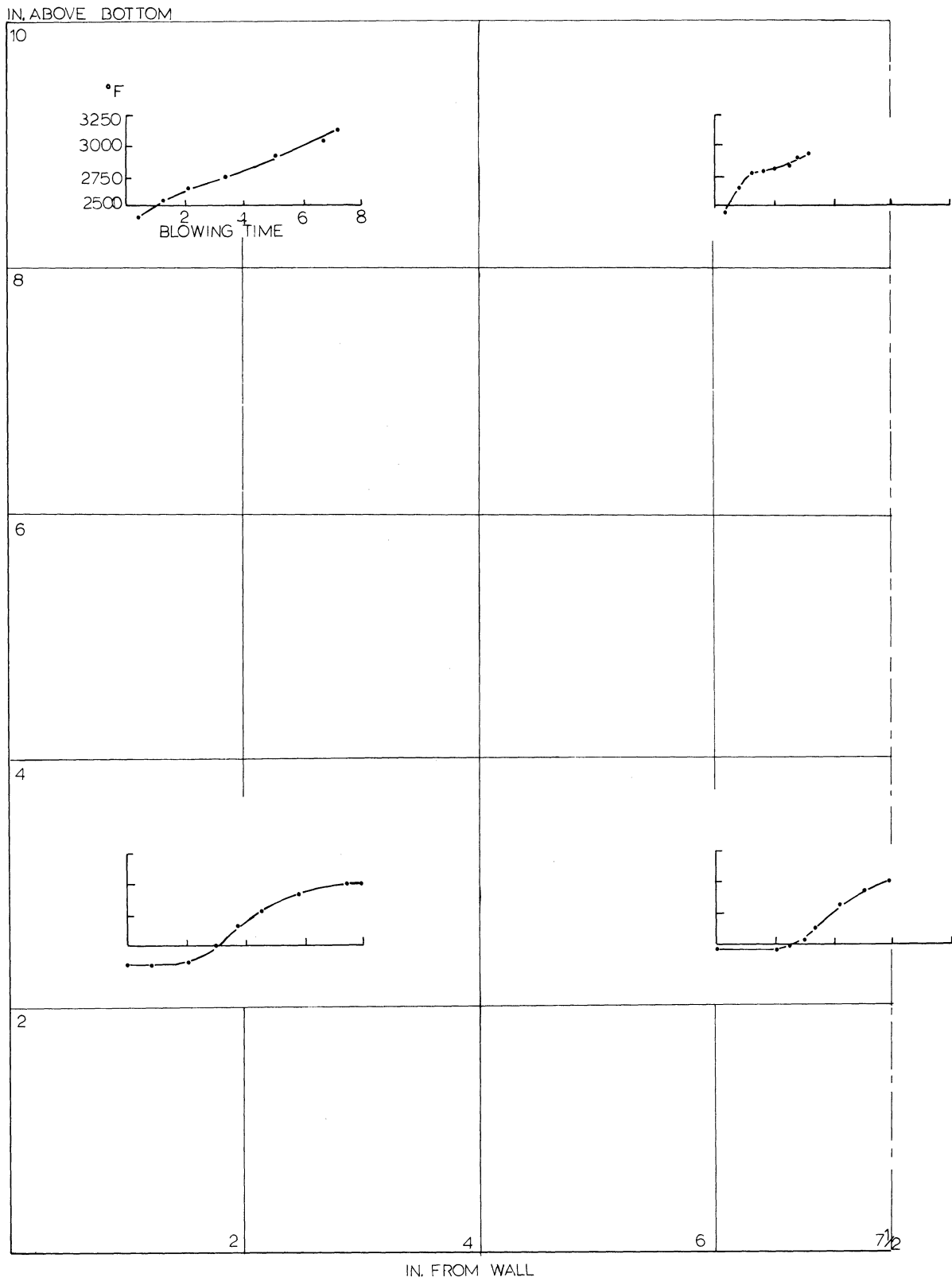
Fig. 39.   Temperature Versus Blowing Time at 4 Locations
(10 in. bath, 7 in. bl. ht. , 20 psig. , 0.316 in. nozzle).
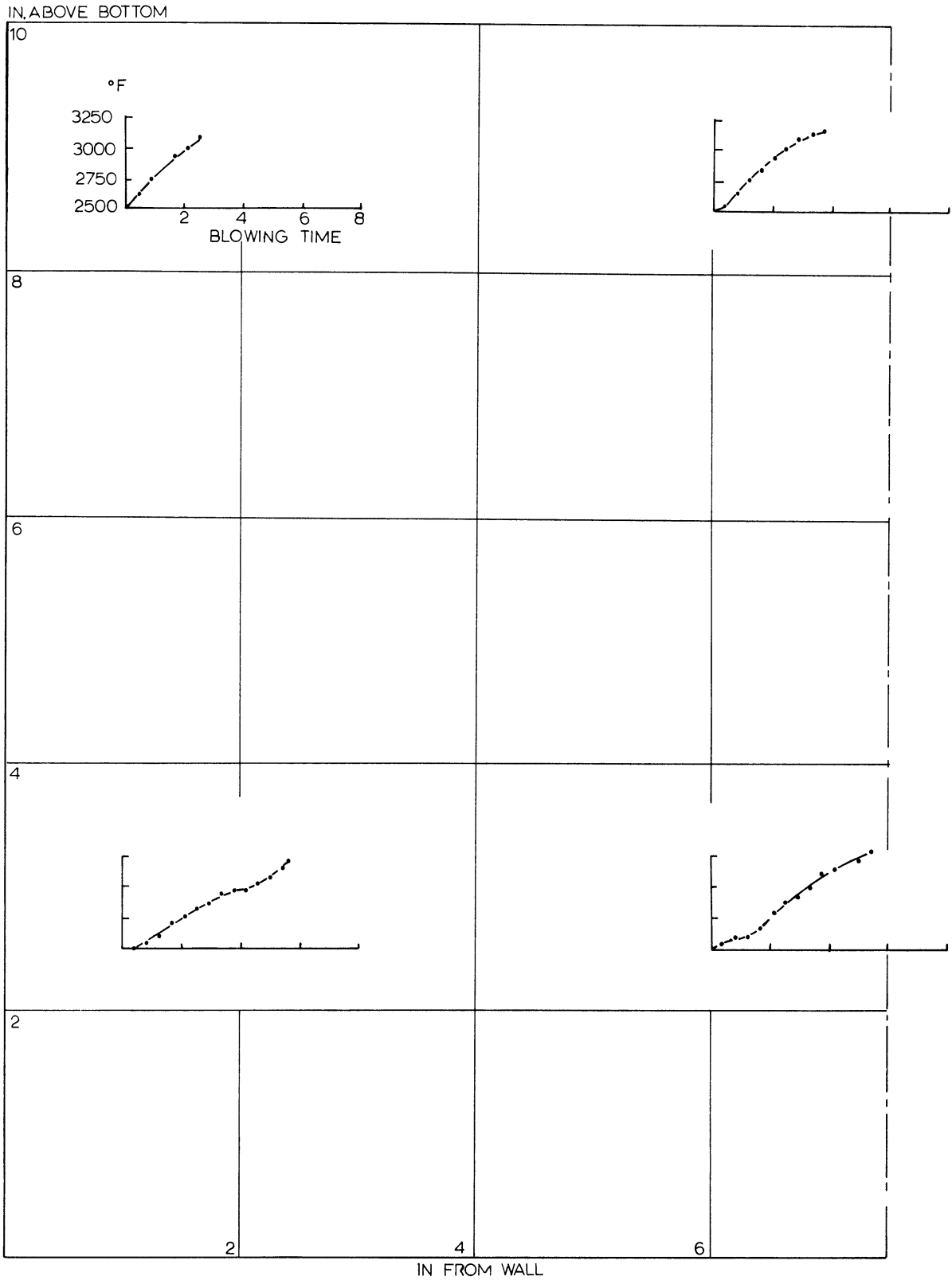
Fig. 40. Temperature Versus Blowing Time at 4 Locations (10 in. bath, 7 in. bl. ht., 35 psig., 0.316 in. nozzle).

d)   Effect of Nozzle Diameter

Temperature-time curves are characterized by long
holds when the bath is blown with a 0.162 inch lance as shown in
Figure 41. Temperatures are constant or are decreasing slightly
for 4 minutes at the bath surface and 6 minutes at the bottom and
then the temperatures increase at approximately $125^\circ F./min.$
throughout the bath.

Summary - Temperature

The maximum rate of temperature increase and minimum
gradient are encountered with deep penetration conditions. By
contrast with shallow penetration, as obtained with a small diameter
nozzle, the temperature at the bottom of the bath actually falls
for several minutes. These temperature distributions show clearly
that the metal which is oxidized and heated near the jet impingement
area moves radially outward at the surface not downward at the
centerline.

IN ABOVE BOTTOM

IN FROM WALL
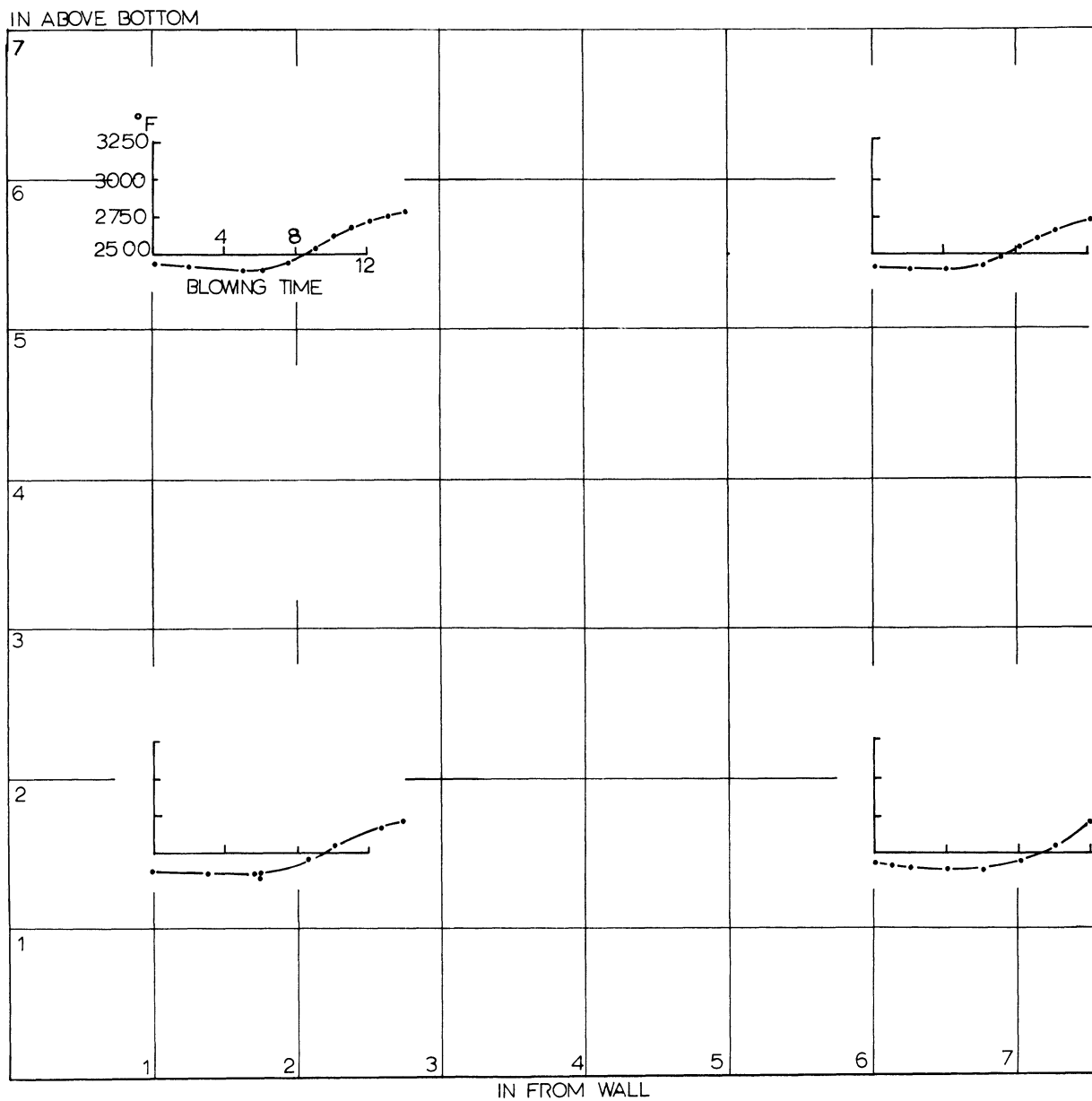
Fig. 41. Temperature Versus Blowing Time at 4 Locations
(6 in. bath, 7 in. bl. ht., 25 psig., 0.162 in. nozzle).

7) <u>Slag</u> <u>Composition</u>

The slag samples provide interesting data when considered with the changes in metal chemistry just discussed. The analyses of all samples taken are given in Appendix I, Data. It is best to begin the discussion with a review of the average slag composition given by the spoon (S-2) samples and then progress to the probe samples to illustrate composition gradients. First the change in P_2O_5 will be discussed and then the oxygen level as FeO.

P_2O_5 Content of Average Slag

a)   Standard Conditions

In Table VII are presented the compositions of four slags taken with a spoon sampler with the vessel turned down after blowing. Under standard conditions these samples represent blowing times in excess of four minutes and were well mixed with the slag sampling spoon.

The P_2O_5 contents of these slags range between 2.3% and 3.3% and represent good bath dephosphorization under a hard blowing condition.

b)   Effect of Blowing Height

By contrast, the analyses of four other slags, with a 21 inch blowing height, are given in Table VII. The range of P_2O_5 contents is 2.6% to 3.5%. This blowing condition produced nearly the same P_2O_5 content as did the standard condition; however, the bath was at a much lower temperature and other conditions were impractical for good steelmaking.

Table VII

Compositions of Homogeneous (Average, S-2) Slag Samples

For All Blowing Conditions

Blowing Time (min.)	SiO_2	Fe_2O_3	FeO	Al_2O_3	CaO	MgO	MnO	P_2O_5
				Slag Composition (weight percent)				

S-2 Samples

Standard Conditions

Blowing Time (min.)	SiO_2	Fe_2O_3	FeO	Al_2O_3	CaO	MgO	MnO	P_2O_5
4:10	15.8	4.6	7.5	2.8	48.8	11.2	3.3	3.3
5:15	13.8	7.3	17.0	1.1	43.5	10.5	2.8	2.4
5:30	9.9	8.9	22.2	0.9	40.0	9.8	3.1	2.3
5:32	9.2	6.3	10.5	4.9	50.8	9.8	2.4	2.8

21 inch Blowing Height

Blowing Time (min.)	SiO_2	Fe_2O_3	FeO	Al_2O_3	CaO	MgO	MnO	P_2O_5
3:46	16.5	---	----	4.8	41.9	11.8	3.6	3.4
4:15	10.4	9.7	28.4	4.6	33.3	6.2	2.7	3.5
5:30	9.2	10.9	31.4	3.9	28.8	9.2	2.8	2.9
5:32	7.2	8.9	39.9	3.2	28.6	6.4	2.0	2.6

10 inch bath, 20 psig.

Blowing Time (min.)	SiO_2	Fe_2O_3	FeO	Al_2O_3	CaO	MgO	MnO	P_2O_5
8:32	12.9	1.8	4.9	0.9	53.6	19.0	2.1	1.8

10 inch bath, 35 psig.

Blowing Time (min.)	SiO_2	Fe_2O_3	FeO	Al_2O_3	CaO	MgO	MnO	P_2O_5
5:30	13.5	7.4	17.7	7.6	24.6	25.2	2.2	1.8

6 inch bath, 25 psig.

Blowing Time (min.)	SiO_2	Fe_2O_3	FeO	Al_2O_3	CaO	MgO	MnO	P_2O_5
13:38	8.9	7.9	7.7	2.4	57.1	8.4	1.3	2.6

c)   Effect of Bath Depth

Only one slag sample is listed in Table VII, at 8: 32, for a heat employing a 10 inch bath blown at 20 psig. The slags are lumpy up until this time and at 8: 32 (the end of the blow) the slag is very stiff. The low P_2O_5 contnet, 1.8%, reflects the poor dephosphorization of the bath.

Increasing the blowing pressure to 35 psig. produced a fluid slag in 5: 30. The P_2O_5 content listed in Table VII is 1.8%; however, the slag volume is large as indicated by the low CaO content, 24.6%. The additional volume was produced by attack of the lining as evidenced by 25.6% MgO. The bath is adequately dephosphorized indicating the importance of deep jet penetration, 7-1/2 inches, as opposed to 4-1/2 inches with 20 psig..

d)   Effect of Nozzle Diameter

The composition of one slag sample, taken at 13: 38, is listed in Table VII for heats blown with the 0.162 inch diameter nozzle. Slags were very lumpy until this time and this is reflected in the poor dephosphorization of the bath.

P_2O_5 Content of Probe Samples

The probe samples provide an interesting comparison with spoon (average) samples taken from other heats at about the same blowing time.

a)   Standard Conditions

In Table VIII the composition of probe samples, taken at 8 and 11 inches from the bottom of the converter, are presented. The 8 inch sample contains 3.7% P_2O_5 while the 11 inch sample contains 2.8% P_2O_5 indicating higher phosphorus contents closer to the bath. Since the average P_2O_5 at this time is about 2.5% this indicates lower P_2O_5 levels higher in the slag.

Table VIII

Composition of Probe Samples Taken From a Homogeneous Slag
and Comparative Average Compositions

Blowing Time (min.)	SiO_2	Fe_2O_3	Slag Composition FeO	Al_2O_3	(weight percent) CaO	MgO	MnO	P_2O_5
Standard Conditions - 8 inch height								
4:40	11.5	5.5	17.5	0.9	36.2	14.2	3.9	3.7
- 11 inch height								
5:21	9.8	8.4	26.0	0.8	38.1	9.5	3.5	2.8
- S-2 for comparison								
5:15	13.8	7.3	17.0	1.1	43.5	10.5	2.8	2.4
21 inch Blowing Height - 9 inch height								
3:15	5.4	9.7	32.6	2.3	21.3	22.4	1.9	0.7
- 11 inch height								
5:00	5.6	20.2	27.0	2.2	22.4	16.7	1.4	0.6
- S-2 for comparison								
4:15	10.4	9.7	28.4	4.6	33.3	6.2	2.7	3.5
0.162 inch diameter nozzle - 8 inch height								
12:15	10.5	7.0	28.4	2.3	27.9	13.2	4.7	0.9
- S-2 for comparison								
13:38	8.9	7.9	7.7	2.4	57.1	8.4	1.3	2.6

b)   Effect of Blowing Height

Compositions of the 9 inch and 12 inch level samples are 0. 6 - 0. 7 P_2O_5 for the 21 inch blowing height conditions, Table VIII.   Since the S-2 samples during the same time period contain 2. 6% to 3. 5% P_2O_5 there is a substantial phosphorus gradient very close to the bath surface.   This is reasonable because the slags produced under this condition are stiff allowing little slag circulation and phosphorus transport.

c)   Effect of Nozzle Diameter

Similar results are obtained by blowing with the 0. 162 inch diameter nozzle. The 8 inch probe sample contained 0. 9% P_2O_5 at 12: 15 in a very stiff slag.   By contrast the average (spoon) sample taken at 13:38 contained 2. 6% P_2O_5.   Here too, a phosphorus gradient is evident between the bath surface and the 8 inch sample height.

FeO Composition of Average Slag

Pronounced differences in FeO content are obtained when standard and soft blowing conditions are compared, Table VII, (p. 86). This is illustrated by average (spoon) samples.

a)   Standard Conditions

Under standard conditions the FeO reaches 7. 5% at 4: 00 and 17% at the end of the heat; therefore, with this type of blowing the FeO content of the slag remains low (8%) throughout the decarburization period of the bath and finally increases to about 17% which is in the composition range reported for commercial operations in Table III.

b) Effect of Blowing Height

Increasing the blowing height to 21 inches increases the FeO content of the slag as shown in Table VII. At 4:15 the % FeO in the slag produced with these conditions is 28.4% as opposed to 7.5 with standard conditions and the FeO content reaches about 35% at 5:30 as compared to 17% with standard conditions. Therefore, the chief difference in this condition compared with the standard is that the FeO contents of the slag are increased before the bath is decarburized. This high reserve of oxygen, coupled with the oxygen being delivered by the lance can lead to very high interface CO evolution and contribute to the slopping condition.

Table VII - Partially Repeated

Compositions of Homogeneous (Average, S-2) Slag Samples

For All Blowing Conditions

Blowing Time (min.)	SiO_2	Fe_2O_3	FeO	Al_2O_3	CaO	MgO	MnO	P_2O_5

S-2 Samples

Standard Conditions

4:10	15.8	4.6	7.5	2.8	48.8	11.2	3.3	3.3
5:15	13.8	7.3	17.0	1.1	43.5	10.5	2.8	2.4
5:30	9.9	8.9	22.2	0.9	40.0	9.8	3.1	2.3
5:32	9.2	6.3	10.5	4.9	50.8	9.8	2.4	2.8

21 inch Blowing Height

3:46	16.5	---	----	4.8	41.9	11.8	3.6	3.4
4:15	10.4	9.7	28.4	4.6	33.3	6.2	2.7	3.5
5:30	9.2	10.9	31.4	3.9	28.8	9.2	2.8	2.9
5:32	7.2	8.9	39.9	3.2	28.6	6.4	2.0	2.6

8) <u>Special Heats</u>

After a review of the preceding data special heats were made to investigate the following points:

a) The role of the basic slag in dephosphorization,

b) The effect of high initial phosphorus on bath dephosphorization,

c) The nature and amount of metal droplets thrown up by the jet,

d) The role of droplets in dephosphorization.

a) The Role of the Basic Slag in Dephosphorization

Heat R-40 was made without a flux addition and started with a clean metal surface to determine what portion of dephosphorization is caused by MgO from the lining or by vaporization of $\underline{P}$ or P_2O_5. The heat was run under standard conditions although it was stopped intermittently to take metal samples.

The results of this heat are summarized in Table IX.

Table IX

Composition of a Bath Blown under
Standard Experimental Conditions but Without Flux

Blowing Time (min.)	% P	% Si	% C	% Mn
0	0.22	0.28	3.90	0.26
1-1/2	0.22	0.01	3.36	0.06
3	0.20	<0.01	1.30	0.06
4-1/2	0.22	<0.01	0.20	0.08

Final Slag: 66.4% SiO_2,   16.9% Fe_2O_3,   5.5% FeO,   3.1% CaO, 0.3% P_2O_5

Silicon, carbon and manganese are all reduced in the usual manner while the phosphorus content is virtually unchanged. The final slag is acid with 0.3% P_2O_5 and 16.9% Fe_2O_3.

Three points are evident in these results. Dephosphorization by vaporization of $\underline{P}$ or P_2O_5 is not obtained. MgO from the furnace lining is not a major factor in bath dephosphorization under normal conditions. The Fe_2O_3 -FeO ratio in the slag is very large in this case compared to a normal run. This indicates the role of the basic slag in a normal run in dephosphorization.

b)   The Effect of High Initial Phosphorus on Bath
Dephosphorization

Heat R-41 was run with 0.76% initial phosphorus. Four sampling locations were placed with centerlines 6 inches above the bottom of the converter. In all other aspects the heat was run under standard conditions using flux.

The results of this heat are compared to the usual experimental data in Figure 42. The dephosphorization rate is higher with higher initial phosphorus, and, as expected, the phosphorus content of the slag is higher.

c)   The Nature and Amount of Metal Droplets Thrown Up
By the Jet

Heat R-39 was run to determine the amount and size distribution of the droplets thrown up by the oxygen jet under various blowing conditions. The techniques used for this heat were described in the Experimental Procedure section.
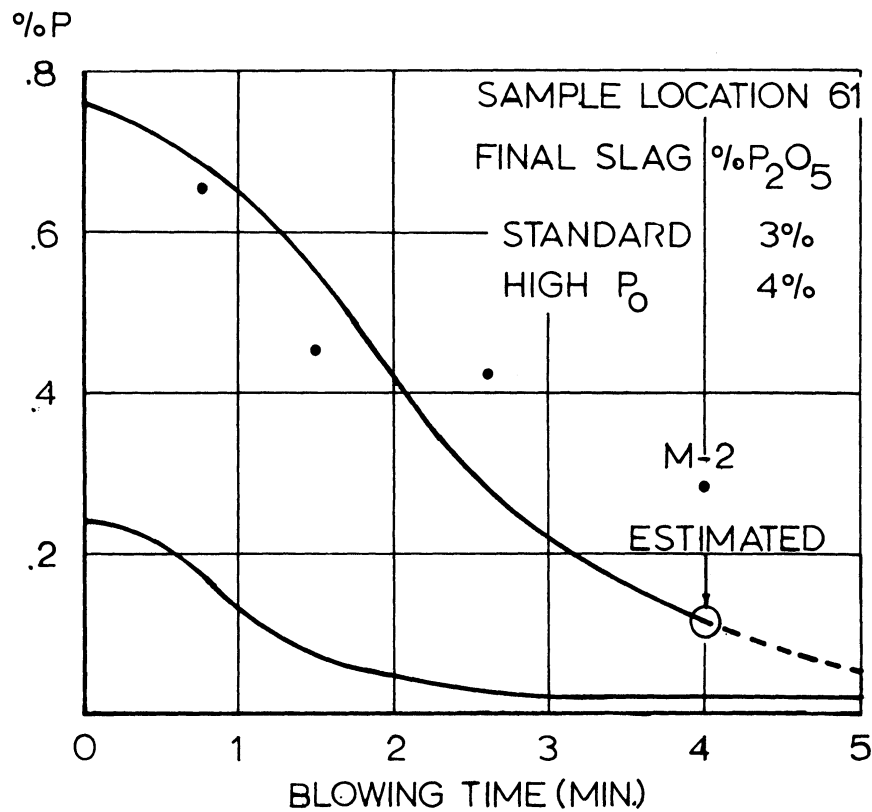
Fig. 42. % Phosphorus Versus Blowing Time at Sampling
Location 61 for Initial % Phosphorus of 0.76% and 0.24%.

The weight of droplets thrown up is tabulated in Table X.

Table X

Distribution of Droplets in the Converter

(Values are lb. of droplets thrown up/min.)

Blowing	Oxygen	Bath Radii			
Ht. (in.)	(psig.)	2 - 3	3-5-1/4	5-1/4-8	Total
7	10	3	2	1	6
7	20	25	12	3	40
7	30	14	40	6	60

The weight of droplets increases with blowing pressure. During
a 5-1/2 minute run with standard experimental conditions the weight
of droplets thrown up is equal to the weight of the bath. Under
standard experimental conditions the flux of droplets across the bath
surface decreases with distance from the center.

The droplets collected are found to range in size from
0. 1 cm. to 0. 6 cm. in diameter. Several were subjected to
metallographic examination and a typical structure is shown in Figure
43.
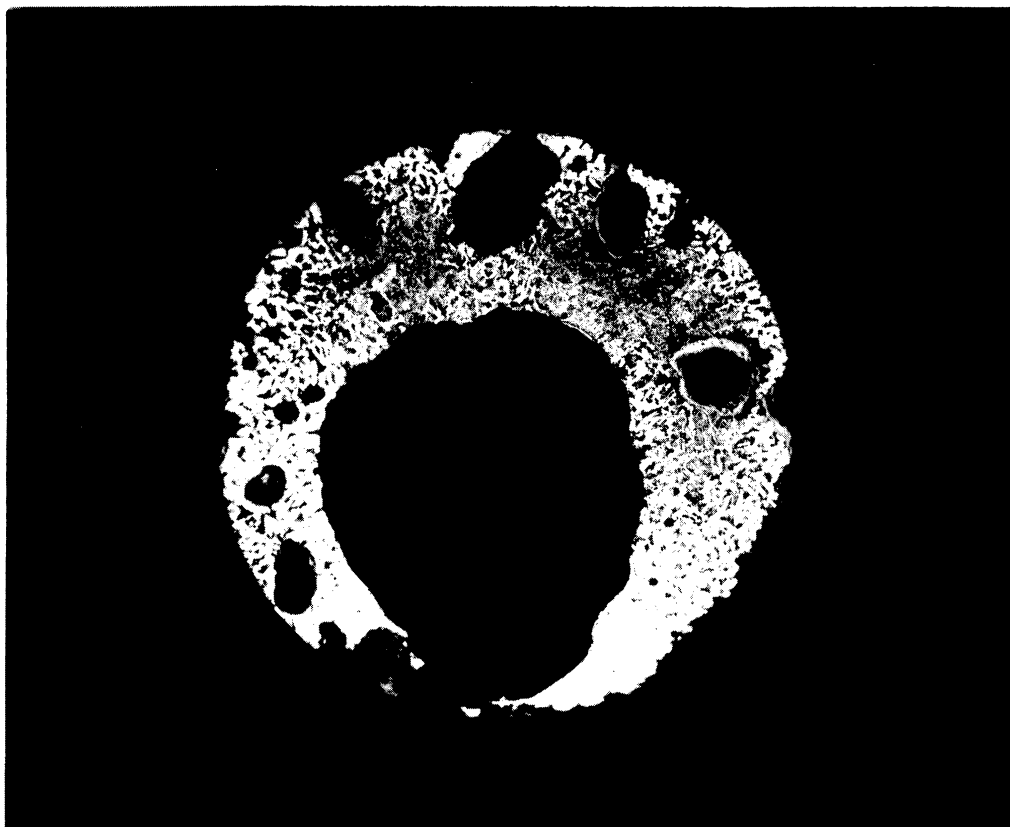
Fig. 43. 0. 6 cm. Diameter Droplet Showing Ferrite,
Pearlite and Gas Holes. 2% Nital Etch, 20X.

The large dark interior areas are gas holes. These gas holes are
found to account for at least 50% of the sample volume, apparent
density $\approx$ 3. 5 gm/c. c. . Of greater importance is that the droplet
is composed of ferrite and pearlite in a ratio indicating about
0. 4% C although the bath contained 3. 6% C at the time.

d)   The Role of Droplets in Dephosphorization

Heat R-38 was run under standard experimental conditions except that all but one of the sampling locations at the bath surface one inch from the wall were protected from falling metal droplets by a refractory shield. Four sampling locations were prepared with centerlines 6 inches above the bottom.

The % P at location 61 of this special heat is compared with standard data in Figure 44. Compared to standard conditions, dephosphorization is retarded at the protected locations and not retarded in unprotected sampling location near the bath surface.
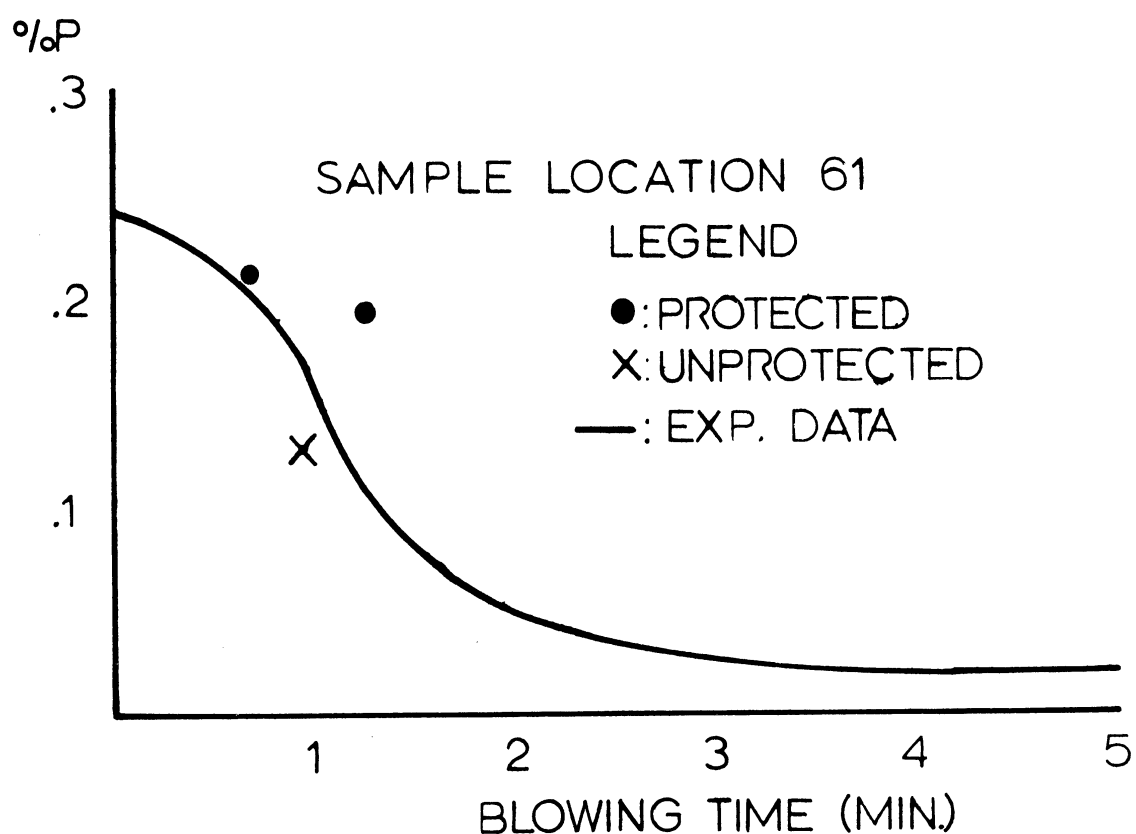
Fig. 44.   % Phosphorus Versus Blowing Time for Protected and Unprotected Samples Taken at Sampling Location 61.

9) Summary of the Results

The changes in bath chemistry and temperature for all
of the blowing conditions are summarized in Figures 45 and 46
by plotting P, Si, and C contents or temperature versus blowing
time at two critical sample locations. The sample locations are
56 and 11 for those conditions employing a 6 inch bath depth or
86 and 21 for that condition employing a 10 inch bath depth.

By using these summary graphs the effect of a given
operating condition upon chemistry and temperature can be seen.

a) Standard Conditions

Dephosphorization is faster and more extensive at the
top of the bath than at the bottom as shown by comparing the curves
marked 1 in Figure 45. Similarly, silicon oxidation, curves 2,
and decarburization, curves 3, proceed faster and more extensively
at the top of the bath than at the bottom, and temperatures are
higher at the top of the bath as shown in Figure 46.

The more extensive oxidation at the top of the bath is due
to the proximity of the slag-metal interface and the falling droplets
in the case of dephosphorization or the proximity of the oxygen
source (the heat source) in the cases of silicon oxidation, decar-
burization and bath temperature.

The completion of silicon oxidation before dephosphorization
or decarburization rates increase is best shown in Figure 45 at
location 56. Silicon oxidation is complete at 1: 00 while the
maximum rates of dephosphorization and decarburization are found
at 2: 00.
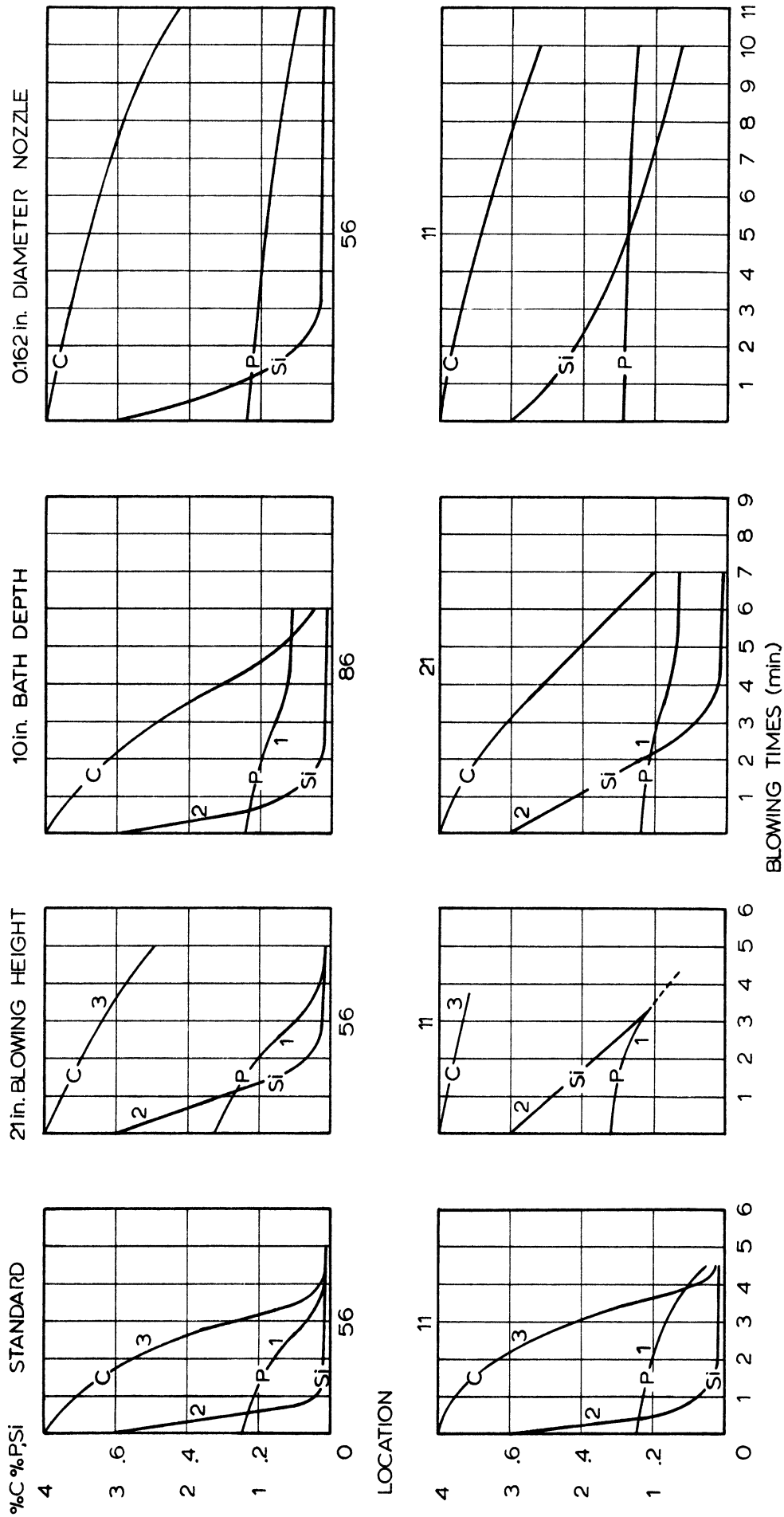
Fig. 45. Summary Plots of P, Si, and C Contents at 2 Sample Locations Versus Blowing Time for all Blowing Conditions.
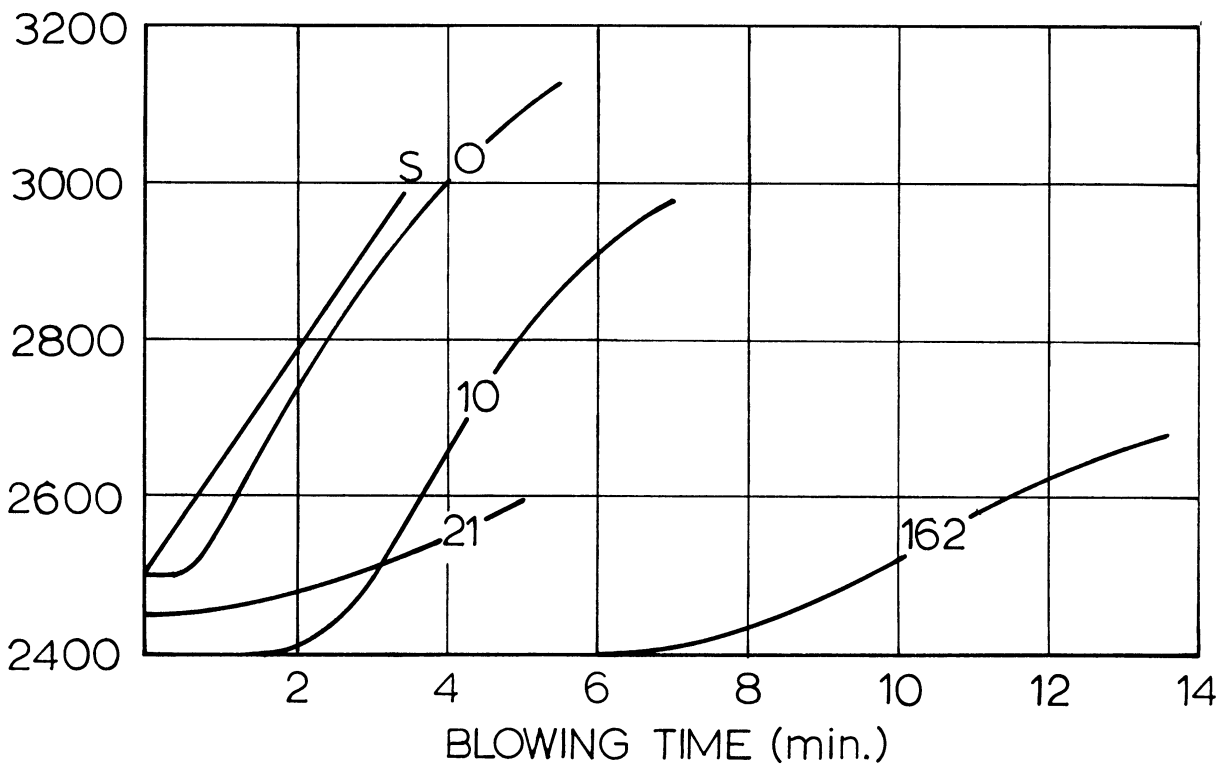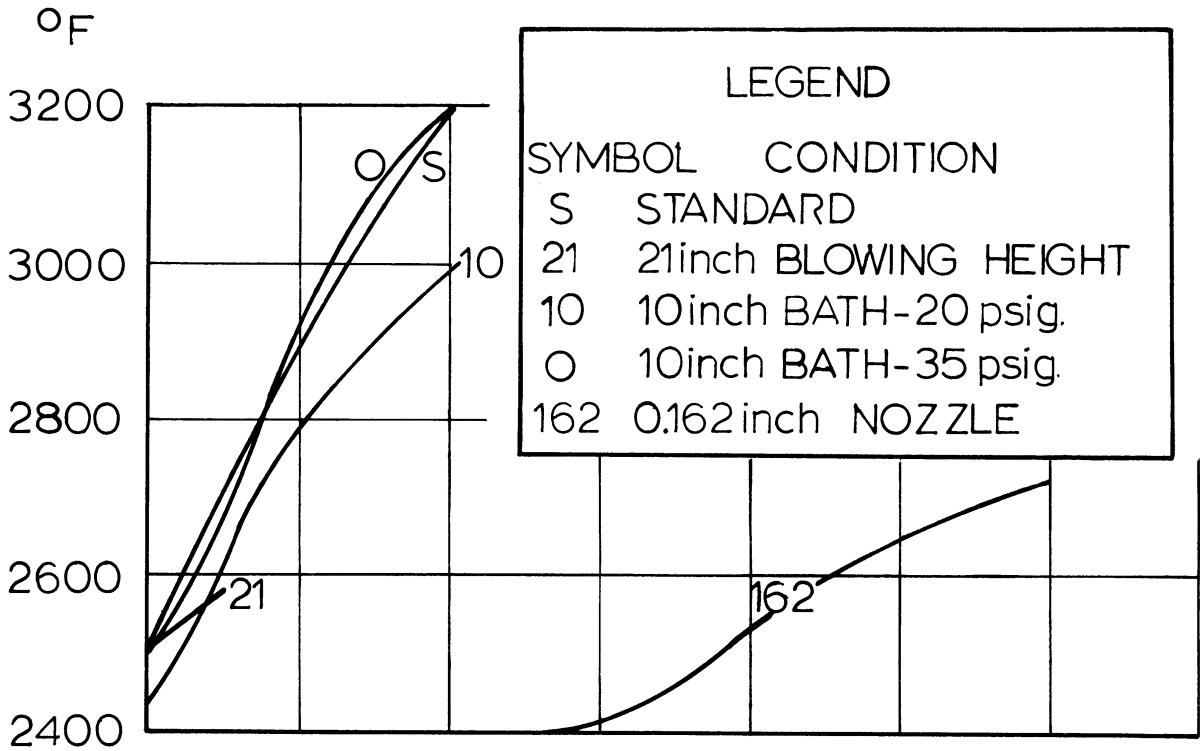
Fig. 46. Summary Plots of Bath Temperature at 2 Locations Versus Blowing Time for all Blowing Conditions.

b)   21 inch Blowing Height

In this case, dephosphorization is faster and more extensive near the bath surface than it is near the bottom as shown in Figure 45.   Similarly, silicon oxidation and decarburization proceed faster and more extensively at the surface and the bath temperature at the surface is higher as shown in Figure 46.

The reasons for these variations are the same as those for standard conditions.   Of greater importance however are the differences produced by increasing the blowing height.   Dephosphorization under these and standard conditions is proceeding rapidly near the bath surface, but near the bottom of the bath dephosphorization is much slower than under standard conditions as seen by comparing the curves marked 1 on the plots.   This is due to greater jet penetration under standard conditions causing greater circulation which transports low phosphorus material to all parts of the bath. The same reason explains the much larger differences in silicon content from the top to the bottom of the bath blown from 21 inches as seen by comparing the curves marked 2.

The differences in carbon content from the top to the bottom of the bath blown from 21 inches are large;   however, the significant comparison regarding decarburization between the two systems is the extent of decarburization at corresponding sampling locations. Under standard conditions the carbon content at location 56 at 5: 00 is 0. 1% while at the same location and time the carbon content of a bath blown from 21 inches is 3%, curves 3.   This difference is not explained by differences in circulation but the data suggest that the character of the jet and of the decarburization mechanism are changed by increasing the blowing height.

c)   10 inch Bath Depth

Dephosphorization, silicon oxidation and decarburization
are faster and more extensive near the top of the bath than near the
bottom, Figure 45.   The effect of a decreased jet penetration -
bath depth ratio on circulation is best shown in Figure 46 by differences
in temperature at the two locations.   Near the top of the bath the
temperature begins to increase at the initiation of blowing and
continues to increase throughout the heat.   At the bottom of the
bath the temperature remains constant for 2 minutes before beginning
to increase.   This two minute delay is caused by the absence of
circulation at the bottom of the bath.

Silicon oxidation and decarburization are slower than with
standard conditions but equally extensive.   The lower rate is due
to decreased oxygen flow rate per pound of bath.   Dephosphorization
is slower and not as extensive as with standard conditions,   curve 1.
The high phosphorus content in the 10 inch bath is not due simply
to the decreased oxygen rate because,   as shown,   silicon is oxidized
to low bath content,   curves 2.   The high final phosphorus content
is due to the dry,   low FeO slag produced under these conditions
emphasizing the importance of a fluid active slag to dephosphorization.

d)   0. 162 inch Diameter Nozzle

Dephosphorization, silicon oxidation and decarburization
are faster near the top of the bath than near the bottom.   The
maximum extent of dephosphorization and decarburization is not
known because the heats were not run to completion.   The effect
of decreasing the nozzle diameter is to decrease the oxygen flow
rate to 30% of that under standard conditions and to decrease jet
penetration to 40% of that under standard conditions thus decreasing

the heating rate and circulation of the bath, Figure 46. The temperature
near the bath surface remains constant during the first four minutes
of the run. During this time the flux is being heated. The temp-
erature near the bottom of the bath remains constant for six minutes.
The additional two minutes are the time required to circulate
hot metal from the top of the bath to the bottom.

10) Mathematical Analyses

In this section the data are subjected to four types of mathematical analyses: a) Mass Balance, b) Oxygen Efficiency and Utilization, c) Comparison Between Equilibrium and Actual Phosphorus Contents and d) Comparison Between Dephosphorization Mechanisms and Data.

a) Mass Balance

The mass balance is performed by calculating the weight of element J which is charged with the hot metal and comparing this with the weight of the element in the metal and slag at the end of a run.* These calculations are made for all blowing conditions. The results are given in Table XI in terms of "accountable element J" which is defined as the ratio of the weight of J at the end of the blow to the weight of J at the beginning of the blow.

The weight of phosphorus and manganese in the system calculated from final metal and slag compositions is close to the weight of phosphorus and manganese charged in the hot metal. The calculated final silicon weight is consistently greater than the initial silicon weight for all experimental conditions.

Table XI

Accountable Element J for All Blowing Conditions

bath depth	6	6	10	10	6
blowing height	7	21	7	7	7
blowing pressure	20	20	20	35	25
nozzle diameter	0.316	0.316	0.316	0.316	0.162
Accountable P	1.1	1.1	1.0	1.3	0.9
Accountable Si	1.5	1.3	1.8	1.5	1.5
Accountable Mn	1.0	1.1	0.8	1.1	0.9

* The mass balance is derived in Appendix II, Calculations.

b)   Oxygen Efficiences and Utilizations

Oxygen efficiences* and utilization are calculated by assuming formation of SiO_2, MnO, P_2O_5, and CO.   When the oxygen efficiency is less than 70%, CO is replaced by CO_2 in the calculation.   Oxygen efficiencies and utilizations are tabulated in Table XII for all the blowing conditions.

The oxygen efficiencies are generally high except in the case of the 21 inch blowing height experiment where oxygen efficiency is 51% assuming all CO or 69% assuming all CO_2.

Table XII

Oxygen Efficiency and Utilization for All Blowing Conditions

O_2 In (lb.)	O_2 to P (lb.)	O_2 to Si (lb.)	O_2 to Mn (lb.)	O_2 to C (lb.)	O_2 to Fe (lb.)	O_2 Eff. (%)
Standard Conditions at 5:30						
23.3	0.53	1.6	0.32	13.3	3.8	84
21 inch Blowing Height at 5:30						
23.3	0.72	1.7	0.27	3.9	5.7	51
23.3	0.72	1.7	0.27	7.8*	5.7	69*
10 inch Bath Depth, 20 psig at 8:32						
36.1	0.58	2.2	0.32	21.4	0.91	73
10 inch Bath Depth, 35 psig at 5:30						
33.12	0.80	2.7	0.46	20.2	7.4	95
0.162 inch Diameter Nozzle at 13:38						
12.7	0.48	1.1	0.19	7.2	1.4	82

* Assumed 100% CO_2.

* An oxygen efficiency calculation is given in Appendix II, Calculation.

Oxygen efficiences and utilizations are calculated at

30 second intervals for standard and 21 inch blowing height conditions.

These calculations are referred to as differential oxygen efficiencies

and utilizations.

Differential oxygen efficiency and utilization for standard

conditions are plotted in Figure 47. Oxygen efficiency is relatively
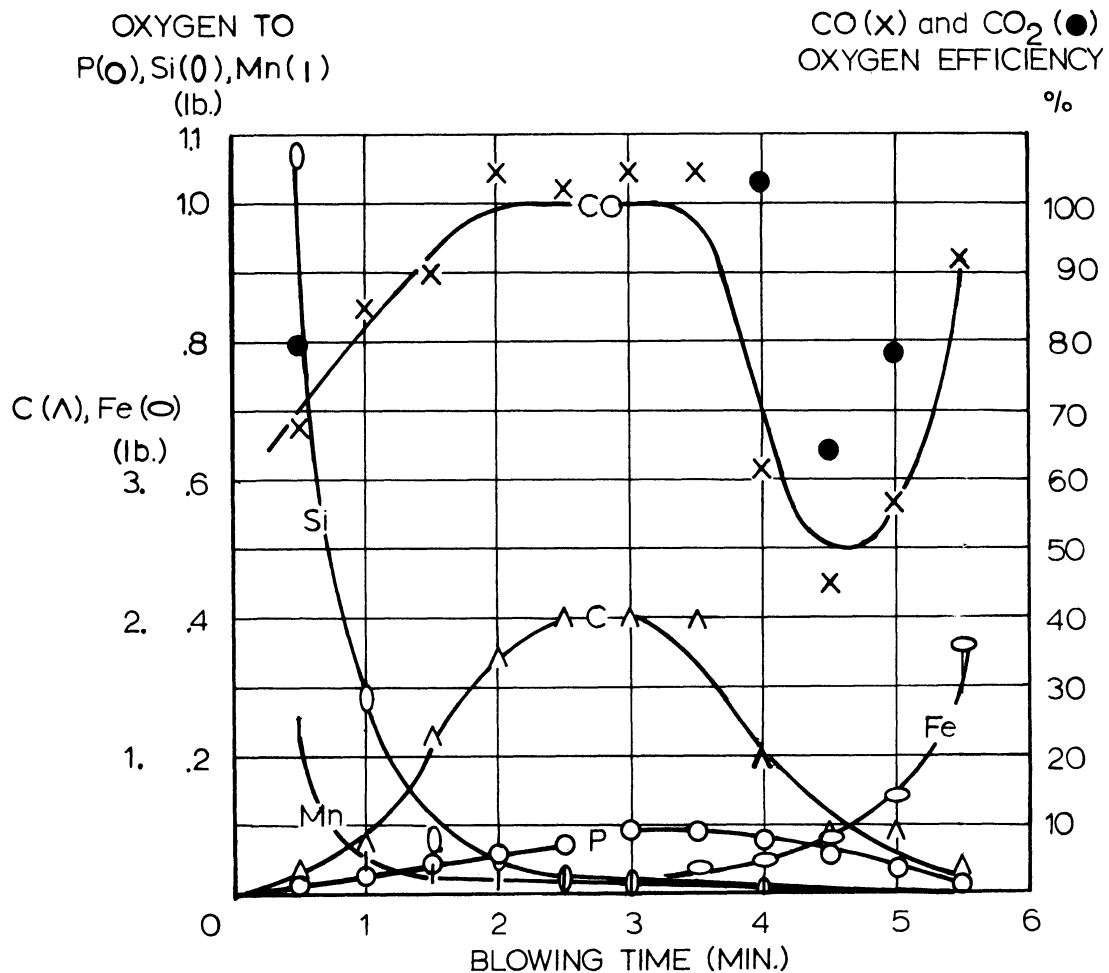
Fig. 47. Differential Oxygen Efficiency and Utilization Versus Blowing Time with Standard Conditions.

high throughout the experiment. The order of occurrence of maximum

oxidation rates is silicon and manganese at 0: 30, carbon at 2: 30,

phosphorus at 3: 00, and iron at 5: 30. One lb. of oxygen is used to

oxidize Si in the first 30 seconds. 2.7 lb. of oxygen are used to oxidize carbon between 2: 00 and 2: 30. 1.9 lb. of oxygen are used to oxidize iron between 5: 00 and 5: 30. The time intervals when oxygen efficiencies are plotted for both CO and CO_2 indicate that sufficient oxygen is available for either gaseous product.

The differential oxygen efficiency and utilization plot for the 21 inch blowing height condition is shown in Figure 48. Silicon
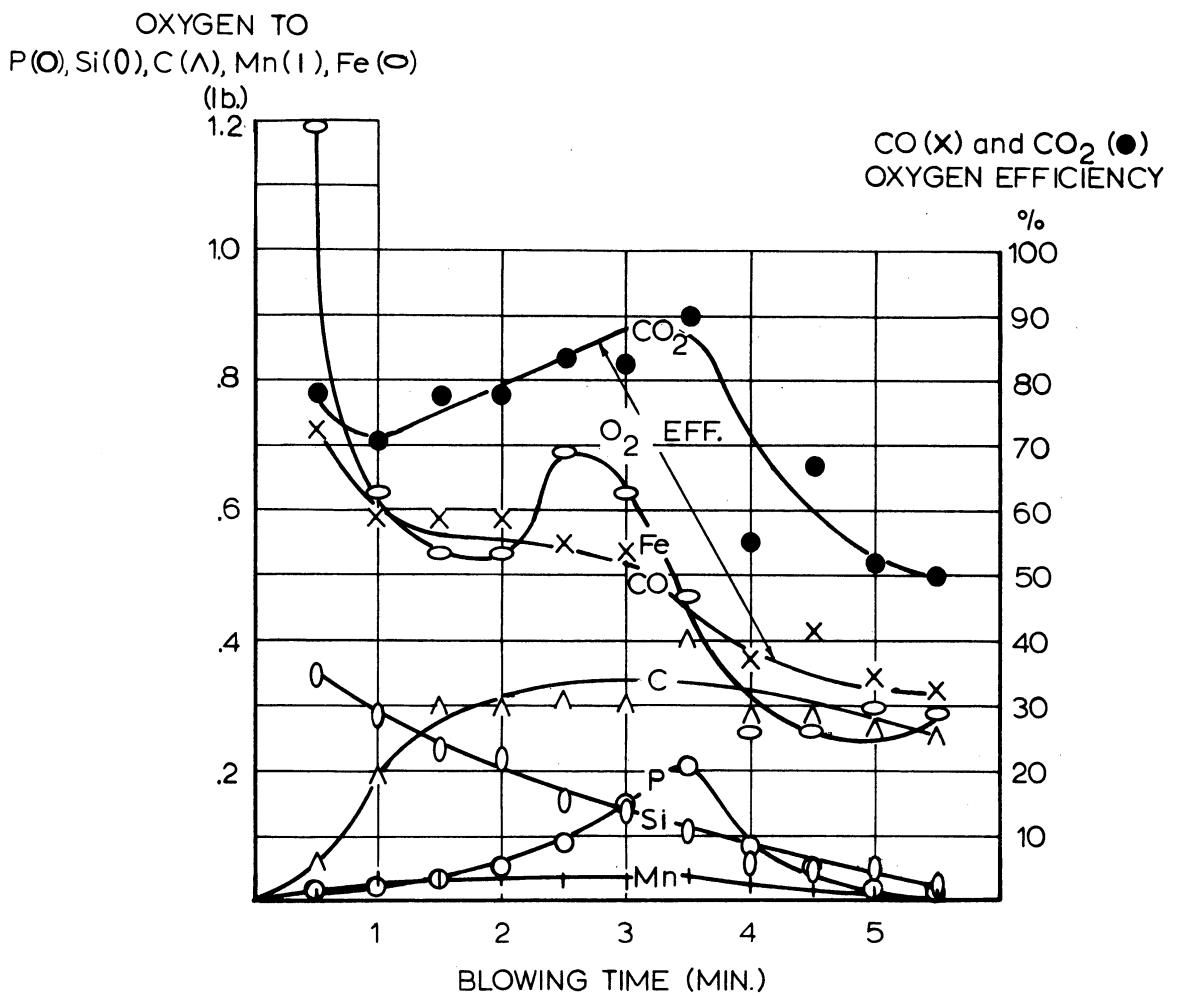
Fig. 48. Differential Oxygen Efficiency and Utilization Versus Blowing Time with 21 inch Blowing Height.

and iron are oxidized first with manganese and carbon not having clear maximum oxidation periods and phosphorus is oxidized most

rapidly at 3:30. 1.1 lb. and 0.35 lb. of oxygen are used to oxidize

iron and silicon respectively during the first 30 seconds. 0.76 lb./

minute and 0.08 lb./minute of oxygen are used to oxidize carbon and

manganese respectively for long periods. 0.21 lb. of oxygen are

used to oxidize phosphorus between 3:00 and 3:30. Oxygen

efficiencies assuming 100% CO are quite low. Higher efficiencies

are attained if all the carbon is assumed to be oxidized to CO_2.

Even in this case, efficiencies decreased toward the end of the blow.

c)   Comparison Between Equilibrium and Actual Phosphorus Contents

Equilibrium phosphorus content in the bath is calculated

on the basis of thermodynamic data reported in the Review of

Literature.. The slag compositions used in these calculations

are final slag compositions and have been reported earlier. The

temperature of the slag is assumed to be less than the temperature

of the metal. The specific temperature used is reported in Table

XIII along with the calculated equilibrium phosphorus content of the

bath surface and the average bath % P.

Equilibrium between the bath and slag phosphorus is not

attained at the end of a run on the basis of the equilibrium calculations.

The slag temperatures assumed are about 300°F below the metal

temperature and an increase in slag temperature to metal temp-

erature would increase equilibrium phosphorus content more than

100 times. For example, if the slag on a bath blown under standard

conditions reached a final temperature of 3200°F the equilibrium

phosphorus content would be 0.4% or almost twice the initial

phosphorus content of the bath.

Table XIII

Comparison of Equilibrium and Actual Phosphorus Contents
for All Blowing Conditions

bath depth	6	6	10	10	6
blowing height	7	21	7	7	7
blowing pressure	20	20	20	35	25
nozzle diameter	0.316	0.316	0.316	0.316	0.162
equilibrium % P	0.004	0.002	0.02	0.004	0.01
bath surface % P	0.019	-----	0.11*	0.022	0.1*
average bath % P	0.021	0.017	----	0.047	0.07*
slag temperature (°F)	2900	2800	2800	2900	2700

* Blowing time is less than that required to fully decarburize.

d) Comparison Between Dephosphorization Mechanisms
and Data

Four mathematical models were developed to test dephos-
phorization mechanisms* under standard conditions. The mechanisms
tested were: 1) bulk diffusion, 2) boundary layer diffusion,
3) dilution by dephosphorized metal droplets, and 4) a combination
of boundary layer diffusion and dilution.

1) Bulk diffusion is suggested as a dephosphorization
mechanism by the higher phosphorus gradient near the slag-metal
interface. The model is calculated with Fick's Second Law by
assuming a phosphorus content of 0.22% at blowing time 1:00 and
calculating the change in the surface concentration with time.

* The models are derived in Appendix II, Calculations.

This model (% phosphorus-time curve 1) is compared

to average bath % phosphorus data (curve D) in Figure 49. The model
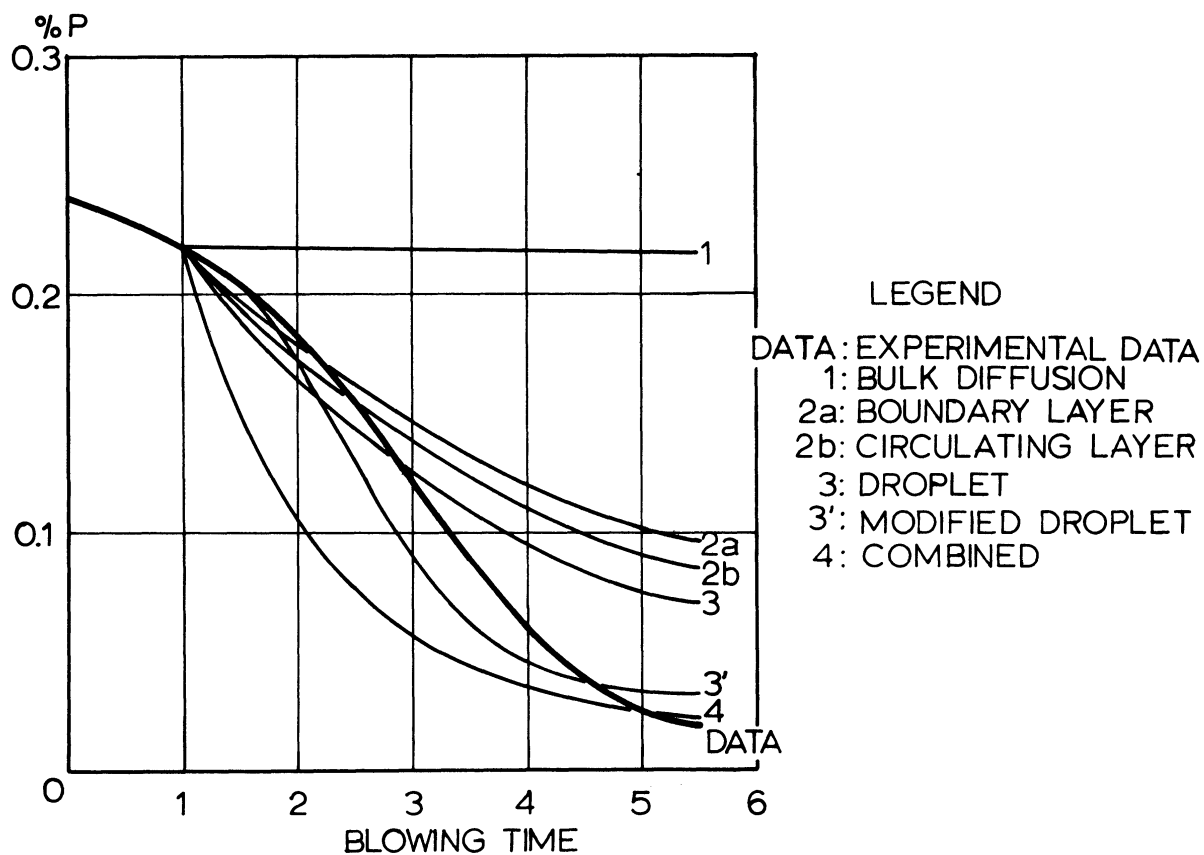
Fig. 49. Average Bath % Phosphorus Calculated from Mass Transfer Models Compared to the Data - Standard Conditions.

does not fit the data indicating that bulk diffusion is not the dephos-

phorization mechanism and that bulk diffusion makes little or no

contribution to phosphorus transfer.

2a) Boundary layer diffusion from a turbulent bath is

suggested by the bath turbulence in the converter. The model is

calculated by assuming on a phosphorus content of 0.22% at 1:00

and then calculating the decrease in average bath % P due to phosphorus

transfer across the metal boundary layer.

This model is plotted as curve 2a in Figure 49. The model and the data agree in magnitude from 1:00 to 2:30; however, the model curve has the wrong slope.

2b) <u>Boundary layer diffusion</u> from a circulating bath is suggested by the bath circulation. The model is calculated by assuming 0.22% P at 1:00 and a surface layer of thickness ℓ through which metal is circulated from the lower bath at the center of the converter outward to the wall. This model checks not only the mechanism but the direction of bath circulation.

This model is plotted as curve 2b in Figure 49. Like 2a, this model and the data agree in magnitude from 1:00 to 2:30; however, the model curve has the wrong slope. The % P in the surface layer calculated from the model is compared to data in Figure 50 at the three sampling locations in the 6-1/2 inch row. The model, curve 2b, does not fit the data well; however, a decrease in phosphorus content from the center to the wall which is predicted by the model is shown clearly in the data indicating that the outward circulation assumed in the model is correct.

3) <u>Dilution by dephosphorized metal droplets</u> is suggested by the effect of metal droplets on dephosphorization which was shown to be an important part of bath dephosphorization in Run R-38. The model was calculated by assuming 0.22% P at 1:00. The droplets are assumed to be thrown up by the jet, fall through the slag, and return to the bath containing 0.04% P from 1:00 to 4:30 and 0.02% P from 4:30 to 5:30. The rate at which droplets are thrown up is 100 cc/sec. for the model.
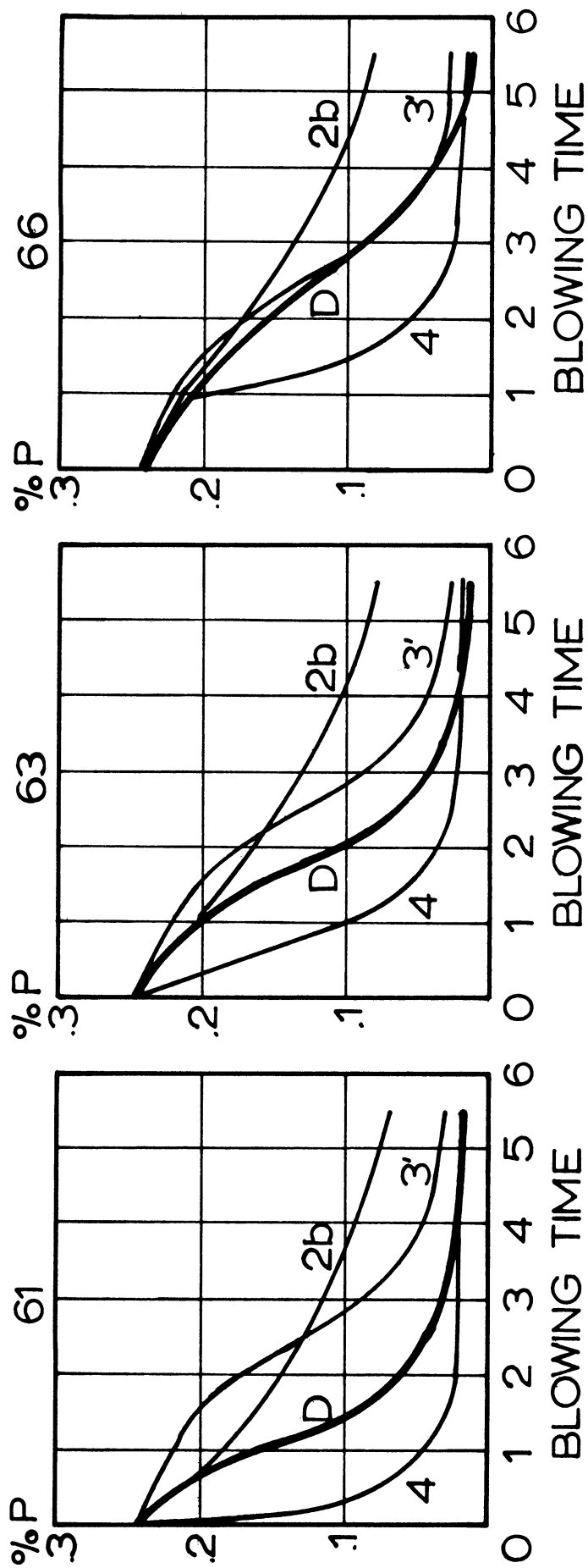
Fig. 50. Surface % Phosphorus Calculated from Mass Transfer Models Compared to the Data - Standard Conditions.

This model is plotted as curve 3 in Figure 49. The model and the data agree in magnitude from 1:00 to 2:30; however, the slope of the model curve is in the wrong direction.

3') This model differs from model 3 in that the rate at which metal droplets are thrown up is assumed to be proportional to the rate of decarburization. The rate at which droplets are thrown up increases from 100 cc/sec. at 1:00 to 300 cc/sec. between 2:30 and 4:00.

This model is plotted as curve 3' in Figure 49. The model does not agree with the data until 4:30; however, the model is significant in that it produces a curve with the same slopes as the data curve. If the model curve is translated to the right a distance equivalent to 30 seconds it fits the data almost exactly. While the model does not predict changes in surface concentration with distance from the center, it is plotted in Figure 50 as curve 3'. The model is in good agreement with the data at sampling location 66 and lagged behind the experiment data at locations 63 and 61.

4) <u>Combination of boundary layer diffusion (2b) and dilution (3)</u> is suggested by these realities of converter operation. The two models are described above and were combined by determining the flux of droplets across the bath surface. The flux is determined from Run R-39 to be $40/r^3$, cc./sq.cm./sec. or cm/sec. The flux decreases rapidly with increased distance, r, from the center.

This model is plotted as curve 4 in Figure 49. The model agrees with the data at 5:00. Before this, phosphorus content calculated by the model is lower than actual bath phosphorus contents.

The surface concentrations at the sampling location calculated from the model are compared to the data in Figure 50. The model is plotted as curve 4. The phosphorus content calculated by the model is lower than the actual phosphorus content at all three sampling locations. As in the case of model 2b, decreasing % P with increasing r is predicted by the model and reflected in the data.

To summarize, the relationship between phosphorus content and blowing time is not calculated from any of the models with sufficient accuracy to deem that model a success; however, the models do serve to emphasize two important features of the results. First the decrease of % P in the surface layer from the center to the wall of the converter is predicted by assumed outward circulation in models 2b and 4. Second, the interrelation of the elements in the metal bath is emphasized in model 3' with which the shape of the dephosphorization curve is predicted by assuming that the droplet volume is proportional to the rate of decarburization.

Conclusions

1. Pronounced chemical and thermal gradients are demonstrated in the bath of a pilot size oxygen converter. The chemical gradients are shown for the first time. Both the chemical and the thermal data indicate a circulation pattern which is up at the center and radially outward at the surface. This is contrary to a large group of publications. These gradients are all strongly affected by operating conditions as indicated in the following conclusions.

2. Dephosphorization occurred most rapidly under conditions of deep penetration, e. g., standard conditions. With soft blowing, good dephosphorization at the slag-metal interface was attained but a severe gradient developed due to poor circulation. Experiments with a 10 inch bath indicated that penetration should be increased to accompany the greater metal depth.

While dephosphorization was encountered at the bath-slag interface with soft blowing, a second mechanism was encountered with hard blowing. The reduced rate of dephosphorization at locations which were protected from metal droplets falling through the slag, showed that these droplets contributed significantly to bath dephosphorization.

3. Silicon oxidation went to completion under all conditions because this reaction did not require direct transfer of the element from the metal to the slag. In other words, silicon could react with oxygen anywhere in the bath to form SiO_2 and then find its way to the slag. Despite this ease of oxidation, silicon gradients were present similar to phosphorus gradients and developed earlier. Manganese behaved similarly but was oxidized more slowly and to a lesser extent than silicon.

4.   Carbon gradients developed later than those for manganese and silicon. It is significant that even at the height of decarburization, steep gradients were present which indicated circulation upward at the centerline.

5.   Compositional gradients were also determined for the slag in a few cases and showed a higher phosphorus content near the metal interface.

6.   The thermal gradients indicated that the metal moved radially outward from the jet impingement zone. The maximum temperature measured during a heat was 3250°F. at the top of the bath, 1-1/2 inches from the centerline. The metal at the bottom of the bath was colder than the metal across the top surface.

7.   The data indicate that best operating practice for dephosphorization is to penetrate deeply, i. e. , beyond the center of the bath, while adding flux at a rate to insure a fluid slag.

Appendix I, Data

The data are presented in Tables XIV and XV below.
Location AB = A + 1/2 in. above the bottom of the converter and
B in. from the wall. Sample M-1 is the chill-cast bath sample
taken before the run. Sample M-2 is the chill-cast bath sample
taken after the run. In Table XV sample S-2 is the slag sample
taken after a run.

In both tables the data are tabulated by blowing conditions:
standard, 21 inch blowing height, 10 inch bath and 0.162 inch
diameter nozzle conditions in that order. For each condition
the data are tabulated from the lowest to the highest samples and
from the wall toward the center of the converter. For example,
data from sample location 11 are the first tabulated and data
from sample location 66 the last.

TABLE XIV

Blowing Time - Metal Composition Data
for all Blowing Conditions

Heat No.	Blowing Time	Metal Composition		(weight percent)	
		P	Si	C	Mn
		Location 11			
26	0:20	.24	.41	4.00	.36
27	0:20	.20	.25	----	.30
23	1:00	.21	.07	3.88	.14
25	1:00	.22	.08	3.80	.13
37	1:15	.21	---	----	---
20	1:45	.25	.02	3.25	.11
25	3:00	---	---	1.19	.13
17	3:15	.17	<.05	1.48	.29
37	3:30	.16	---	1.58	.18
20	3:45	.21	.02	1.61	.20
27	4:30	.05	<.02	0.10	.11

Heat No.	Blowing Time	Metal Composition (weight percent)			
		P	Si	C	Mn

Location 13

23	1:00	.18	---	3.42	.17
24	1:00	.23	.10	3.85	.14
25	1:00	.20	---	3.34	.15
37	1:15	.21	<.05	----	---
26	2:00	.07	<.05	0.15	.13
37	3:30	.18	---	----	.20
20	3:45	.18	.04	1.33	.22

Location 16

27	0:20	.23	.35	3.57	.38
25	1:00	.19	.08	3.26	.19
37	1:15	.18	<.05	3.15	---
26	2:00	.05	.10	----	.11
23	3:00	.09	.06	1.69	.18
25	3:00	.12	.04	1.88	.14
37	3:30	.16	---	1.38	.19
20	3:45	.16	---	----	.21

Location 31

26	0:35	.22	.17	3.46	.19
37	0:40	.24	---	----	---
20	1:30	.24	.03	3.44	.10
23	2:16	.14	<.05	2.80	.17
37	2:46	.18	---	----	---
17	3:00	.27	<.05	1.76	.25
27	3:45	.03	.02	0.10	.10
26	5:00	.02	.01	0.04	.11

Location 33

20	1:30	.24	.03	2.98	.13
37	2:46	.17	---	----	---
17	3:00	.18	<.05	1.55	.33
27	3:45	.04	<.02	0.10	.10
25	4:00	.09	<.05	1.16	.14
26	5:00	.02	.02	<0.10	.10

Heat No.	Blowing Time	Metal Composition (weight percent)			
		P	Si	C	Mn

Location 36

Heat No.	Blowing Time	P	Si	C	Mn
37	0: 40	.20	<.05	3.04	.12
37	2: 46	.14	---	1.26	.17
17	3: 00	.17	.08	1.75	.30
27	3: 45	.04	<.01	0.10	.12
25	4: 00	.10	<.01	1.06	.15
26	5: 00	.02	.01	0.06	<.10

Location 51

Heat No.	Blowing Time	P	Si	C	Mn
24	0: 45	.14	.17	3.28	.15
25	0.45	.22	.08	3.90	.15
25	2: 00	.14	<.05	2.92	.13
26	3: 00	.09	.07	2.85	.18
37	3: 00	.17	---	1.91	.17
26	4: 15	.02	<.05	<.10	<.10
27	4: 15	.09	.11	----	.13
27	5: 00	.01	.01	0.04	---

Location 53

Heat No.	Blowing Time	P	Si	C	Mn
24	0: 45	.20	---	3.35	.12
25	0: 45	.20	.12	3.34	.20
37	1: 30	.18	---	----	---
37	3: 00	.13	---	----	---
26	4: 15	.02	.06	0.05	<.10
27	5: 00	.02	.02	0.06	<.10

Location 56

Heat No.	Blowing Time	P	Si	C	Mn
24	0: 45	.23	.09	3.54	.12
23	0: 46	.09	<.05	----	.20
25	2: 00	.09	<.05	----	.17
14	2: 45	---	.02	1.81	.25
27	5: 00	.02	.01	.06	<.10

Location 61

Heat No.	Blowing Time	P	Si	C	Mn
23	1: 45	.07	<.01	1.79	.13
37	2: 00	.22	---	2.31	.28
37	3: 16	.15	---	1.35	.20
27	3: 30	.02	<.05	0.04	<.10
27	4: 45	.02	---	0.06	<.10

Heat No.	Blowing Time	Metal Composition		(weight percent)	
		P	Si	C	Mn

Location 63

23	0:34	.12	---	2.24	.15
20	1:00	.20	.02	1.72	.19
17	2:30	.17	<.05	1.46	.25
37	3:16	.15	---	1.49	.21
27	4:45	.02	.06	0.06	<.01

Location 66

26	0:05	.16	.08	3.06	---
23	0:34	.21	.08	3.70	.14
20	1:00	.19	.02	----	.20
37	2:00	.14	---	1.25	.18
17	2:30	.16	.05	1.40	.24
37	3:16	.18	---	----	---
27	4:45	.02	<.05	0.04	.10

Sample M1

17		.43	.55	3.99	.60
20		.33	.52	3.97	.48
23		.22	.50	4.16	.41
24		.24	.53	4.14	.48
25		.24	.53	4.14	.48
26		.23	.41	4.00	.36
27		.25	.54	3.99	.57
37		.22	.58	4.00	.48
38		.201	.48	4.03	.50
39		.03	.10	3.96	.04
40		.218	.28	3.90	.26
41		.760	.50	3.70	.48

Heat No.	Blowing Time	Metal Composition (weight percent)			
		P	Si	C	Mn

Sample M2

Heat No.	Blowing Time	P	Si	C	Mn
17	3:46	.192	<.05	1.19	.26
27	5:31	.020	.003	0.064	.07
25	4:04	.068	.004	0.91	.15
26	5:04	.021	.005	0.058	.069
37	3:53	.151	.08	1.28	.12
38	3:45	.14	.045	1.29	.18
39	1:00	.031	.01	3.60	.05
40	1:30	.218	.01	3.36	.06
40	3:00	.198	nil	1.30	.06
40	4:30	.218	nil	0.20	nil
41	4:03	.290	.02	0.84	.15

6 in. bath   20 psig. pressure
21 in. blowing height   0.316 in. dia. nozzle

Location 11

Heat No.	Blowing Time	P	Si	C	Mn
12	1:22	.32	.45	4.22	.47
5	2:05	.28	.37	3.73	.36
11	2:43	.15	.23	3.88	.38
8	3:25	.20	.20	3.60	.36

Location 13

Heat No.	Blowing Time	P	Si	C	Mn
12	1:22	.31	.40	4.16	.52
5	2:05	.27	.40	3.93	.39
11	2:43	.16	.21	3.77	.28
8	3:25	.11	.25	3.70	.34

Location 16

Heat No.	Blowing Time	P	Si	C	Mn
12	1:22	.30	.45	4.20	.50
5	2:05	.24	.45	3.93	.43
11	2:43	.13	.20	3.90	.40

Location 31

Heat No.	Blowing Time	P	Si	C	Mn
12	1:08	.35	.50	4.22	.50
11	2:28	.18	.19	3.94	.44
13	4:05	.20	.27	3.65	.37

Heat No.	Blowing Time	Metal Composition		(weight percent)	
		P	Si	C	Mn

Location 33

Heat No.	Blowing Time	P	Si	C	Mn
12	1: 08	.26	.40	4.06	.46
5	1: 55	.25	.42	3.83	.42
9	2: 28	.18	.18	3.80	.32
11	2: 28	.14	---	3.90	.40
13	4: 05	.11	.14	3.46	.28
36	5: 25	.07	---	----	---

Location 36

Heat No.	Blowing Time	P	Si	C	Mn
36	0: 45	.18	---	----	---
12	1: 08	.32	.50	4.10	.47
13	1: 08	.21	.38	3.67	.37
5	1: 55	---	---	3.87	---
9	2: 28	.19	.13	3.72	.32
11	2: 28	.11	.10	3.89	.40
13	4: 05	.06	.11	3.45	.27
36	5: 25	.07	---	----	---

Location 51

Heat No.	Blowing Time	P	Si	C	Mn
36	1: 00	.19	---	----	---
5	1: 30	.27	.33	3.84	.48
9	2: 13	.26	---	3.70	.38
11	2: 14	.08	.15	3.74	.32
13	3: 50	.12	.07	3.48	.33

Location 53

Heat No.	Blowing Time	P	Si	C	Mn
12	0: 55	.28	.40	4.14	.40
36	1: 00	.18	---	----	---
9	2: 13	.08	.08	3.50	.36
13	3: 50	.11	.11	3.62	.30

Location 56

Heat No.	Blowing Time	P	Si	C	Mn
12	0: 55	.28	.35	4.16	.47
36	1: 00	.23	---	----	---
5	1: 30	---	---	2.78	---
9	2: 13	.09	.05	3.36	.24

Heat No.	Blowing Time	Metal Composition P	Si	(weight percent) C	Mn
		Location 63			
36	1:15	.06	---	----	.17
		Location 66			
36	1:15	.07	---	----	.17
36	5:25	.05	---	1.98	---
		Location 71			
12	0:42	.24	.25	3.88	.42
5	1:15	.09	.30	3.80	.46
11	2:00	.08	.15	3.52	.32
		Location 73			
12	0:42	.24	.35	3.64	.36
11	2:00	.09	.10	3.75	.30
8	2:40	.10	.06	3.54	.24
13	3:35	.12	.08	3.44	.31
		Location 76			
12	0:42	.26	.25	3.72	.40
11	2:00	.08	.10	3.89	.34
8	2:40	.09	.05	3.52	.26
		Sample M1			
5		.279	.85	4.24	.60
8		.300	.65	----	.60
9		.380	.55	4.28	.62
11		.304	---	4.36	.62
12		.353	---	4.28	.64
13		.405	.62	3.96	.61
15		.424	.51	3.91	.54
36		.235	.55	3.99	.48

Heat No.	Blowing Time	Metal Composition (weight percent)			
		P	Si	C	Mn

Sample M2

12	1:36	.297	---	3.98	.43
5	2:15	.272	.45	3.82	.42
9	2:40	.110	.10	3.82	.32
11	3:00	.040	.10	3.85	.32
8	3:46	.13	.08	3.56	.30
13	4:15	.028	<.05	3.62	.22
36	5:30	.017	.055	1.89	.10
15	6:15	.107	<.05	2.94	.21

10 in. bath   20 psig. pressure
7 in. blowing height   0.316 in. dia. nozzle

Location 21

31	0:32	.24	.52	2.95	.40
31	2:42	.18	.10	2.71	.28
29	4:00	.19	.02	2.60	.17
29	7:02	.13	.01	1.03	---

Location 23

31	0:32	.16	.11	3.10	.26
31	2:42	.19	.05	2.78	.22
29	4:00	.20	.02	2.70	.24

Location 26

31	0:32	.24	.43	3.40	.37
31	2:42	.19	.05	2.97	.21
29	4:00	.18	.02	2.62	.25
29	7:02	.14	.01	0.24	.22

Location 51

31	1:10	.25	.20	2.81	.22
31	2:50	.19	.07	2.75	.24
29	3:45	.16	.01	1.41	.16

Heat No.	Blowing Time	Metal Composition P	Si	(weight percent) C	Mn
		Location 53			
31	2:50	.17	<.05	2.82	.20
29	3:45	.12	<.05	----	.14
29	6:15	.12	<.05	0.29	.23
		Location 56			
31	1:10	.24	.10	3.02	.17
31	2:50	.19	.09	2.96	.23
29	3:45	.13	.09	1.63	---
29	6:15	.15	<.05	0.40	---
		Location 81			
31	0:50	.23	.33	3.23	.38
31	2:30	.14	.10	2.80	.21
29	3:30	.19	.02	2.70	.24
29	6:00	.12	.01	0.21	---
		Location 83			
31	0:50	.22	---	3.55	---
31	2:30	.16	<.05	2.79	.19
29	6:00	.13	<.05	0.20	.20
		Location 86			
31	0:50	.23	.16	3.44	.22
31	2:30	.18	<.05	2.80	.23
29	6:00	.11	.02	0.25	---
		Location 101			
31	0:15	.16	.02	2.74	.23
31	1:30	.21	.02	2.98	.20
29	3:00	.19	.02	2.15	.21
29	5:00	.11	.07	0.19	.31
		Location 103			
31	0:15	.17	<.05	2.76	.23
31	1:30	.19	<.05	2.66	.18
29	5:00	.11	.05	0.22	.29

Heat No.	Blowing Time	Metal Composition P	Si	(weight percent) C	Mn
		Location 106			
31	0:15	.18	<.05	2.59	.20
31	1:30	.16	<.05	2.90	.21
29	5:00	.12	<.05	0.22	.16
		Sample M1			
29		.25	.48	4.06	.47
31		.24	.38	4.03	.47
		Sample M2			
31		.15	<.01	2.78	.14

10 in. bath   35 psig. pressure
7 in. blowing height   0.316 in. dia. nozzle

Heat No.	Blowing Time	P	Si	C	Mn
		Location 21			
32	0:45	.27	.12	3.55	.25
		Location 51			
34	5:22	.03	.02	0.04	.12
		Location 101			
32	0:30	.24	.15	3.74	.30
		Location 103			
32	0:30	.23	.14	3.47	.20
34	5:15	.03	---	0.03	.12
		Location 106			
32	0:30	.27	.12	3.48	.23
34	5:15	.02	.01	0.08	.06
		Sample M1			
32		.26	.46	3.86	.55
33		.28	.44	4.10	.55
34		.25	.60	3.81	.55

Heat No.	Blowing Time	Metal Composition (weight percent)			
		P	Si	C	Mn

Sample M2

| 33 | 2:00 | .15 | .013 | 3.33 | .56 |
| 34 | 5:30 | .047 | <.01 | 0.02 | .043 |

6 in. bath   25 psig. pressure
7 in. blowing height   0.162 in. dia. nozzle

Location 11

21	1:45	.21	---	3.97	.44
22	1:46	.24	.44	3.66	.37
35	10:00	.15	.23	2.62	.18

Location 13

| 22 | 1:46 | .20 | .37 | 3.99 | .36 |
| 35 | 10:00 | .17 | .04 | 3.18 | .39 |

Location 16

22	1:46	.23	.42	3.36	.40
35	10:00	.16	.06	3.18	.22
35	13:00	.13	<.05	2.95	.18

Location 31

22	1:30	.23	.28	4.01	.37
21	1:32	.23	---	4.06	.51
22	3:00	.19	.32	----	.39
35	8:20	.15	<.05	2.71	.20
35	12:00	.09	<.05	2.17	.15

Location 33

22	1:30	.20	.42	3.91	.26
22	3:00	.20	.32	3.21	.37
35	8:20	.12	<.05	2.22	.20
35	12:00	.10	<.05	2.13	.18

Location 36

22	1:30	.19	.28	3.57	.35
22	3:00	.19	---	3.70	---
35	8:20	.12	<.05	2.95	.15
35	12:00	.11	<.05	2.17	.13

Heat No.	Blowing Time	Metal Composition (weight percent)			
		P	Si	C	Mn

		Location 51			
22	1:15	.17	.28	3.65	.27
21	1:17	.21	.08	3.56	.23
21	2:47	.19	.09	3.37	.13
		Location 53			
22	1:15	.20	.46	3.44	.28
21	1:17	.20	.15	3.39	.19
21	2:47	.18	.09	3.33	.13
35	9:30	.14	<.05	2.42	.18
35	11:45	.09	<.05	2.30	.17
		Location 56			
22	1:15	.18	.33	3.48	.33
21	1:17	.20	.08	3.52	.24
21	2:47	.22	<.05	3.27	.23
35	9:30	.12	.10	2.15	.17
35	11:45	.11	<.05	2.58	.18
		Location 61			
21	1:01	.21	.08	3.67	.18
22	1:01	.18	.26	3.76	.26
21	2:30	.19	.07	3.75	.11
22	2:30	.20	.19	3.66	.24
35	9:00	.10	<.05	2.17	.46
35	11:30	.10	<.05	2.08	.46
		Location 63			
22	1:01	.19	.33	3.64	.26
21	2:30	.19	.10	3.50	.19
35	9:00	.12	<.05	2.56	---
35	11:30	.10	.01	1.98	.17

Heat No	Blowing Time	Metal Composition (weight percent)			
		P	Si	C	Mn
		Location 66			
21	1:01	.20	.12	3.27	.14
22	1:01	.18	.22	3.54	.22
21	2:30	.17	.08	3.75	.13
22	2:30	.18	---	2.62	.16
35	9:00	.10	<.05	2.34	.17
35	11:30	.09	.005	2.28	.15
		Sample M1			
22		.253	.68	3.96	.54
21		.230	.68	4.21	.46
35		.272	.48	4.29	.46
		Sample M2			
22	4:01	.193	.17	3.64	.24
21	5:42	.182	.05	3.58	.14
35	13:45	.065	.025	2.18	.12
		Special Heats R-38 Location 31			
S	2:15	.21	---	----	.17
O	2:30	.20	.004	2.97	.17
S	2:45	.18	---	1.53	.24
S	3:15	.16	---	1.32	.21
		Location 33			
	2:45	.14	---	1.28	.34
	3:15	.18	---	1.42	.23
		Location 36			
	2:15	.15	---	----	.25
	2:45	.17	---	1.53	.24
		Location 61			
S	0:40	.21	---	3.46	.10
O	0:53	.13	---	3.25	.20
S	1:16	.20	---	1.19	.12

Heat No.	Blowing Time	Metal Composition		(weight percent)	
		P	Si	C	Mn
		Location 63			
	0: 53	.16	---	1. 36	.25
		Location 66			
	0: 53	.16	---	1. 31	.22
	2: 00	.17	---	1. 44	.27
		Sample M1			
		.210	.48	4. 03	.50
		Sample M2			
	3: 45	.139	.045	1. 29	.18
		Special Heat R-39			
		Sample M1			
		.028	.10	3. 96	.04
		Sample M2			
		.031	.01	3. 60	.05
		Special Heat R-40			
		Sample M1			
	0: 00	.218	.28	3. 90	.26
		Sample M2			
	1: 30	.218	.01	3. 36	.06
		Sample M3			
	3: 00	.198	nil	1. 30	.06
		Sample M4			
	4: 30	.218	nil	0. 20	.08

Heat No.	Blowing Time	Metal Composition (weight percent)			
		P	Si	C	Mn

Special Heat
R-41

Location 61

	0:45	.650	---	----	---
	1:30	.47	---	----	---
	2:38	.46	---	----	---

Location 63

| | 1:30 | .45 | --- | ---- | --- |
| | 2:38 | .43 | --- | ---- | --- |

Location 66

| | 1:30 | .46 | --- | ---- | --- |
| | 2:38 | .47 | --- | ---- | --- |

Sample M1

| | | .760 | .50 | 3.70 | .48 |

Sample M2

| | 4:03 | .290 | .02 | 0.84 | .15 |

TABLE XV

Blowing Time - Slag Composition Data for all Blowing Conditions

Heat No.	Blowing Time	SiO$_2$	Tot. Fe	Fe$_2$O$_3$	FeO	Al$_2$O$_3$	CaO	MgO	MnO	P$_2$O$_5$
8 in. sample ht.	6 inch bath, 7 inch blowing height, 20 psig. pressure, 0.316 inch. dia. nozzle									
26	1:30	17.1	12.9	3.6	13.4	0.75	37.9	15.9	6.2	1.5
23	2:43	22.4	17.0	1.1	20.9	7.7	21.0	15.7	6.0	3.0
27	2:45	23.8	13.1	1.3	15.7	0.8	29.6	12.4	8.4	4.4
17	3:30	20.1	9.4	3.1	9.3	3.8	33.2	15.9	5.5	5.5
26	3:45	21.1	19.3	4.0	21.2	1.1	27.3	12.8	6.9	3.9
27	4:40	11.5	17.4	5.5	17.5	0.9	36.2	14.2	3.9	3.7
11 in. sample ht.										
26	2:17	8.8	15.6	6.0	14.7	6.0	42.5	14.7	2.5	1.9
26	3:15	20.7	23.8	4.2	26.8	1.1	23.5	11.1	7.1	3.4
27	4:00	17.5	22.1	7.4	21.5	0.9	27.3	11.1	6.3	--
27	5:21	9.8	26.0	8.4	26.0	0.8	38.1	9.5	3.5	2.8
S-2 Samples										
24	1:27*	14.2	7.9	4.5	6.1	4.6	49.2	12.2	3.0	4.2
17	3:46*	15.9	5.5	3.6	3.8	4.0	50.5	11.8	3.4	4.9
23	3:48*	13.7	7.4	4.2	5.8	6.0	48.0	14.5	2.8	2.7
20	3:57*	13.8	5.3	3.9	3.3	3.8	52.4	14.2	2.7	3.4
25	4:10	15.84	9.1	4.6	7.5	2.8	48.8	11.2	3.3	3.3
26	5:15	13.8	18.3	7.3	17.0	1.1	43.5	10.5	2.8	2.4
27	5:30	9.9	23.5	8.9	22.2	0.9	40.0	9.8	3.1	2.3
18	5:32	9.2	12.6	6.3	10.5	4.9	50.8	9.8	2.4	2.8

Slag Composition (weight percent)

Heat No.	Blowing Time	SiO$_2$	Tot. Fe	Fe$_2$O$_3$	FeO	Al$_2$O$_3$	CaO	MgO	MnO	P$_2$O$_5$
9 in. sample ht.	6 inch bath, 21 inch blowing height, 20 psig. pressure, 0.316 inch dia. nozzle									
36	1:30	10.0	22.5	7.91	21.9	1.4	33.5	16.5	2.9	1.0
36	3:15	5.4	32.1	9.7	32.6	2.3	21.3	22.4	1.9	0.7
12 in. sample ht.										
36	2:45>	6.1	36.8	7.9	40.2	2.7	19.3	17.3	2.2	0.5
36	5:00	5.6	35.1	20.2	27.0	2.2	22.4	16.7	1.4	0.6
S-2 samples										
12	1:36	8.6	17.5	---	---	1.4	58.9	3.8	2.8	1.6
12	1:36*	7.3	24.1	10.3	21.7	2.2	49.2	3.8	2.1	2.1
5	2:15*	9.1	26.1	10.1	24.7	2.5	44.8	5.1	2.2	2.0
9	2:40	10.6	24.0	---	---	3.8	37.4	8.4	3.3	3.4
11	3:00	10.7	26.2	---	---	3.5	36.3	5.9	2.8	3.0
8	3:46	16.5	13.4	---	---	4.8	41.9	11.8	3.6	3.4
13	4:15	10.4	28.9	9.7	28.4	4.6	33.3	6.2	2.7	3.5
36	5:30	9.2	32.1	10.9	31.4	3.9	28.8	9.2	2.8	2.9
19	5:32	7.2	37.2	8.9	39.9	3.2	28.6	6.4	2.0	2.6
13 in. sample ht.	10 inch bath, 7 inch blowing height, 20 psig. pressure, 0.316 inch dia. nozzle									
31	1:45	19.5	10.8	2.9	11.4	0.6	38.0	12.0	7.5	1.8
31	3:05	16.7	6.9	2.3	6.7	0.6	48.0	10.1	5.8	1.9
29	4:30	20.1	8.5	4.1	7.3	0.7	34.4	19.9	5.2	3.7
S-2 samples										
31	3:26*	14.9	5.5	2.5	4.8	0.8	49.8	16.9	3.8	1.5
29	8:32	12.9	4.0	1.8	4.9	0.9	53.6	19.0	2.1	1.8

Heat No.	Blowing Time	Slag Composition (weight percent)								
		SiO$_2$	Tot. Fe	Fe$_2$O$_3$	FeO	Al$_2$O$_3$	CaO	MgO	MnO	P$_2$O$_5$
13 in. sample ht. 10 inch bath, 7 inch blowing height, 35 psig. pressure, 0.316 inch dia. nozzle										
34	4:45	10.9	15.3	5.2	15.0	5.2	40.8	12.4	3.2	3.4
S-2 sample										
34	5:30	13.5	18.5	7.4	17.1	7.6	24.6	25.2	2.2	1.8
8 in. sample ht. 6 inch bath, 7 inch blowing height, 25 psig. pressure, 0.162 inch dia. nozzle										
35	8:30	18.4	23.5	2.4	28.1	5.31	18.0	12.9	9.5	1.3
35	12:15	10.5	27.0	7.0	28.4	2.3	27.9	13.2	4.7	0.9
11 in. sample ht.										
35	10:30	---	24.1	---	---	---	---	---	---	---
S-2 sample										
22	4:01*	17.2	2.0	0.3	2.3	---	---	---	0.8	0.2
21	5:42*	16.4	9.9	0.7	12.1	2.9	39.7	15.7	3.8	0.9
35	13:38	8.9	11.5	7.9	7.7	2.4	57.1	8.4	1.3	2.6
Special Heats S-2										
38	3:45*	10.4	4.5	2.2	3.9	5.6	60.2	10.7	2.2	1.4
40	4:30	69.6	16.1	16.9	5.5	2.0	1.5	3.9	1.4	0.3
41	4:03	9.8	3.5	2.3	2.5	3.3	63.3	10.8	1.8	4.1

* Sample contained lumps of undissolved lime and was considered inhomogeneous; therefore it was not included in the review of slag data.

Appendix II, Calculations

a.   Calculation of Average Batch %J

b.   Mass Balance and Oxygen Utilization

c.   Equilibrium Calculations

d.   Mass Transfer Models

a.   Determination of Average Bath %J

The average bath content of J is determined from the
analysis of final metal samples whenever such data are available.
During the early portion of an experiment no data are available so
average bath %J is determined as shown by the example below.

$$J \ = \ P, \qquad t \ = \ 1:00 \text{ blowing time}$$

Conditions: 6 in. bath, 7 in. blowing height,

20 psig. pressure, 0.316 in. lance

Constant composition curves from Figure 17 are redrawn
as on Figure 51.   The axes are height and distance from the center
of the converter squared.   The product of the axes is proportional
to bath volume.   The sum of graph areas between two constant
composition lines multiplied by the intermediate %P is proportional
to the weight of phosphorous in the bath.   The sum of the products
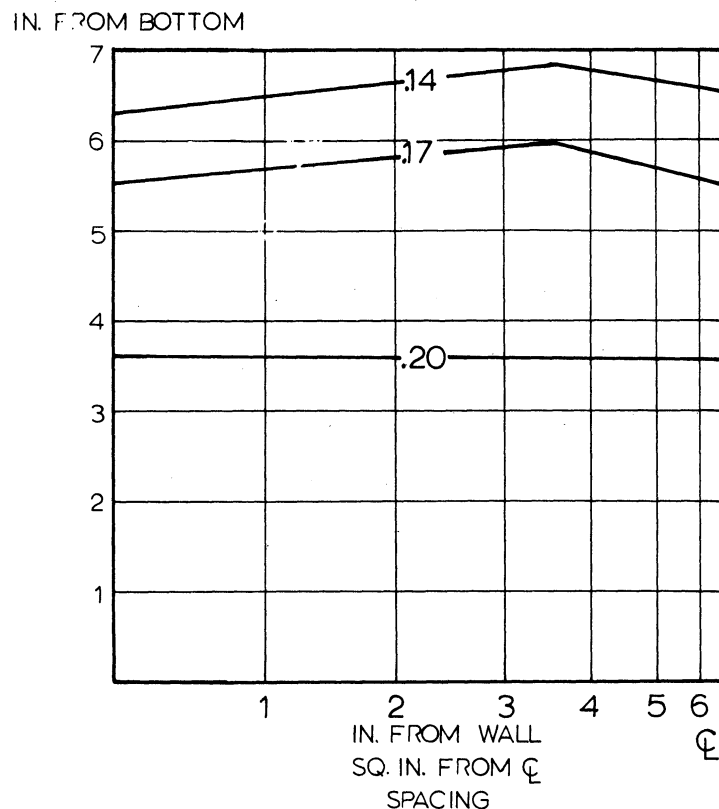is divided by the total graph area yielding average %P.

Fig. 51.   Volume Plot Used in Calculating Average Bath % P.

b.   Mass Balance and Oxygen Utilization

Mass balance and oxygen utilization calculations can be
made when sufficient data are available on the slag and metal
compositions variation with time.   The mass balance and oxygen
utilization equations are derived below.

Mass Balance

The slag weight is determined assuming no loss of CaO.
In other words, while slag and metal are thrown out of the converter
during a run CaO was presumed to be thrown out in amounts propor-
tional to its fraction of the total slag.

Slag wt.   =   lb. CaO in/fraction CaO in the slag

Metal wt. at time t =   metal wt. charged – wt. by time t

of elements lost to the slag including

Fe in the slag.

wt. of elements in the metal   =   % element J x metal wt. /100.

wt. of elements in the slag   = $\%J_a O_b$ x slag wt. /(100 x mol. wt.

$$J_a O_b \text{ /a x mol. wt. } J).$$

Total wt. of all J   =   J in metal + J in slag.

Accountable J   =   (Total wt. J/initial total wt.) x 100%.

Whenever data were available on the compositions of slag
and metal during an experiment mass balance calculations were made
at incremental times; otherwise, the calculations were made only
at the end of an experiment on the basis of beginning and final metal
composition and final slag composition.

Oxygen Utilization

The oxygen used to oxidize each metal impurity was calculated assuming the formation of specific oxides. Here SiO_2, MnO, P_2O_5, CO, FeO and Fe_2O_3 were the oxides initially considered.

wt. of J in the metal = wt. of metal x %J/100.

wt. of J oxidized in time t = initial wt. of J - wt. of J at time t.

Oxygen to oxidize J = wt. of J oxidized x b x mol. wt. O/ a x mol. wt.

Total oxygen used = Σ oxygen to J.
$\quad\quad\quad\quad\quad\quad\quad\quad$ J

Oxygen efficiency = (total oxygen used/total oxygen in) x 100%.

In cases where data were sufficient, differential efficiencies were calculated by subtracting the weight of J in the metal at time t - Δt from the weight of J in the metal at time t. Oxygen efficiencies were calculated for the time increment Δt.

As a matter of interest whenever the oxygen efficiency was less than 70% an additional calculation was made assuming 100% CO_2.

c.   Equilibrium Calculations

Equilibrium phosphorus concentrations have been calculated from metal and slag composition data and thermodynamic constants.

Slag temperatures were assumed to lag behind metal temperature. After 5: 30 blowing time at standard conditions, $2910^{\circ}F$. was assumed to be the slag temperature. The following calculations of equilibrium %P were made using Winkler's (38) thermodynamic data.

TABLE XVI

Calculation of Mole Fraction $J_a O_b$ in the Slag

t = 5: 30,   T = $2910^{\circ}F$. = $1600^{\circ}C$. ,   Sample: 27S-2

Compound	SiO_2	Al_2O_3	Fe_2O_3	P_2O_5	MgO	MnO	CaO	FeO
mol wt.	60	102	160	122	40.3	71	56	72
wt. %	9.9	0.9	8.9	2.3	9.8	3.1	40.0	22.2
mol/100 lb.	.165	.009	.056	.019	.243	.044	.715	.308
mol frac.	.10	.01	.03	.01	.16	.03	.46	.20

B = CaO + MgO + MnO = 0.69

A = SiO_2 + $2P_2O_5$ + $1/2 Fe_2O_3$ + $1/2 Al_2O_3$ = 0.14.

B/A = 4.9.

FeO = 20 mol. %.

$(P_2O_5) / (\%P^2)$ ≈ 600.   Figure 11 Winkler and Chipman (38)

(P_2O_5) = 0.01.

%P = $(0.01/600)^{1/2}$ = 0.004%.

d. Mass Transfer Models

Four models have been developed for dephosphorization under standard blowing conditions. The four models are 1) Bulk Diffusion, 2a) Boundary Layer Transfer from a Turbulant Bath, 2b) Boundary Layer Transfer from a Circulating Bath, 3) Bath Dilution from Metal Droplets Falling through a Dephosphorizing Slag, and 4) Combination of Circulation and Droplet Models. Each of the models is derived separately below.

1) Bulk Diffusion

This model is based on a stagnant bath being dephosphorized by diffusion of phosphorus to an infinite surface sink at 0%P. This situation is best described by Fick's Second Law.

P = %P, t = time in seconds

h = distance from the bath surface in cm

D = 1.5×10^{-4} cm^2/sec.

RHO = density of liquid steel = 7 gm/cc

$$(RHO/100) \frac{dP}{dt} = (RHO/100) D \frac{d^2P}{dh^2} \qquad (1)$$

B. C.

%P = 0.22 at $t = 0$ and $0 < h < \infty$

a semi infinite bath is assumed

%P = 0 at $h = 0$ and $0 < t < \infty$.

With these boundary conditions the integrated form of (1) is:

$$(0.22 - \%P) / (0.22 - 0) = 1 - erf ((h)/(2 \sqrt{Dt})) \qquad (2)$$

%P for various h and t is calculated with (2). %P is calculated to be 0.19% after 10,000 seconds, roughly 3 hrs., at a distance of

2.5 cm., 1 inch, from the bath surface. The dephosphorization rate is 0.01%/hr.. Clearly, this model is not appropriate.

2a) Boundary Layer Transfer From a Turbulent Bath

Wagner (47) has described this general model in detail. In this case phosphorus loss is given by

$$\dot{m} = (D/\delta) A (P - P^*) \tag{3}$$

δ = diffusion distance = .003 cm.

P^* = equilibrium phosphorus content (gm/cc.)

P = phosphorus content at time t (gm/cc.)

Equation (3) has been modified for use with %P, X.

$$m = (D/\delta) A (RHO/100) (X - X^*) \tag{4}$$

$$X \text{ at } t - [(m \times 100\%)/(bath\ wt.)] \Delta t = X \text{ at } t + \Delta t \tag{5}$$

Equation (5) has been used in calculations of X as a function of blowing time.

2b) Boundary Layer Transfer From a Circulating Bath

A schematic drawing of this condition is shown in Figure 52.

$M(r)$ = flow velocity of the circulating layer at r (cm/sec).

ℓ = thickness of the circulating layer (cm.)

$$C_1 = M \ell\ 2\pi\ r = constant\ (c.c./sec.) \tag{6}$$

$$(D/\delta) (RHO/100) (X_B - X^*) = phosphorous\ flux\ gm./cm^2/sec.$$

$X_B(r)$ = %P in circulating layer at r.

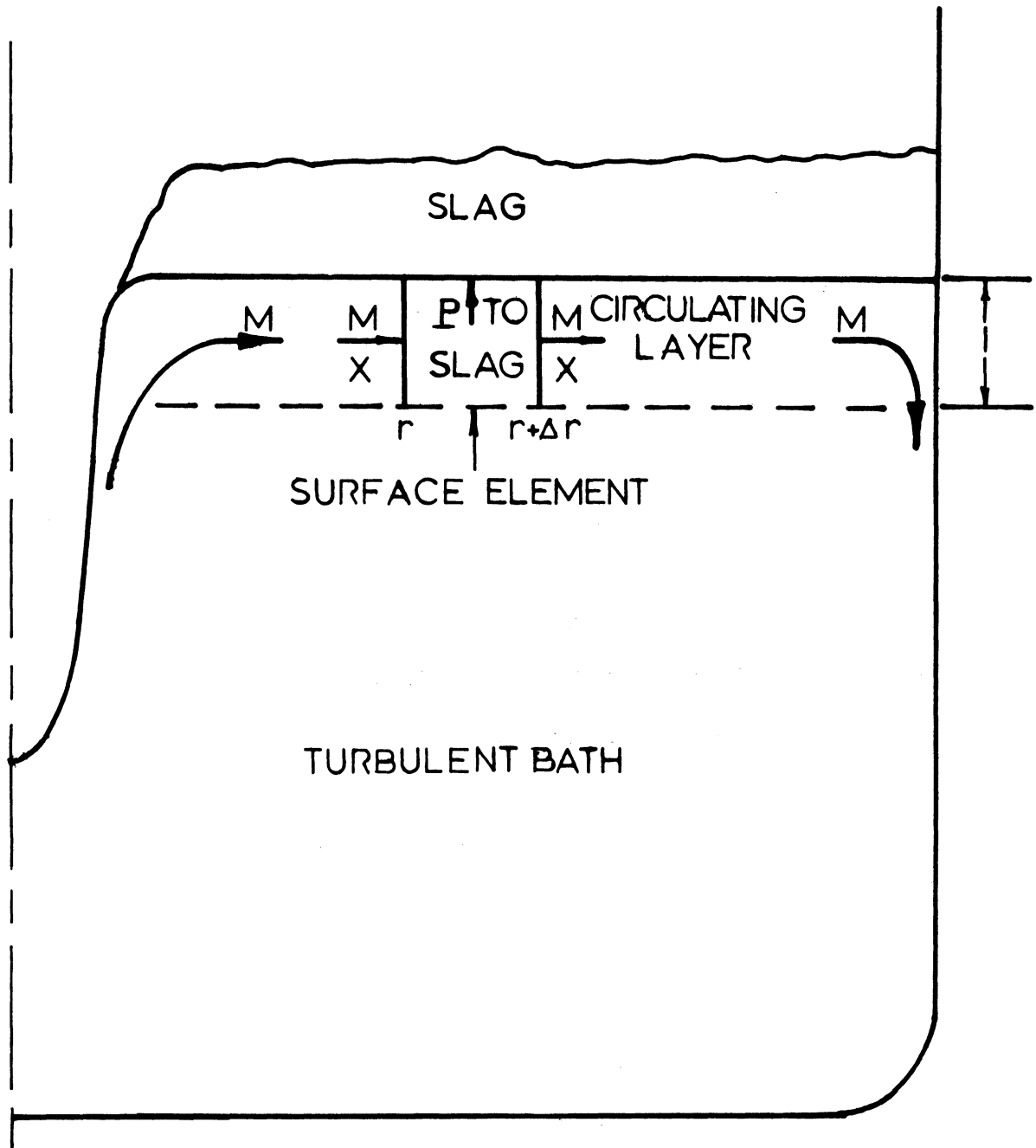Fig. 52. Schematic Drawing of Mass Transfer Conditions of Model 2b.

$$-(RHO/100)(C_1 X_B{}_r - C_1 X_B{}_{r+\Delta r}) = (D/\delta)(2\pi r \Delta r)(RHO/100)(X_B - X*)$$

(7)

$$(dX_B)/(dr) = -(D/\delta)(2\pi/C_1)(X_B - X*)r \qquad (8)$$

$$(dX_B)/(X_B - X*) = -(D/\delta)(2\pi/C_1)(X_B - X*)rdr \qquad (9)$$

$$\text{In }(X_B - X*) = -(D/\delta)(\pi/C_1)r^2 + K \qquad (10)$$

$$X_B - X* = K \exp\left[-(D/\delta)(\pi r^2/C_1)\right] \qquad (11)$$

$$\text{at } r = 2.54 \quad X_B = X \text{ (Bulk \%P)} \qquad (12)$$

$$X_B = (X - X*) \exp\left[(D/\delta) C (\pi/C_1)(r^2 - 6.452)\right] + X* \qquad (13)$$

X_B was calculated at r's corresponding to the 3 sampling locations at the bath surface with equation 13.

The change in the bulk phosphorous content is determined by assuming that there is no interaction between the bulk of the bath and the surface layer except when new metal at bulk concentration flows in at r = 2.54 and when refined metal flows out at the wall.

$$V = 16.51 - \ell$$

$$VX_t - VX_{t+\Delta t} = C_1 (X - X_B) \qquad (14)$$

$$X_B = \text{surface \%P at r = wall}$$

$$-\left[(dX)/(X - X_B)\right] = (C_1/V) dt \qquad (15)$$

$$(X - X_B) = A \exp\left[(-C_1/V)\Delta t\right] \qquad (16)$$

$$\text{at } t = 0 \quad X = X_0 = \text{\%P} \qquad (17)$$

$$X = (X_0 - X_B) \exp(-t C_1/V) + X_B \qquad (18)$$

The bulk phosphorus concentration can be calculated for any blowing time with (18).

3) Bath Dilution From Metal Droplets Falling Through a Slag

This model is analogous to liquid from a tank being run into a refining unit and then back into the tank.

Let SPRAY = volume of droplets thrown up per second.

$$V X \Big|_t - V X \Big|_{t+\Delta t} = SPRAY (X - X_E) \tag{19}$$

X_E = %P in droplets leaving the slag

$$X_E \geq X^* \tag{20}$$

$$X = (X_0 - X_E) \exp(-SPRAY\, t/V) + X_E \tag{21}$$

3') This model was modified such that SPRAY is proportional to the rate of decrease of the bath %C, e. g., SPRAY α d%C/dt.

4) Combination of Circulation and Droplet Models

The two models, 2b and 3, have been described separately. The combination is derived below.

Mass balance on a surface element

$$C_1 \Big|_r - C_1 \Big|_{r+\Delta r} + 2\pi r \Delta r L - 2\pi r \Delta r L = 0 \tag{22}$$

surface layer volume is constant

C_1 is constant

L(r) = distribution of droplets over the surface

$$L(r) = C_3/r^3, \quad C_3 = constant \tag{23}$$

Phosphorous balance around surface layer element

$$(RHO/100)(C_1X_B) \Big|_r - C_1X_B \Big|_{r+\Delta r} + 2\pi r \Delta r L X_X - 2\pi r \Delta r L X_B) =$$

$$(D/\delta)(2\pi r \Delta r)(RHO/100)(X_B - X^*) \qquad (24)$$

$$-C_1[(dX_B)/(dr)] = 2\pi r[(D/\delta)(X_B - X^*) + L(X_B - X_E)] \qquad (25)$$

$$\text{If } X^* = X_E \qquad (26)$$

$$-C_1(dX_B)/(dr) = 2\pi 4[(D/\delta) + L](X_B - X_E) \qquad (27)$$

$$(dX_B)/(X_B - X_E) = [(-2\pi)/(C_1)][(D/\delta)/L] rdr \qquad (28)$$

$$L = C_3/r_3 \qquad (23)$$

$$(dX_B)/(X_B - X_E) = ((-2\pi)/C_1)[(Dr/\delta) + (C_3/r^2)] dr \qquad (29)$$

$$\ln(X_B - X_E) = (-2\pi)/(C_1)[(Dr^2/2\delta) - (C_3/r)] + K \qquad (30)$$

$$X_B - X_E = K \exp[(-2\pi/C_1)\{(Dr^2/2\delta) - (C_3/r)\}] \qquad (31)$$

$$\text{at } r = 2.54 \qquad X_B = X \text{ (bath } \%P) \qquad (32)$$

$$X_B = (X-X_E) \exp(-2\pi/C_1)(D/2\delta)(r^2 - 6.462) \ldots$$

$$-C_3[(1/r) - 0.3937] + X_E \qquad (33)$$

$X_B(r)$ was calculated for r corresponding to the sampling locations at the bath surface.

The time dependence $\%P$ in the bath is derived below:

Phosphorus balance

RHO/100 has been cancelled out.

$$VX \Big|_{t+\Delta t} - VX \Big|_t = -C_1X \Big|_{r=2.54} + C_1X_B \Big|_{r=wall} \ldots$$

$$-X L2\pi rdr + LX_B 2\pi rdr \qquad (34)$$

$$-C_1 X \Big|_{r=2.54} = -C_1 X \tag{35}$$

$$C_1 X_B \Big|_{r=wall} = C_1 [(X-X_E) \exp(---) \Big|_{r=wall} + X_E] \tag{36}$$

$$= C_1 X \exp(---) - C_1 X_E \exp(---) + C_1 X_E \tag{37}$$

$$X \int L 2\pi r \, dr = 2\pi X C_3 \int_{2.54}^{r^2} [1/(r^2)] \, dr \tag{38}$$

$$= 2\pi X C_3 (0.3937 - 1/r^2) \tag{39}$$

$$\int L X_B \, 2\pi r \, dr = 2\pi C_3 \int (1/r^2) [(X-X_E) \exp(---) + X_E] \, dr \tag{40}$$

$$= 2\pi C_3 X \int (1/r^2) [\exp(---)] \, dr - 2 C_3 X_E \int (1/r^2) \dots$$

$$[\exp(---)] \, dr + 2\pi C_3 X_E \int (1/r^2) \, dr \tag{41}$$

Combining equations 34, 35, 37, 39, and 41:

$$VX \Big|_{t+\Delta t} - VX \Big|_{t} = -C_1 X + C_1 X \exp(---) - C_1 X_E \exp(---) + \dots$$

$$C_1 X_E - 2\pi C_3 X [0.3937 - (1/r^2)] +$$

$$2\pi C_3 X \int (1/r^2) \exp(---) \, dr - 2\pi C_3 X_E \int (1/r^2) \exp(---) \, dr \, .$$

$$+ 2\pi C_3 X_E [(0.3937) - (1/r^2)] \tag{42}$$

Grouping terms in 42:

$$B = -C_1 + C_1 \exp(---) - 2\pi C_3 [0.3937 - (1/r^2)] + \dots$$

$$2\pi C_3 \int (1/r^2) \exp(---) \, dr \tag{43}$$

$$V dX/dt = BX - BX_E \qquad (44)$$

$$(dX) / (X - X_E) = (V/B)dt \qquad (45)$$

$$\ln (X - X_E) = (V/B) t + K \qquad (46)$$

$$X - X_E = K \exp [(V/B) t] \qquad (47)$$

$$\text{at } t = 0, \qquad X = X_0 \qquad (48)$$

$$X = (X_0 - X_E) \exp [(V/B) t] + X_E \qquad (49)$$

Evaluation of $\int (1/r^2) \exp (---) dr$ was done graphically for $r = 2.54$ to $r = 19.05$.

Bibliography

1.   A. L. Hodge. *Iron and Steel Engineer*. 1966, V. 44, pp. 97-100.

2.   P. W. A. Lanzing and R. Smit. *Journal of Metals*. 1962, V. 14, pp. 510-514.

3.   T. Ikida, op. cit. pp. 518-520.

4.   G. Grosvenor. *Journal of Metals*. 1961, V. 13, pp. 621-624.

5.   J. N. Albaugh. op. cit. p. 631.

6.   Panel Discussion. *Open Hearth Proc*. 1965, V. 48, pp. 120-135.

7.   T. J. Murray, F. E. Williams and E. C. Vice. *Journal of Metals*. 1964, V. 16, pp. 644-650.

8.   J. A. Glasgow. *Journal of Metals*. 1961, V. 13, pp. 625-627.

9.   R. B. Morgan. op. cit. pp. 628-630.

10.   G. Massobrio and F. Santini. *Open Hearth Proc*. 1965, V. 48, pp. 115-119.

11.   R. A. Flinn, R. D. Pehlke, R. D. Glass and P. O. Hayes, *A. I. M. E. Trans*. to be published.

12.   J. A. Glasgow. *Journal of Metals*. 1962, V. 14, pp. 514-516.

13.   C. G. Campbell. op. cit. pp. 516-517.

14.   K. F. Behrens and J. Koenitzer. *Open Hearth Proc*. 1964, V. 47, pp. 54-72.

15.   F. Petrilli. op. cit. pp. 73-77.

16.   O. Cuscoleca, K. Rosner and W. Kuhnelt.   O. A. M. Bull.
        Jan. 1952.

17.   W. O. Philbrook.   Journal of Metals.   1958, V. 10, pp. 477-
        482.

18.   T. P. Calclough.   J. I. S. I.   1959, 192, pp. 201-215.

19.   H. Trenkler.   Revue Universelle des Mines.   V. 96, 1953,
        pp. 644-657.   Brutcher Trans. no. 3238.

20.   O. Cuscoleca.   Stahl und Eisen.   Vol. 72, no. 17,
        Aug. 14, 1952, pp. 989-992.

21.   H. Trenkler.   op. cit. pp. 992-997.

22.   K. Rosner.   op. cit., pp. 997-1004.

23.   W. Kuehnelt.   op. cit., pp. 1004-1010.

24.   G. Tromel.   Stahl und Eisen.   Vol. 73, no. 1, 1953,
        pp. 19-22.   Brutcher Trans no. 3227.

25.   H. Trenkler.   Inbetriebnahme Breitbandstrasse Blasstahlwerk
        Jan. 5, 1953, pp. 17-18, 20-22.

26.   H. Hauttman.   op. cit., pp. 23-30.   Private Translation

27.   T. E. Suess   "Method of Carrying Out Melting Processes"
        U. S. Pat. 2,800,631,   July 23, 1957.

28.   H. Rellermeyer, H. Knueppel and J. Sittard.   Stahl und
        Eisen.   1957, V. 77, pp. 1296-1303.

29.   C. Holden and A. Hogg.   J. I. S. I.   1960, V. 196, pp. 318-
        332.

30.   H. Krainer, K. Borowski and J. Maatsch.   Krupp Tech.
        Rev.   1965, V. 23, pp. 53-66.

31.   T. Kootz.   J. I. S. I.   1960, V. 196, pp. 253-258.

32.   W. O. Philbrook.   Journal of Metals.   1961, V. 13, pp. 613-
        620.

33.   G. C. Smith and D. A. Dukelow. Journal of Metals. 1964, V. 16, pp. 357-361.

34.   T. E. Suess. Iron and Steel Engineer. 3-1952, V. 29, pp. 91-93.

35.   J. Pearson. Iron and Coal Trades Review. 1960, V. 181, pp. 1407-1413.

36.   B. S. Holmes and M. W. Thring. J. I. S. I. 1960, V. 196, pp. 259-261.

37.   G. Perbix. Journal of Metals. 1966, V. 18, pp. 824-831.

38.   T. B. Winkler and J. Chipman. Trans Met. Soc. AIME. 1946, V. 167, pp. 111-133.

39.   L. von Bogandy, W. Dick and I. N. Stranski. Archri fur das Eisenhuettenwesen. 1958, V. 29, pp. 329-337.

40.   T. Kootz and H. Neuhaus. Stahl und Eisen. 1961, V. 81, pp. 1810-1815.

41.   T. Kootz, K. Behrens, H. Maas and P. Boumgarten. Stahl und Eisen. 1965, V. 85, pp. 902-907.

42.   T. Kato, J. Imai, and K. Fujiwara. Tetsu-to-Hagane. 1962, V. 48, pp. 465-467. Brutcher Trans. no. 5675.

43.   Physical Chem. of Steelmaking Comm. A. I. M. E. Basic Open Hearth Steelmaking. Chilton Company, New York, N. Y., 1964.

44.   T. F. Pearson, A. S. Venkatadri and J. O'Hanlon. J. I. S. I. 1966, V. 205, pp. 997-1006.

45.   L. A. Baker, N. A. Warner and A. E. Jenkins. Trans. Met. Soc. AIME. 1967, V.   pp. 857-863.

46.   C. Wagner. The Physical Chemistry of Steelmaking. The M. I. T. Press, Cambridge, Mass., 1958.